THE PHYSIOLOGY AND SIMULATION OF ALPHA MOTONEURONS IN THE HUMAN SPINAL CORD

by

Kelvin E. Jones

B.Sc., Simon Fraser University, 1991

THESIS SUBMITTED IN PARTIAL FULFILLMENT OF

THE REQUIREMENTS FOR THE DEGREE OF

DOCTOR OF PHILOSOPHY

in the Department

of

Kinesiology

SIMON FRASER UNIVERSITY

September 1995

APPROVAL

NAME: Kelvin E. Jones

DEGREE: Doctor of Philosophy

TITLE OF THESIS: The Physiology and Simulation of Alpha Motoneurons in the Human Spinal Cord

EXAMINING COMMITTEE:

Chair: Dr. John Dickinson

Dr. Parveen Bawa
Senior Supervisor
Professor, School of Kinesiolgoy

Dr. Eric Banister
Professor, School of Kinesiology

Dr. Tom Calvert
Professor & Director
Centre for Systems Science

Dr. Charles Krieger
Department of Medicine, UBC

Dr. Hal Weinberg
Internal Examiner
Professor, School of Kinesiology

Dr. Eberhard Fetz
External Examiner
Department of Physiology and Biophysics
University of Washington

Date Approved: 19 September '95

PARTIAL COPYRIGHT LICENSE

I hereby grant to Simon Fraser University the right to lend my thesis, project or extended essay (the title of which is shown below) to users of the Simon Fraser University Library, and to make partial or single copies only for such users or in response to a request from the library of any other university, or other educational institution, on its own behalf or for one of its users. I further agree that permission for multiple copying of this work for scholarly purposes may be granted by me or the Dean of Graduate Studies. It is understood that copying or publication of this work for financial gain shall not be allowed without my written permission.

Title of Thesis/Project/Extended Essay

THE PHYSIOLOGY AND SIMULATION OF ALPHA MOTONEURONS IN THE HUMAN SPINAL CORD.

Author:_
(signature)

Kelvin Edward Jones
(name)

SEPT. 26, 1995
(date)

Abstract

The present thesis addressed two broad questions about the physiology of human alpha motoneurons: 1) how does the central nervous system recruit the neurons in a motoneuron pool when performing various tasks; and 2) can the biophysical properties of human motoneurons be indirectly assessed and compared with those of the cat?

For the recruitment studies two sets of experiments were performed. The first set examined the hypothesis that the motoneurons innervating the flexor carpi ulnaris (FCU) muscle are fractionated into subpopulations, and that each of these subpopulations is recruited during a distinct task. The results of the present study did not support this hypothesis, but instead suggested that motoneurons in the motoneuron pool are recruited in the same order during the tasks presented in this study. The second set of recruitment experiments examined the order of recruitment of first dorsal interosseus (1DI) motoneurons during natural motor behaviour. The results of these experiments demonstrated that recruitment proceeds in the same fashion during a behavioral task as that during the more restrictive condition of an isometric contraction.

The present investigation of the biophysical properties of human motoneurons was accomplished by measuring motoneuron excitability during rhythmic firing. The excitability of motoneurons was measured by the probability of their response to inputs from two sources: 1) muscle stretch receptors; and 2) neurons in the motor cortex. The results of these experiments demonstrated that the level of ongoing activity of the motoneuron, as determined by its firing rate, is a significant factor affecting its ability to respond to an input. In an effort to explain these results, a computer simulation of motoneuron stimulus/response behaviour was undertaken based upon known properties of the cat motoneuron. The result of this modeling suggests that the basic biophysical properties of the cat motoneuron are sufficient to account for the observed responses of human motoneurons to synaptic inputs.

Dedication

To my Granny, who through her life and now
in her death has exemplified that "all is vanity" unless
it is done Soli Deo gloria.

Acknowledgments

I recognize that without the input of several people I might have well left the pages in this thesis blank.

I will never forget my senior supervisor, Dr. Parveen Bawa, for her years of diligent labor and superior mentoring. She is a generous person of the highest integrity, qualities that I hope have rubbed off on me.

My committee members, Drs. Eric Banister and Tom Calvert, I thank you for your discussions and for your willingness to contribute to an area in which you don't often venture.

I am grateful to Dr. Charles Krieger, chaperone par excellence, for a full year of stimulating experimentation and learning. The time spent in his lab was invaluable as I was exposed to a completely new area of neuroscience. I thank him also for his encouraging words and discussions about the future for young researchers in Canada.

Thank you to those who have spent time with me in K8601; Stephen Riek, Tao Zhong, Gordon Chalmers, Simon Adams, Claudia Edwards, and Christianne Rossi-Durand. You have made research more fun when we did it together and non-research time became an experience when you were simply yourselves.

The staff in the School of Kinesiology have all left pleasent impressions on me and I can't wait to start sending postcards. Thanks to Mel and Rob for their technical expertise and musical taste. Thanks to Laurie, Shona, Fiona and everyone else in the Kinesiology office for their administrative support and friendship.

Finally, to the members of my family and my friends, the fact that I've emerged from the lab with a thesis in hand is really a reflection of your support and encouragement. Thanks especially to Renée and Dylan who stood by me in the craziness of these past few months.

Table of Contents

List of Tables

List of Figures

Chapter 1
INTRODUCTION

The primary function of the motoneuron seems clear - the control of muscle tension through contraction of extrafusal muscle fibers; however, the mechanism(s) by which this function is achieved in natural motor behavior remain to be fully understood. The majority of research on motoneurons has been done in the feline spinal cord (predominately in the lumbosacral area) using the technique of both extracellular and intracellular signal recording in a reduced preparation. Much has been learned from these studies about the intrinsic properties of this cell and its role in the integration of the input from a number of separate segmental and supraspinal sources (for review see Burke and Rudomin, 1977). It is from cat experiments that we have begun to gain an appreciation of the role cell morphology plays in the overall function of the motoneuron. From this literature base on properties of cat motoneurons, several conceptual models and experimental paradigms have been designed to study the physiology of the human spinal motoneuron. The concern of the present thesis was to develop further understanding of the human motoneuron, both behaviorally and biophysically, utilizing the core principles already established in the cat motoneuron.

Anatomical structure of motoneurons

Motoneurons are cells that consist of a cell body (or soma) from which a number of branching processes arise. The cell body of a motoneuron in the cat lumbar cord, which is typically represented as a sphere with a diameter ranging from 45 to 60 μm (Cullheim et al., 1987; Clements and Redman, 1989), occupies the ventral horn in Rexed lamina IX of the mammalian spinal cord. Within lamina IX, motoneurons are organized in a longitudinal fashion and are identified in four columns: the ventromedial column, the central column, the ventrolateral column and the dorsolateral column (Brown, 1981; Schoenen, 1982). The motoneurons innervating the

axial musculature are located in the medial columns and those supplying the limbs are located more laterally. This pattern of motoneuron organization gives rise to the relative prominence of the ventro- and dorso-lateral columns in the cervical and lumbosacral enlargements from which the plexuses for innervation of the limbs arise. A single axon originates from the cell from a protrusion of the soma termed the axon hillock. Prior to myelination, this region of the axon is referred to as the initial segment. Following myelination the axon continues through the ventral root into the periphery with a variable length to its target muscle.

In the cat lumbar cord, each motoneuron gives rise to 8 to 22 primary dendritic trunks which have an average length to termination of approximately 1.2 mm (Barrett and Crill, 1974; Cullheim et al., 1987; Clements and Redman, 1989). Each primary dendrite branches a number of times resulting in an average of 13.5 terminations[1] increasing the complexity of the dendritic tree (Cullheim et al., 1987). The resulting complex branching pattern of the dendrites constitutes > 97% of the total membrane surface area of a motoneuron. The branching of the dendrites in the mammalian spinal cord is arranged in an architectural fashion which is dependent on the location of the cell body. Dendritic branching of motoneurons occurs in a predominately longitudinal fashion (along the rostrocaudal axis) for all columns except the dorsolateral column in which the dendrites are organized in a multipolar fashion (Brown, 1981; Schoenen, 1982). In columns where longitudinal organization is present, the dendrites overlap throughout several segments and it is common for the motoneurons whose cell bodies may be separated by several hundred

---

[1] This average is given for motoneurons of both S and F type motor units. However, it is important to note that there is a significant differences between the total number of terminations for type S and F motoneurons, 127.8 vs. 181.3 respectively (Cullhiem et al., 1987). This is a major factor contributing to the finding that the motoneuron innervating a fast-twitch muscle unit is larger, in terms of total membrane area, than one innervating a slow-twitch muscle unit of the cat triceps surae. The difference in branching pattern of the F- and S-type motoneurons led the above authors to conclude that the S-type motoneurons are not simply a smaller version of the F-type cells, but are instead a distinct though overlapping specific cell type.

microns, to have dendrites which are juxtaposed.[2] The dendrites in columns may be organized into bundles, extending both in the rostrocaudal axis and transversely, in which dendrites from a given column are found in intimate contact with one another. Conversely, motoneurons in the dorsolateral column have dendritic domains which overlap only for cell bodies which are relatively close and are characterized by a lack of significant dendritic bundles. The motoneurons innervating the distal musculature reside in this column.

The particular significance of the anatomy of a motoneuron to its function, lies in the allocation of the functions of the cell to its anatomical divisions. The majority of synaptic input is conveyed and processed by the dendrites. The dendritic input is integrated in the soma and the resulting membrane voltage change is initially transduced by the initial segment into spikes which are conducted down the axon to the neuromuscular junction and back into the soma eliciting a full action potential with its accompanying afterhyperpolarization. Thus it seems appropriate to consider the morphology of the cell as well as its electrical properties when thinking about the function of a specific motoneuron or the group action of several motoneurons.

Intrinsic properties of motoneurons

Within the current conceptual framework, the neuron may be considered an individual computing device and an analogy drawn for it to the area of computing science. An input is directed toward the dendrites which then transmit the input to a CPU-like soma for integration and the output signal conveyed by an axon to the post-synaptic target. Underlying this simple input-output relationship is the unique intrinsic property of each neuron type which endows them with distinct computational behaviors (Llinás, 1988). These latter properties may be grossly defined as

---

[2] Shoenen (1982) suggests that such juxtaposition favors synchronization of such motoneurons. Therefore, in motoneurons innervating proximal musculature or calf muscles there would be a predisposition for synchronization especially for those inputs whose synaptic terminations are oriented parallel to the longitudinal dendritic branches of these cells. This may be to the advantage of motoneurons whose muscle units are involved in gross movements or postural maintenance where fine control of movement is not a requirement.

the active and passive properties of the neuron. In the motoneuron the active properties are represented by the various ionic channels which may be activated by ligand binding or by variations in membrane potential (reviews Schwindt and Crill, 1984; Llinás, 1988; Hille, 1992). It is the active properties that give rise to the excitability of the membrane and the ability to generate action potentials. The passive properties, on the other hand, are those electrotonic characteristics which filter and blend the transmission of current throughout the neuron. The origin of these properties is the structural composition of the neuron, which behaves as if it were a simple electrical circuit composed of resistors, capacitors and batteries.

Passive properties

Passive properties are also called the cable properties of the neuron. Much of the structure of the motoneuron may be represented by cylinders of various lengths and diameters. This is especially true of the dendrites and the axon, whereas the soma is often represented as a sphere. The description of the electrical properties of a cylinder are equivalent to the mathematics of electrical cables and hence much theoretical work has been done to apply the equations to the cylindrical structure of the motoneuron. Much of the work on the cable properties of neurons has focused on the function of the dendrites and much of this pioneered by Wilfrid Rall (reviewed in Segev et al., 1995). In short, the cable properties describe how a current input at some location in the neuron is transmitted to the adjacent regions resulting in changes in potential across the membrane in a time and distance dependent manner.

One may easily imagine that when current is applied to one end of an electrical cable current will flow, by virtue of the movement of charges, both inside the cable and, depending on the type of insulation, across the outer surface of the cable. The same can be said of a cylindrical portion of neuronal membrane. Current injected into one end of the cylinder will flow, by virtue of the movement of ions, along the inside core of the cylinder and across the neuronal membrane to the extracellular space. The distribution of this current both inside and across the cylinder depends on the resistive and capacitive properties of the cytoplasm and membrane. The capacitive

properties are imparted by the charge holding characteristics of the membrane and the resistive properties by the passive ionic channels. For a unit length of cylinder, the resistance posed by material inside the cylinder is termed the axial resistance, r_i (Ω/cm), that posed by the membrane is the membrane resistance, r_m (Ω-cm), and the capacitive property is the membrane capacitance, c_m (F/cm). Thus for a cylinder of length l, the total resistance of the cytoplasm is $r_i l$ (Ω), the total resistance of the membrane is r_m/l (Ω), and the total membrane capacitance is $c_m l$ (F).[3] These components make up the equivalent electrical circuit which describes the properties of a cylindrical portion of neuronal membrane. As mentioned above an injection of current into the cylinder will result in a change in membrane potential (V_m) which varies as a function of time and distance:

$$\frac{1}{r_i}\frac{\partial^2 V_m}{\partial x^2} = c_m \frac{\partial V_m}{\partial t} + \frac{V_m}{r_m},$$

where V_m is membrane potential (mV), x is distance (cm) from the point of current injection (I_{inj}), and t is time (ms). This is the cable equation which has many solutions depending on the length and termination of the cylindrical structure being considered. Multiplying both sides of the equation by r_m gives:

$$\lambda^2 \frac{\partial^2 V_m}{\partial x^2} = \tau_m \frac{\partial V_m}{\partial t} + V_m,$$

where λ is the dimensionless space constant, and τ_m is the membrane time constant (ms). The space constant has important physical meaning in that it describes how the membrane potential under steady state conditions decreases with distance from the point of current injection in an

---

[3] Often values of the passive properties are given in terms of specific membrane resistivity (R_m, Ω-cm^2), specific membrane capacitance (C_m, F/cm^2) and specific intracellular resistivity (R_i, Ω-cm). The reason for this is that these latter values are independent of whether the part of the neuron being considered is represented by a cylinder, sphere or some other geometrical structure. These specific properties are related to the cylinder specific parameters by:

$$R_i = \pi\rho^2 r_i; \qquad R_m = 2\pi\rho r_m; \qquad C_m = c_m / 2\pi\rho$$

where ρ is the radius of the cylinder in cm.

infinite or semi-infinite cable. The distance at which the potential has decayed to 37% ($1/e$) of its maximum value at the point of current injection is $\lambda = \sqrt{\frac{r_m}{r_i}}$. Similarly, the membrane time constant describes an important physical parameter as it describes the time dependent charging properties of the membrane. If a depolarizing step current is applied to the cylinder the membrane potential increases in an exponential manner to a maximum value. The time at which V_m reaches 63% ($1\text{-}e^{-1}$) of its maximum value is the membrane time constant and is equal to $r_m c_m$. When V_m is at its maximum value, V_{ss} or V_{max}, the input resistance is defined as $R_N = Vmax/I_{inj}$.

Implications of passive properties to the function of dendrites

It seems appropriate to pause here and highlight the importance of these passive properties to the unified functioning of the motoneuron. If we assume that the dendrites are entirely passive, i.e. that their electrical behavior is not dependent on voltage, then we may assess the influence the passive properties have on current input at some point on the dendrites and the resulting voltage transient measured at the soma (Rall, 1967). Physiologically such a current input to the dendrites would result from the synaptic transmission of some presynaptic source such as the primary afferent of the muscle spindle. If we consider an excitatory synaptic input with the same conductance time course and peak amplitude applied at various distances from the soma the resulting excitatory post-synaptic potentials (EPSPs) show a gradation in size and shape dependent on its distance from the soma (Rall, 1967). The more distal the input from the soma, the smaller the amplitude and the longer the time to peak and half-width of the resulting EPSP recorded in the soma. While attenuation and filtering of the membrane potential with distance is due in part to the space and time constants, the electrotonic length and the termination of the dendrite also play a significant role (Rall, 1959). Electrotonic length, L, is defined as the length of the cylinder representing the dendrite divided by the space constant. The shorter the L, the lower the attenuation of the voltage signal from the distal dendrites. The significance of this is the effect the passive properties have on the spatio-temporal summation of synaptic inputs. For a motoneuron, where L is generally less than 2 (Fleshman et al., 1988), the soma integrates input

from the entire dendritic domain. The proximally located input produces a larger and faster EPSP which is effective in triggering a threshold crossing while the input located distally will contribute to the background level of depolarization (or hyperpolarization if an inhibitory input). It clearly is the function of the dendrite not only to convey input to the soma but in doing so structure it in a functional manner.

Active properties

The active properties of the motoneuron are characterized by another set of elements, the variable resistors, or conductors, and batteries. Physiologically, these elements represent the ligand- or voltage-activated ionic channels and the reversal potentials of the ions which permeate these channels. It is these elements which are responsible for neuronal excitability, that is, its ability to fire an action potential. Hodgkin and Huxley's initial work on the squid giant axon (Hodgkin and Huxley, 1952) resulted in a method of describing quantitatively the ionic membrane currents that has since been applied to many other excitable membranes. The squid giant axon was a convenient preparation for the initial formulation of a theoretical framework of neuronal excitability not only because of its size, but also because of its simplicity in expressing only two types of voltage-activated ionic conductance, the fast sodium and potassium conductance respectively. The mammalian motoneuron, on the other hand, expresses a wide range of voltage- and ligand-activated ionic conductances which may vary between species, muscles innervated and with the organism's stage of development (Schwindt and Crill, 1984; Llinás, 1988; Viana et al., 1993a, b). To date, in the adult cat spinal motoneuron five ionic conductances in the membrane comprising the initial segment, soma, and proximal dendrites have been described as relevant to repetitive firing behavior: 1) a fast tetrodotoxin (TTX) sensitive transient sodium conductance (Araki and Terzuolo, 1962; Barrett and Crill, 1980; Schwindt and Crill, 1982); 2) a fast tetraethylammonium (TEA) sensitive potassium conductance (Barrett et al., 1980; Schwindt and Crill, 1981; Zhang and Krnjevic, 1988); 3) a slow potassium conductance which is most likely calcium-dependent (Krnjevic et al., 1978; Schwindt and Crill, 1981; Zhang and Krnjevic, 1987);

4) a high voltage-activated (HVA) calcium conductance (Schwindt and Crill, 1980b); and 5) a low voltage-activated (LVA) calcium conductance (Schwindt and Crill, 1980a; Schwindt and Crill 1982).[4]

As in the squid giant axon, the sodium conductance results in an inward current with fast kinetics and is activated at different voltage depolarizations in the initial segment and soma (Barrett and Crill, 1980). In the initial segment the sodium channel is activated at depolarizing steps of 10-20 mV whereas the somatic sodium channels are activated by voltage steps of 25-40 mV positive to rest. The reversal potential for this inward current ranges between 100-120 mV positive to rest. It is the inward sodium current that generates the depolarizing spike of the action potential in the motoneuron. Another feature of this sodium channel is that it inactivates with time constants of 0.2 to 2 ms dependent on membrane voltage. This inactivation is required for the generation of repetitive firing in the motoneuron for without inactivation of sodium channels the membrane would remain in a depolarized state (Schwindt and Crill, 1984). The lower voltage threshold for sodium current in the initial segment confirms the suggestion that it is the initial segment which is responsible for establishing the threshold for firing of the motoneuron (Coombs et al., 1957; Calvin and Schwindt, 1972). The inward current produced during the initial segment spike is conducted to the soma-dendritic membrane producing sufficient depolarization to activate sodium channels resulting in the soma-dendritic spike. The resulting spike of the motoneuron action potential may have a peak of 60-100 mV above rest depending on the input resistance of the cell and the density of sodium channels.

The inward current generated by opening of the sodium channels is quickly followed by an outward current, which in the cat motoneuron is generated by slow and fast potassium conductances with reversal potentials in the range of -6 to -21 mV relative to resting potential

[4] It seems misleading to introduce these as 5 conductances as there is a multiple number of high and low voltage activated calcium conductances and different calcium-dependent potassium channels identified in other motoneuron preparations in addition to other neurons of the CNS. However, since these are not well described for adult cat spinal motoneurons I will not consider them here.

(Barrett et al., 1980). The fast potassium conductance is similar to the voltage-dependent delayed rectifier conductance described in the squid axon and is responsible for assisting in the rapid repolarization of membrane potential following the spike. Activation of this conductance occurs at a depolarization near +30 mV with a time constant for activation of 4 - 5 ms. At a more depolarized level the time constant falls to a value near 1 ms. An important feature of the fast potassium conductance is that it does not inactivate during depolarization, thus at all potentials greater than its activation threshold the conductance is persistent. This conductance may be blocked by TEA resulting in an increased duration of the action potential (Schwindt and Crill, 1981). The significance of this conductance for repetitive firing is its role in regulating action potential duration. An increase in action potential duration following a block of the fast potassium conductance results in an enhanced afterhyperpolarization which would tend to lower the repetitive firing rate to a given current injection (Schwindt and Crill, 1981).

The slow potassium conductance on the other hand has much slower kinetics with a time constant in the range of 20 - 50 ms near its activation threshold. The slow potassium conductance is activated by a less positive depolarization than the fast potassium conductance, nearer to 10 mV positive to resting potential, and is insensitive to extracellular iontophoresis of TEA. In many neurons from other species, a potassium conductance with the kinetics and a functional role similar to the slow potassium conductance in the cat motoneuron, has been shown to be activated by intracellular calcium concentration (Barrett and Barrett, 1976; Viana et al., 1993b). There are good reasons to believe that the slow potassium conductance in the cat motoneuron is also mediated by the cellular calcium concentration (Krnjevic et al., 1978; Barrett et al., 1980; Zhang and Krnjevic, 1987), however the calcium-dependence remains to be fully characterized. Regardless of whether it is a calcium-dependent conductance, the functional role of the slow potassium conductance seems clearly to be the generation of the afterhyperpolarization (AHP) of the action potential and through this mechanism to modulate repetitive discharge of the motoneuron in the primary firing range (Kernell, 1965b; Baldissera and Gustafsson, 1971;

Schwindt and Calvin, 1973; Traub, 1977; Traub and Llinás, 1977; Barrett et al., 1980; Powers, 1993).[5]

The presence of HVA and LVA calcium conductances support the hypothesis that the slow potassium conductance could be mediated by calcium. However, their mere presence does not unequivocally link them to regulation of calcium-dependent potassium conductances. A calcium channel would need to be co-localized with the slow potassium channels in the plasma membrane to be effective in modulating their conductance and data describing the distribution of ionic channels in the adult cat spinal motoneuron is not available. In a slice preparation of neonatal rat hypoglossal motoneurons, it has been demonstrated that an HVA calcium conductance is the one that gives rise to the calcium influx responsible for activation of the potassium current underlying the AHP (Viana et al., 1993a). Recently, three types of calcium channels, N-, P-, and L-type, have been identified as contributing to the HVA whole-cell calcium currents seen in the neonatal rat hypoglossal motoneurons (Umemiya and Berger, 1994, 1995).[6] It appears as though these channels have a differential distribution for the dendritic and somatic membrane, which has yet to be fully described. Of particular interest is the N-type channel which is least predominant in the somatic patches (Umemiya and Berger, 1995) and is apparently the main channel for supplying the calcium influx needed to activate the calcium-dependent potassium conductance underlying the AHP (Umemiya and Berger, 1994). These results suggest that the N-type channel may be preferentially located in the dendritic membrane and, therefore, the associated AHP generating potassium conductances would also be located in the dendrites. This would support the modeling study on spinal motoneurons in which a calcium-dependent potassium conductance underlying the

---

[5] A notable exception to the relationship between the AHP and repetitive discharge has been shown during fictive locomotion in decerebrate cats (Brownstone et al., 1992). In this case the AHP is still present during the repetitive firing behavior, however, it seems to bear little relation to the interspike interval. The slow potassium conductance mediating the AHP is likely under the influence of neuromodulatory factors during locomotor-like activity as the AHP is clearly depressed (Schmidt, 1994).

[6] The finding of multiple channels contributing to a single whole-cell recorded current should alert us to the possibility of a similar finding for the other conductances described. There are multiple types of voltage- and calcium-dependent K^+ channels which may contribute to what has been labelled as fast and slow potassium conductance in this thesis.

AHP had to be preferentially located in the dendritic compartments for adequate simulation of normal motoneuron firing behavior (Traub and Llinás, 1977).

The LVA calcium conductance described in adult cat spinal motoneurons is a persistent conductance which is activated weakly in the voltage range traversed during slow repetitive firing but is tonically active during fast firing rates (Schwindt and Crill, 1980a, 1982). It appears that this conductance plays a role in regulating the transform of current input to firing rate by adjusting the slope of the f-I curve (Schwindt and Crill, 1982, Powers, 1993) and increasing the maximum firing rate (f) of the cell (Schwindt and Crill, 1982). In the neonatal rat hypoglossal motoneuron, a T-type LVA calcium channel has been identified (Umemiya and Berger, 1995). In this neuron the transient calcium conductance is thought to contribute to the afterdepolarization following the repolarizing phase of the action potential but contributes little to the calcium influx needed for generation of the AHP. The afterdepolarization in young animals (< 4 days old) may be large enough to lead to burst firing but this tendency becomes absent in older animals (> 10 days). The possibility of the presence of a transient LVA calcium conductance in adult cat spinal motoneurons is an attractive hypothesis since these cells display delayed depolarizations similar to the afterdepolarizations observed in the rat hypoglossal motoneurons (Calvin, 1974). In adult cat spinal motoneurons the delayed depolarization has been implicated in the firing of doublet spikes at low levels of current injection. The similarity between burst firing associated with afterdepolarizations in the neonatal rat hypoglossal motoneurons and the doublet firing associated with delayed depolarizations in adult cat spinal motoneurons although interesting, is currently without experimental evidence supporting a LVA transient calcium current in the cat.

The combination of the passive properties of the motoneuron and the active conductances give rise to its ability to receive input from various sources, integrate that input and produce a functional output. The dendrites are important not only for their role in collecting input from various sources but also for their function in filtering and differential attenuation of an input. The majority of the active conductances are currently presumed to be located on or near the soma and are responsible for transducing the input signals into patterns of spike outputs. The axon of the

motoneuron faithfully conducts the output signals to its target muscle producing a contraction and, in many cases, movement.

The importance of the intrinsic properties for the studies presented in this thesis are the role they play in the recruitment and excitability of the human motoneuron. The input resistance of a motoneuron, by virtue of Ohm's law, plays a significant role in the transduction of an input current into membrane voltage. For two cells with different input resistance, one large and one small, the injection of the same amount of current into both cells results in a larger change in membrane voltage in the cell with the larger input resistance. This change in membrane potential is the mechanism by which the active properties are engaged and, therefore, the cell with the higher input resistance is more likely to be recruited. The input resistance of a motoneuron is inversely correlated to its surface area, so the smaller the cell the larger the input resistance and, therefore, the more likely it is to be recruited. Once recruited the motoneuron may continue to fire repetitively. Following each spike in the repetitively firing neuron is a period of depressed excitability, the absolute and relative refractory periods. During the absolute refractory period the sodium channels, which have just previously opened to produce the spike, are inactivated and are not available for reactivation. This effectively prevents two spikes from occurring within a short period of time, e.g. 2 ms. Following the absolute refractory period is a relative refractory period when the membrane excitability is depressed but, given a large enough stimulus, may fire another action potential. During this period the membrane potential is hyperpolarized due to the activation of potassium conductances. The assessment of recruitment and post-spike membrane excitability of the human motoneuron are the topics addressed in this thesis.

Recruitment

In considering the intrinsic properties of motoneurons the notion of threshold for excitation has been briefly mentioned. The process by which an inactive motoneuron is brought to threshold and caused to fire one or more action potentials is known as recruitment. Recruitment

is more than the mere excitation of a motoneuron. Its true significance in the regulation of motor output, lies in its relative order of recruitment, expressed as rank order, within a larger group of motoneurons. In studies of recruitment the group of motoneurons generally considered is that innervating an entire muscle and this is called the motoneuron "pool" for that muscle. Each motoneuron of a pool projecting to a limb muscle may innervate between 100 and 1000 muscle fibers. The motoneuron together with all the muscle fibers which it innervates represents a single functional unit called the motor unit (Sherrington, 1906). The nervous system uses recruitment of motor units as a means of varying the force exerted by a skeletal muscle. In doing so, the relative activation of the motor units for a given muscle follow an orderly sequence, ranging from those that produce small forces and are fatigue resistant to those that produce large forces but are easily fatigued (Henneman and Mendell, 1981; Calancie and Bawa, 1990). This has come to be known as the size principle of motoneuron (or motor unit) recruitment and its formulation in large part is due to the work of Elwood Henneman and coworkers in the cat (Henneman, 1957, 1985; Henneman et al., 1965,1974; Bawa et al., 1984). The size principle of motor unit recruitment was later extended to humans for a variety of inputs including both voluntary and artificially produced peripheral and descending inputs to the motoneuron pool (Milner-Brown et al., 1973b; Henneman et al., 1976; Desmedt and Godaux, 1977, 1979, 1981; Bawa, 1981, 1982; Calancie and Bawa 1985a, b; Riek and Bawa, 1992; Bawa and Lemon, 1993).

The size principle

The initial studies by Henneman and coworkers were done in the decerebrate cat. The size of a motoneuron was implied by the amplitude of the extracellularly recorded spike from a ventral root filament. The basis for this size implication is the positive correlation between the amplitude of the recorded impulse and the diameter of the axon conducting it, the diameter being proportional to motoneuron surface area. The authors found that as the excitatory input to the motoneuron pool was increased, there was a clear tendency for smaller motoneurons to be recruited prior to larger ones. This was true for both peripheral and a variety of descending

inputs. As a result of these studies Henneman proposed that the excitability of a motoneuron was inversely proportional to its cell size and therefore recruitment of motoneurons occurs from small to large cells, i.e. the "size-principle" (Henneman, 1985).

The recruitment of motoneurons in an orderly sequence tells us little about the functional effect of recruitment on force production in the periphery. The answer to this lies in the relationship between motoneuron size and the heterogeneity of the muscle fibers in a typical limb muscle. The muscle fibers comprising a given motor unit have similar histochemical and morphological characteristics which result in physiological differences between motor units (Burke, 1967, 1981; Burke et al., 1971; Kugelberg, 1981). Three types of motor units are widely recognized: slow (S); fast fatigue resistant (FR); and fast fatiguable (FF)[7] and these may be identified using quantitative measures of their physiological differences (Burke et al., 1977). Identification of motor unit types and later reconstruction and measurements of motoneuron size (Cullheim et al., 1987) demonstrated a tendency for the S type motor units to consist of a smaller motoneuron in terms of total membrane surface area than FF type motor units. Therefore, in functional terms, the S type motor units are recruited prior to the FR, which is recruited prior to the FF type motor units. Such a recruitment scheme provides for a smooth increment in force production while maximizing the fatigue resistance of the muscle.

Orderly recruitment of human motoneurons was first demonstrated by Stein and coworkers (Milner-Brown et al., 1973b) in the first dorsal interosseus (1DI) muscle. These authors used the spike-triggered average twitch tension as an indicator of motor unit size. The twitch amplitude of a motor unit was expressed in relation to the level of force at which the unit was recruited. It was shown that as the level of voluntary isometric force was increased, motor units with larger twitch tensions were recruited indicating recruitment of 1DI motor units according to the size of the twitch tension. Later studies confirmed orderly recruitment of human

[7] A fourth type of motor unit is sometimes identified this being the F(int) type motor unit whose characteristics make it neither an FF nor an FR type unit but something in between (Burke, 1981).

motor units in this and other muscles using different contraction paradigms and reflex recruitment (Desmedt and Godaux, 1977, 1979; Calancie and Bawa, 1985a, b, 1990).

Exceptions and the role of task groups

In natural motor behaviors, animals are capable of carrying out a wide repertoire of tasks that include ballistic, eccentric as well as concentric and isometric contractions. A question that may be asked in light of the limited set of motor behaviors where the size principle has been demonstrated, whether the central nervous system is hard wired to perform all tasks under the same recruitment scheme, or are there exceptions to the size principle? Since the size principle states that motoneurons are recruited in sequence from small to large, an exception would entail motoneurons be recruited in a sequence from large to small. A number of authors have presented data which suggests that in some cases recruitment does not occur according to the size principle.

Perhaps the most influential evidence for systematic exceptions to the size principle has come from studies utilizing cutaneous input to the motoneuron (Burke et al., 1970; Kanda et al., 1977; Stephens et al., 1978; Garnett and Stephens, 1980, 1981). In decerebrate cats it was shown that cutaneous input from the sural nerve superimposed on stretch reflexes or tendon vibration reflexes tended to decrease the firing rate of relatively low threshold medial gastrocnemius motoneurons while at the same time higher threshold motoneurons were receiving powerful excitation (Kanda et al., 1977). This was interpreted as giving evidence for an input system which deviated from the Ia synaptic system that had been the basis for the size principle. In the experimental input system, a large motoneuron was proposed to receive, preferentially, a greater amount of excitatory input over a smaller counterpart which received a proportionally larger amount of inhibition. Activation of this input system would tend to recruit the larger motoneuron prior to the smaller motoneuron. Such a recruitment scheme could be considered a true exception to the size principle. However, the study did not give evidence for a reversed recruitment scheme but for selective inhibition of low threshold motoneurons which were tonically firing, i.e., a selective deactivation of the small motoneurons (Cope and Clark, 1995).

A confirmation of these findings has been attempted under similar conditions by Clark et al. (1993) in the decerebrate cat. These authors found that in a small percentage of medial gastrocnemius motor units, units with slow axonal conduction velocity exhibited slowing of their firing rates during cutaneous input produced by skin pinch. However, when pairs of motor units were recruited purely by tendon vibration, or skin pinch or electrical stimulation of the sural nerve, recruitment order was always the same and 90% of the time the lower threshold unit had the slower conduction velocity. Thus the size principle recruitment scheme was utilized during both peripheral Ia and cutaneous input to the medial gastrocnemius motoneuron pool.

In humans, cutaneous stimulation has also been used to demonstrate the possibility of alternative recruitment strategies to the size principle (Stephens et al., 1978; Garnett and Stephens, 1980, 1981). In this case electrical stimulation of the digital nerves of the index finger subsequent to recruitment of a pair of first dorsal interosseous (1DI) motor units by isometric abduction of the index finger resulted in selectively silencing the lower threshold motor unit (Stephens et al., 1978). This effect was hypothesized to be due to the differential synaptic effects of the cutaneous stimulation on low and high threshold 1DI motor units, where slow twitch motor units (i.e. small, low threshold motor units) show a predominately inhibitory response and fast twitch units showed a predominately excitatory response (Burke et al., 1970; Garnett and Stephens, 1980). It was clearly demonstrated in later studies that electrical stimulation of the digital nerves of the index finger did have an effect on the recruitment threshold of 1DI motor units (Garnett and Stephens, 1981). In this study motor units with relatively high recruitment thresholds prior to cutaneous stimulation exhibited a reduction in recruitment threshold while low threshold units exhibited increased recruitment threshold during the cutaneous stimulation. These authors suggest that although the order of motor unit recruitment during voluntary activation remains relatively stereotyped, i.e. the size principle of motor unit recruitment is followed, perhaps cutaneous input during grasp could serve to alter the recruitment pattern making the fast twitch motor units preferentially excitable (Garnett and Stephens, 1981).

Other studies on human motor unit recruitment have described deviations from size ordered recruitment during different voluntary tasks (Thomas et al., 1978; Desmedt and Godaux, 1981; ter Harr Romeny et al., 1982, 1984; Nardone et al., 1989; Gielen and Denier van der Gon, 1990). In one study recruitment of 1DI motor units was examined when the muscle was functioning as a prime mover, during isometric abduction of the index finger, and compared with the recruitment when the muscle was functioning as a synergist, during isometric flexion of the index finger (Desmedt and Godaux, 1981). This study showed that, overall, recruitment of pairs of motor units proceeded according to the size principle but some pairs showed reversals in recruitment order between the two tasks. The authors reported that when the 1DI muscle was acting as a synergist, the motor unit pairs showed a reversal of recruitment order in 8% of the sample. This percentage of reversals is not unlike that reported by Henneman et al. (1965) and more likely reflects the fuzzy nature of size ordered recruitment resulting from random error rather than a systematic deviation from size ordered recruitment (Clark and Cope, 1995).

However, other examples of an alternative recruitment strategy during voluntary activation of multifunctional muscles are not so easily dismissed. In the human biceps brachii muscle it has been clearly demonstrated that the recruitment threshold of a motor unit depends on the task being performed (ter Haar Romeny et al., 1982). Motor unit recruitment was examined during three tasks: 1) isometric flexion of the elbow joint; 2) isometric supination of the forearm; and 3) isometric exorotation of the humerus. These authors found that some motor units were preferentially recruited for one task and that other motor units were preferentially recruited for other tasks. It was this preferential recruitment during various tasks that prompted the authors to interpret the work as a possible exception to the size principle (Gielen and Denier van der Gon, 1990). Similar task-dependent recruitment results have been obtained in human extensor digitorum communis (EDC) and abductor pollicis brevis (APB) muscles (Thomas et al. 1978). A methodological criterion when examining pairs of motor units in this latter study was that the two units be recruited at similar levels of effort. This clearly is a concern as random error in the recruitment process is more likely to result in random recruitment reversals between units with

small differences in thresholds. The authors report that recruitment between pairs of APB motor units could be alternated by contractions of distinctly divergent direction and that alternation of recruitment of pairs of EDC motor units was easily achieved as units seemed to be preferentially associated with extension of different digits. The alternation in recruitment of motor unit pairs was interpreted as evidence for a departure from the classically stated size principle of motor unit recruitment.

Another interesting case of departure from size principle recruitment has been presented by Nardone et al. (1989). In this case motor units in the human triceps surae muscles were investigated during the tasks of concentric and eccentric contractions about the ankle joint. These authors found that some units were active only during the concentric contraction, others only during the eccentric contraction and still others which were recruited during the concentric contraction and gradually derecruited during the eccentric contraction. The units recruited exclusively during the eccentric contractions were judged to be fast-twitch units and typically displayed a higher level of recruitment threshold. These results were interpreted as supporting the preferential recruitment of large, fast-twitch motor units during the task of eccentric contraction.

Clearly the results from the human studies on biceps brachii, EDC, APB and triceps surae deviate from the idea that the motoneurons of a pool are recruited in a stereotyped rank order (Henneman et al., 1974) but do they constitute an exception to the size principle? In order to clearly answer this, the question of the "pool" of motoneurons in which recruitment can be compared must be readdressed (Burke, 1985). Should the definition of the "pool" be based on an anatomical basis, as the classically defined motoneuron pool, or on a physiological basis, such as the notion of task groups proposed by Loeb (1985)? A clear illustration of the need for considering the idea of task groups has been given by Cope and Clark (1995). When investigating the recruitment of two motor units, MU1 and MU2, MU2 is defined as the larger unit based on one of any number of good predictors of recruitment order such as conduction velocity or tension (Cope and Clark, 1991). If MU2 is recruited prior to or in the absence of recruitment of MU1 does this constitute an exception to the size principle? The answer of course

is more complex than it first appears. If the two motor units are recorded from different muscles during entirely different tasks, the question is likely to be answered as no, this does not constitute an exception to the size principle because the two motor units are located in separate muscles active during different tasks. If, however, the motor units have been recorded from the same muscle the answer is less obvious. The concept of task groups may help at this point.

The concept of task groups was developed in part to account for the differential recruitment of motoneurons innervating the anterior portion of the sartorius muscle in the cat during locomotion (Hoffer et al., 1987). The sartorius muscle displayed two bursts of EMG activity during the step cycle of walking, one during the swing phase when the muscle was shortening and the other during the stance phase when the muscle was lengthened. Motoneurons projecting to anterior sartorius were recruited during only one of the phases, that is, during only one of the tasks. In this case the motoneuron pool innervating this anatomically distinct muscle was suggested to be divided into functionally separate motoneuron groups, each of which was independently recruited to perform a particular task. The authors then suggested that such a finding should serve as an impetus for the modification of existing theory of orderly recruitment of motoneurons comprising an anatomically defined motoneuron pool.

Thus the anomalous recruitment reported for human motor units in biceps brachii, EDC, APB and triceps surae (Thomas et al., 1978; Desmedt and Godaux, 1981; ter Harr Romeny et al., 1982, 1984; Nardone et al., 1989; Gielen and Denier van der Gon, 1990), may be examples of task groups in multifunctional human muscles. A full examination of the recruitment of human motor units within task groups has been done for EDC (Riek and Bawa, 1992). The important discussion emerging from these authors' work was that the presence of task groups does not imply an exception to the size principle. These authors defined a task group as all the motor units activated, or that could possibly be activated, during the performance of a particular task. It was shown that the EDC muscle has independent intramuscular task groups for middle finger and ring finger extension. Recruitment of motor units within a task group was examined by plotting the spike triggered averaged twitch tension for a single motor unit against its recruitment threshold.

The results showed that the size principle recruitment scheme was utilized within both the middle and ring finger task groups. Another important point arising from these authors work was the fact that the separation of motor units into task groups was not related to motor unit type in EDC, rather each task group was comprised of motor units whose properties spanned the boundaries of any one particular motor unit type.

The size principle, or orderly recruitment, persists as an explanation of the sequence in which motoneurons are recruited (Cope and Clark, 1995). It holds for reflex and supraspinal input to a motoneuron pool in the cat as well as for voluntary and reflex input to a motoneuron pool or task group in humans. While recruitment order can usually be predicted by some measure of size, it is clear that the threshold for recruitment may be modulated by cutaneous input. However, under natural cutaneous input the effect is not production of a reversal in the recruitment order, but a change in the recruitment gain (Kanda and Desmedt, 1983). That is, high threshold units exhibit reduced recruitment thresholds so that a greater proportion of the motor units in a muscle are recruited at a given level of tension production. The functional consequence of this orderly sequence of recruitment is a smooth gradation of force at all levels of effort, minimization of fatigue and a reduced need of cumbersome neuronal circuitry.

Objectives of recruitment studies

Two questions have been addressed in this thesis with regard to the recruitment of motoneurons in humans. Firstly, Denny-Brown (1949) reported that the motoneuron pool of the human flexor carpi ulnaris (FCU) muscle was fractionated into subpopulations, each subpopulation being activated during a different voluntary motor task: wrist flexion; wrist ulnar deviation; and grasping. The question considered in the present report (Chapter 2; Jones et al., 1993) is whether these separate subpopulations exist. Secondly, a question which plagues the recruitment literature is recruitment order during normal behavior versus that seen in the restrictive setting of the laboratory. Most recruitment experiments in human subjects have used tasks which are considered anatomical, that is, the tasks are defined in anatomical terms, for example

flexion/extension or abduction/adduction. The question asked in this thesis is whether there is a difference between recruitment during restrictive "anatomical" tasks compared with more natural "behavioral" tasks (Chapter 3; Jones et al., 1994).

Excitability of human motoneurons

Motoneuronal excitability, as used in this thesis, implies the probability of response of a repetitively firing motoneuron to a transient excitatory input. The response probability depends both on the intrinsic properties of the cell and on the nature and strength of synaptic inputs to the cell. Neither of these factors is readily accessible in human studies and for this reason results from animal studies, especially on cat motoneurons, are cautiously extrapolated to the human spinal cord. For example, this extrapolation has been carried out to study neuronal circuitry in man. The spinal neuronal circuits involving peripheral afferents from muscle spindles, golgi tendon organs and cutaneous receptors, or segmental input from propriospinal neurons, or supraspinal inputs from the cortex that were initially described in the cat or monkey. These data formed the conceptual model for elucidating the presence of these circuits in man. Similarly, the intrinsic properties of motoneurons gathered from animal studies have served as the starting data for describing the biophysical characteristics of human motoneurons.

The intrinsic properties of a motoneuron are determined by the underlying passive and active properties of the cell. For example, the amplitude of current step increment needed to evoke a single action potential in a motoneuron, called rheobase, is an intrinsic property of the motoneuron. It is a result of the unified functioning of the passive properties (e.g. input resistance) with the active properties responsible for generating the action potential. Similarly, the relationship between the firing rate of a motoneuron and the amount of depolarizing step current injected in the soma, the *f*/I curve, may be considered as an intrinsic property of the motoneuron. Certainly, presynaptic inputs are responsible for generating the depolarizing current and even

perhaps altering the slope of the *f*/I curve (Binder et al., 1993), however, the final spike train output is a property organized by the passive and active properties of the motoneuron.

Repetitive firing

During repetitive firing of a motoneuron the intrinsic properties give rise to a soma-dendritic spike followed by an afterhyperpolarization (AHP; Calvin and Schwindt, 1972). The voltage trajectory of the AHP between two spikes is a particularly interesting intrinsic property of the cell as it is believed to have a significant role in the regulation of repetitive firing (Baldissera and Gustafsson; 1971, 1974) and the response of a motoneuron to transient inputs (Fetz and Gustafsson, 1983). In cat motoneurons the voltage trajectory of the AHP between spikes has been qualitatively described by an initial scoop portion, where the membrane potential reaches a minimum value, followed by a ramp-like rise in membrane potential toward threshold (Schwindt and Calvin, 1972). The scoop and ramp of the AHP change systematically with increasing firing rate in the motoneuron. Within the primary firing range (for our purposes we will define this range as having a maximum value of 40 imp/s) an increase in firing rate is accompanied by a decrease in the scoop depth of the AHP while the slope of the ramp remains relatively unchanged (Schwindt and Calvin, 1972).

Human motoneuron trajectories

The AHP trajectories in repetitively firing human motoneurons cannot be measured *in vivo* and therefore in seeking to understand the intrinsic properties of human motoneurons it seems appropriate to start with the assumption that they are similar to those recorded in the cat. This was the approach taken by Ashby and Zilm (1982a, b) in their formulation of a model of "effective"

AHP trajectories[8] in human motoneurons. The original model was formulated in such a way that immediately following a spike, the trajectory was set to a scoop depth proportional to the interspike interval (ISI) and the trajectory then rose to threshold at a constant rate (Ashby and Zilm, 1982a). By modeling the effective trajectory this way the authors attempted to match the behavior of cat motoneuron AHP trajectories with increases in firing rate. Thus, an increased firing rate was modeled by a trajectory whose scoop depth became shallower while the ramp remained constant.[9] The authors used this model to explore the relationship between a composite Ia EPSP and the peri-stimulus time histogram (PSTH) constructed between the stimuli and the spikes of the motoneuron model. The magnitude of the resulting short latency excitatory peak in the PSTH was considered as a measure of motoneuron excitability.

From their computer simulations, Ashby and Zilm (1982a) found that the magnitude of the peak in the PSTH varied as a function of the mean background firing rate of the model, the faster the firing rate the greater the peak of the PSTH (expressed in terms of counts per 100 stimuli). This result was predictable from the nature of the change in the effective trajectory of the model with an increase in firing rate. At a faster firing rate the trajectory was shallower and, therefore, an EPSP of a constant amplitude would be within reach of threshold for a greater proportion of the ISI than at a slower rate. Therefore, at the faster firing rate the model predicted that the motoneuron would be more excitable. However, their subsequent experimental observations on human tibialis anterior motoneurons did not support the model. This led them to reassess the model and propose a new model describing the behavior of trajectories in human motoneurons

---

[8] The authors did not claim to model the specific membrane voltage trajectory between spikes, rather, their trajectories represent the effective distance of an EPSP from threshold at any time during the interspike interval (ISI). In this way the specific contributions of factors such as the membrane voltage trajectory, threshold changes during the ISI, variations in membrane conductance and changes in EPSP amplitude with membrane potential are lumped into a single process.

[9] Although the authors suggest that their trajectories are not equivalent to membrane voltage trajectories but instead represent an effective trajectory, they modeled the firing rate-dependent change in the trajectory exclusively on the membrane voltage trajectory in cat motoneurons. In doing so they implicitly suggest that the effective trajectory behaves the same as the membrane voltage and therefore the other factors, such as membrane conductance and threshold, play little or no role in a change in the effective trajectory with firing rate.

(hereafter referred to as the A-Z model; Ashby and Zilm, 1982b). The A-Z model of human motoneuron trajectories was characterized by a scoop of constant depth and a ramp whose slope varied proportionally with the firing rate. The faster the firing rate, the steeper the slope of the ramp. The impetus for the proposal of this model of human motoneuron trajectories was the finding that, contrary to the above prediction, an increase in the discharge rate of a human motoneuron resulted in either a decrease or no change in the peak of the PSTH. The prediction of the A-Z model is that an EPSP of a constant amplitude would be within reach of threshold for a constant proportion of the ISI regardless of firing rate and, therefore, motoneuron excitability in response to an EPSP would be independent of firing rate.

Since its inception, the A-Z model has gained considerable support in the literature and is currently the basis for the interpretation of many human studies. The assumptions of the A-Z model have served as a foundation for proposing negative feedback loops from the motoneuron to the corticospinal neurons which project to it (Brouwer et al., 1989), for proposing methods of estimating the post-synaptic potential in human motoneurons and the effect of synaptic noise on such estimations (Midroni and Ashby, 1989; Miles et al., 1989; Poliakov et al., 1994; Turker and Cheng, 1994), and for proposing methods for estimating the strength of common input to human motoneurons (Nordstrom et al., 1992). It is also apparent that the use of the A-Z model in the literature has drifted from the cautious "effective" trajectory as it was first proposed, to being considered a model of the membrane potential trajectory underlying repetitive firing in the human motoneuron.

The excitability of repetitively firing human motoneurons is an important property to understand if a coherent theory of motor control is to be formulated. Also, if the intrinsic membrane properties giving rise to membrane excitability are understood, then a deviation from the normal pattern of excitability in any neurogenic disorder may identify the intrinsic properties affected.

Objective of the excitability studies

The objective was to determine some of the details of the biophysics governing repetitive firing behavior in human motoneurons. In order to achieve this objective four studies have been done.

The goal of the first study (Chapter 4) was to determine whether background firing rate had an affect on the probability of response of a motoneuron to a transient input from peripheral Ia afferents. Changes in the response probability at different firing rates were predicted for human motoneurons because cat motoneurons demonstrate characteristic changes in AHPs with changes in motoneuronal firing rate that could lead to changes in motoneuronal excitability (Schwindt and Calvin, 1972). Previous human motoneuron data, however, suggests that response probability is independent of firing rate (Asbhy and Zilm, 1982b; Miles et al., 1989).

The goal of the second study (Chapter 5) was to examine the response probability of a motoneuron at sequential times following a spike to characterize the nature of the refractory period. This was done in motoneurons innervating a relatively slow muscle, soleus, and a relatively fast muscle, flexor carpii radialis (FCR). In the fast muscle responses were collected during two modes of firing: 1) rhythmic single spike firing; and 2) doublet firing. Differences in the nature of the refractory period were expected because cat motoneurons show characteristic differences in AHPs between fast and slow motoneurons and following doublets (Kernell, 1965b; Calvin, 1974).

The goal of the third study (Chapter 6) was to examine the response of human motoneurons to two different input systems: 1) peripheral Ia input; and 2) descending corticomotoneuronal input. Previously reported responses of human motoneurons to descending input (Olivier et al., 1995) were qualitatively similar to the results obtained using peripheral Ia input (Chapters 4 and 5), suggesting that the two input systems are similar. To verify this similarity, it was important to compare both peripheral and descending input under the same experimental conditions. If motoneuronal responses to two different input systems are similar,

this suggests that the responses are due to the postsynaptic properties of the motoneuron rather than to a particular input system.

The goal of the fourth study (Chapter 7) was to understand the biophysical basis for the observed human motoneuron responses (Chapters 4 and 5). Direct measurement of the biophysical properties of human motoneurons, however, is not possible. To estimate the human motoneuron membrane properties, a motoneuron was modeled from the known biophysical properties of adult cat spinal motoneurons. If a transient input to the modeled cat motoneuron gave a similar response to that observed in the human studies, this would suggest a similarity in membrane properties of cat and human motoneurons and enable further understanding of the human motoneuron in both health and disease.

Chapter 2

RECRUITMENT OF MOTOR UNITS IN HUMAN FLEXOR CARPI ULNARIS

Introduction

Denny-Brown (1949) reported observing recruitment of separate subpopulations of the human flexor carpi ulnaris (FCU) muscle for different motor tasks. The tasks tested were flexion and ulnar deviation of the wrist, and grasping. It is true that most of the mammalian limb muscles are activated during multiple tasks or contractions, leading to movement throughout a wide range of directions. This, however, does not necessarily imply that the motoneuron pool of each of these multi-functional muscles is fractionated into subpopulations, making a subpopulation responsible for each particular task. Fractionation has been reported for some muscles (Loeb, 1985; Riek and Bawa, 1992), but it does not seem to hold true for two of the four main extensor and flexor muscles of the human wrist, namely, flexor carpi radialis (FCR) and extensor carpi radialis (ECR; Riek and Bawa, 1992). Based on Denny-Brown's (1949) observations, the question arises, is the spinal cord organization of human ulnaris muscles quite different from the synergistic radialis muscles?[1]

Methods

To answer this question the following experiments were carried out on five healthy human subjects (2 male, 3 female, aged 23 - 48 years). These experiments were approved by the Ethics Committee at Simon Fraser University.

---

[1] This chapter has been published in Brain Research, Jones et al., 1993. Data collection and analysis was done at Simon Fraser University under the supervision of Dr. Bawa. Dr. McMillan had joined the lab to learn single motor unit recording from limb muscles and observe analysis.

Details of surface EMG and SMU recording

Surface electromyographic (EMG) activity was recorded with pairs of Ag-AgCl disc electrodes from FCU and wrist extensors. The surface EMG activity was preamplified (Grass P15, 30 Hz - 3kHz, gain = x100) and the output of the preamplifier was directed to an AC conditioning amplifier (10 Hz high pass filtered). Single motor unit (SMU) action potentials were recorded with bipolar needle electrodes. The electrodes consist of two enamel (HML) coated 37 or 50 μm diameter stainless steel wires which were fixed with epoxy inside a 25 gauge needle. The wires and epoxy were ground down flush with the needle point leaving the two small non-insulated tips of the wires exposed. The two tips were separated by two or three diameters which allowed recording from a very small number of surrounding muscle fibers. The SMU electrodes were connected to a preamplifier (Grass P15, 100 Hz - 10 kHz bandpass filtered, gain = x100) whose output was fed to an AC conditioning amplifier (10 Hz high pass filtered). The output from the amplifier was recorded on tape (Vetter PCM Recorder) together with the surface EMG activity. SMU activity was displayed on an oscilloscope and fed to an audio monitor for visual and auditory feedback to subjects.

Force recording during the four tasks

Subjects were seated with their right forearms supported by a padded horizontal platform, as shown in Figure 2-1. The forearm was fixed with the palm oriented vertically by clamping the wrist between two vertical plates. During the task of isometric flexion the subjects were asked to exert a flexion torque against a vertical handle positioned along the metacarpophalangeal joints of the palmar surface of the hand. The handle was fixed in a position such that the subjects wrist was at an angle of approximately 10 degrees of flexion. Torque measurement was achieved by the use of a strain gauge mounted on a horizontal bar lying in the same plane as the palm. This bar was fixed on one end to a stable vertical shaft, which is coaxial to the axis of wrist rotation,

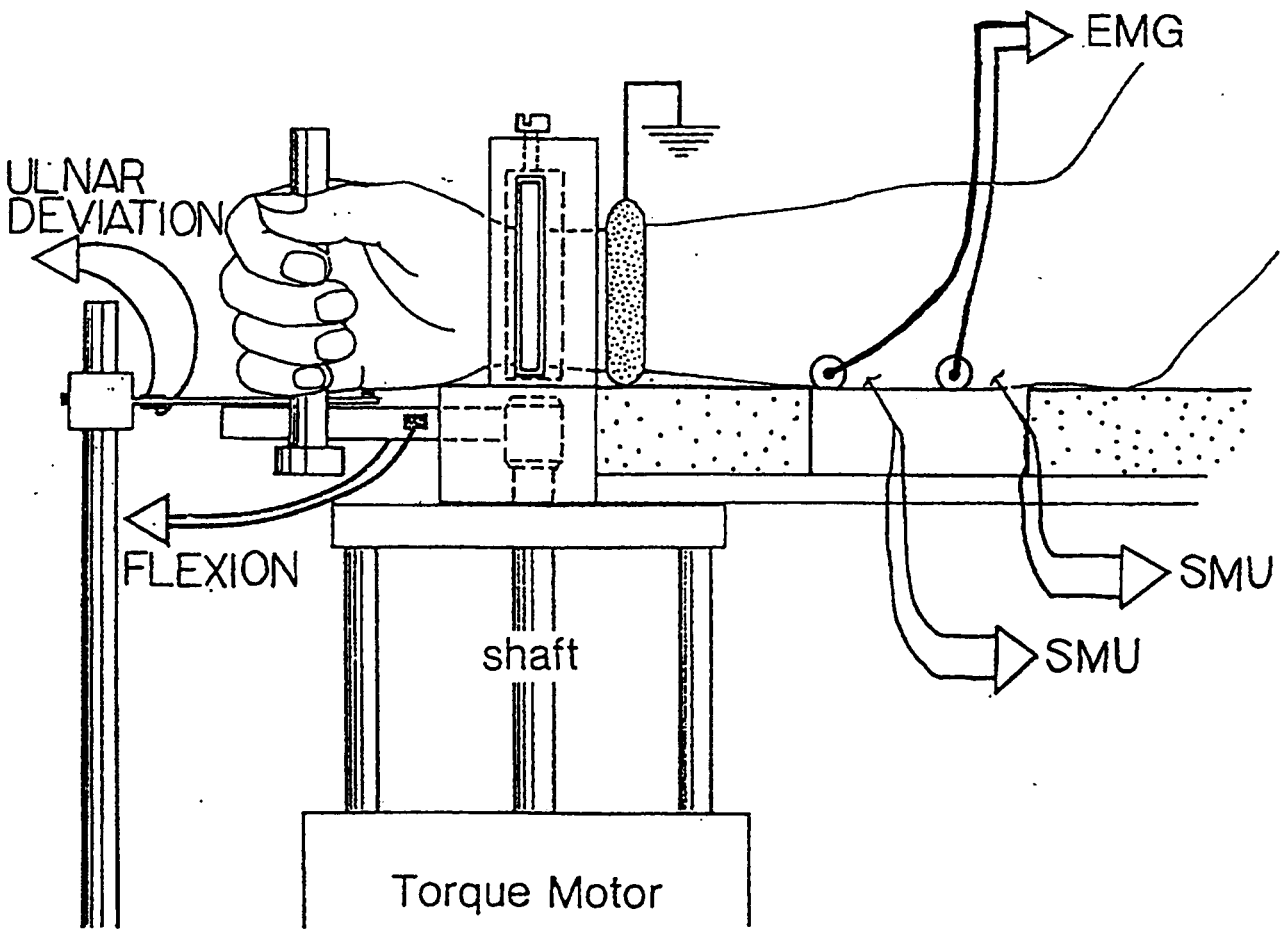

Fig. 2-1 Experimental setup for recording from FCU during four tasks. The subject was seated with the right forearm resting on the horizontal platform and the wrist fixed in position. The shaft from the torque motor could be fixed during isometric flexion or freed to respond to the torque motor. Strain gauges were mounted on bars perpendicular to the direction of torque being measured. A ground electrode was attached to the subject's forearm near the wrist. Two SMU needle electrodes were carefully positioned such that they recorded FCU activity and not the underlying FDP or FDS activity. Surface EMG recorded from the wrist extensors is not shown. [Figure modified from Calancie, 1984]

while the handle is mounted on the non-fixed end. To accommodate subjects of varying size the handle was moved along the strain gauge bar.

During non-isometric flexion, a torque motor was used to apply an extension load to the handle via the vertical shaft and strain gauge bar. By loading the flexor muscles with the torque motor a large change in the angle of the wrist with flexion was avoided, thus maintaining a stable recording. The size of the load was varied according to the threshold force of the SMU being recorded. The subject was required to move the handle against this load through a range of motion. A potentiometer was used to provide the subject with visual feedback of the handle position and torque was measured as for isometric flexion.

To study ulnar deviation, strain gauges mounted on a horizontal bar perpendicular to the plane of the hand were positioned so that the distal edge was in contact with the medial surface of the hand at the 5th metacarpophalangeal joint. The distance between this point and the axis of rotation of the wrist was measured for torque calculation. A subject produced an ulnar deviation torque against the strain gauge bar to elicit motor unit recruitment.

For all force measurements the output from the strain gauges was directed to bridge amplifiers (DC - 1 kHz, gain = 2x100). Calibration of the strain gauges was made with respect to the output of the bridge amplifiers. Output from the bridge amplifiers was separated into two signals: 1) AC force, filtered (0.1 - 300 Hz); and 2) DC force, unfiltered; before further amplification. The AC force was used during spike triggered averaging to extract the motor unit twitch tension. The DC force signal was used to measure the threshold of recruitment for the SMUs and as a visual feedback to the subject for maintenance of force levels. The two force signals were recorded on tape (Vetter PCM Recorder).

The final task of cocontraction was achieved by asking the subject to cocontract the forearm muscles without clenching the fist. No record of force was measured during this task.

Procedure

Once a subject was seated and their forearm positioned with the force measuring devices in place, the FCU muscle was stimulated to ascertain correct positioning for the surface EMG and SMU electrodes. The skin was prepared for the surface electrodes and the Ag-AgCl electrodes were secured over the muscles. Activity from the wrist extensors was recorded to observe muscle activity during cocontraction. The SMU needle electodes were then inserted percutaneously into the FCU muscle of the subject, making sure that the electrodes were not recording from the surrounding finger flexors, flexor digitorum profundus (FDP) and flexor digitorum superficialis (FDS) by ensuring that there were no SMUs recruited by pure finger flexion.

Following this check, the subject was asked to exert an isometric flexion force until the first clear SMU was recruited. Using visual and auditory feedback of SMU firing the subject maintained the SMU firing rate $\leq$ 10 imp/s for 1 - 2 minutes. This period of recording was later used during spike triggered averaging to compute twitch tension for this particular SMU. Following this the subject relaxed and then steadily increased their flexion torque past the threshold for recruitment of the first SMU until a second SMU was recruited on either electrode. Again this unit was held at a minimum rhythmic firing rate for 1 - 2 minutes before the subject relaxed. This procedure was repeated until such time as there were no more clear SMUs recorded in this electrode position. The subject was then asked to produce an ulnar deviation torque in a ramp like manner until the first SMU was recruited. The SMU size and shape were used to identify whether it was definitely the same unit as one of those units recruited in the isometric flexion paradigm. The SMU was fired at a low rate for spike triggered averaging analysis, the subject relaxed and the procedure was repeated as above.

The order of recruitment of SMUs in the two directions was then compared with the order of recruitment when the subject was asked to cocontract the wrist musculature. The cocontraction was generally accompanied by cocontraction of the more proximal musculature around the elbow and shoulder joints. The subject was asked to increase the cocontraction effort until the

previously identified SMUs were recruited. The order of recruitment with cocontraction was then compared to that in the previous two tasks.

Following the completion of these three tasks and recording of a maximum number of clearly discernible SMUs, the needle electrodes were moved to a new position and the above procedures were repeated.

For the task of non-isometric flexion the subject was asked to maintain the handle in a fixed position while a slowly increasing extension load was applied. As the load was increased SMUs were recruited in a particular order (2 - 3 SMUs) and a recruitment order established. The load was then decreased below the thresholds for all the units and the subject was asked to flex the wrist to recruit those same units. This established a recruitment order for isometric and non-isometric flexion which was then used for paired comparison. The needle electrodes were then moved to a new position and the procedure is repeated.

Analysis

Analysis was done off-line from the tape recordings using a Dell 310 microcomputer and software from RC Electronics. The threshold force of an SMU was evaluated from the amplitude of the DC force record when the unit began to fire repetitively. The twitch tension for the SMU was computed by the method of spike triggered averaging (Milner-Brown et al., 1973a). This was achieved by discriminating the SMU of interest via the use of logic circuitry and generating a transistor-transistor logic (TTL) pulse when the time/amplitude criteria are met. This pulse was used to trigger an averaging cycle of the computer thus extracting from the AC force record the motor units twitch. The amplitude of the twitch was read off the computer and converted to torque values using calibrations for the strain gauges and subject moment arms.

The TTL pulse was also used to generate a first order interval histogram of the spike train (ISTH). This histogram provided the mean and standard deviation of the interspike interval (ISI; inverse of firing rate) of the SMU. Any units with ISIs > 100 ms were rejected due to the likelihood of the twitch characteristics being affected by partial fusion (Calancie and Bawa, 1986).

A test for synchronization was applied to the SMUs as the basic assumption for the validity of the spike triggered averaging technique for twitch tensions is the asynchronous firing of motor units. This involved spike triggered averaging of rectified and unrectified surface EMG (Milner-Brown et al., 1973a). When synchronization is present the rectified-averaged EMG does not show clear coincident peaks with the unrectified-averaged EMG. Also a slow rise in base line levels of the rectified-averaged EMG is present ± 10 ms prior to the onset of the unrectified-averaged EMG peak if there is synchronization of motor unit firing. The area in the rectified-average lying between background levels and base line and the total area of the unrectified-averaged EMG were subtracted from the total area in the rectified-averaged EMG. The resulting area was expressed as a percentage of the total unrectified EMG area and must be ≤ 10 % to meet the non-synchronization criteria. If the value exceeded 10 % the SMU was rejected, however, the frequency of synchronization tested with this method was low and resulted in few rejections.

Results

The first observation was that the FCU motoneuron pool did not exhibit distinct subpopulations for any of the four contractions tested. Every motor unit recruited for isometric flexion was recruited during the other three tasks (although very few motor units could be tested repeatedly for all four tasks).

We then tested the order of recruitment of motoneurons by paired comparisons. The distinction between two motor units was made on the basis of differences in the size and shape of their action potentials as shown in Fig. 2-2. The recruitment order of two single motor units (SMUs) is shown for the four tasks tested. SMU 1 was recruited before SMU 2 repeatedly for all four tasks. Surface EMG data for flexor and extensor muscles are shown for each task. It is noteworthy that, while these two units were recruited with very little total EMG during isometric flexion, they required a very strong effort during cocontraction. The recruitment of FCU units during cocontraction always required a strong voluntary effort indicating that the FCU muscle is

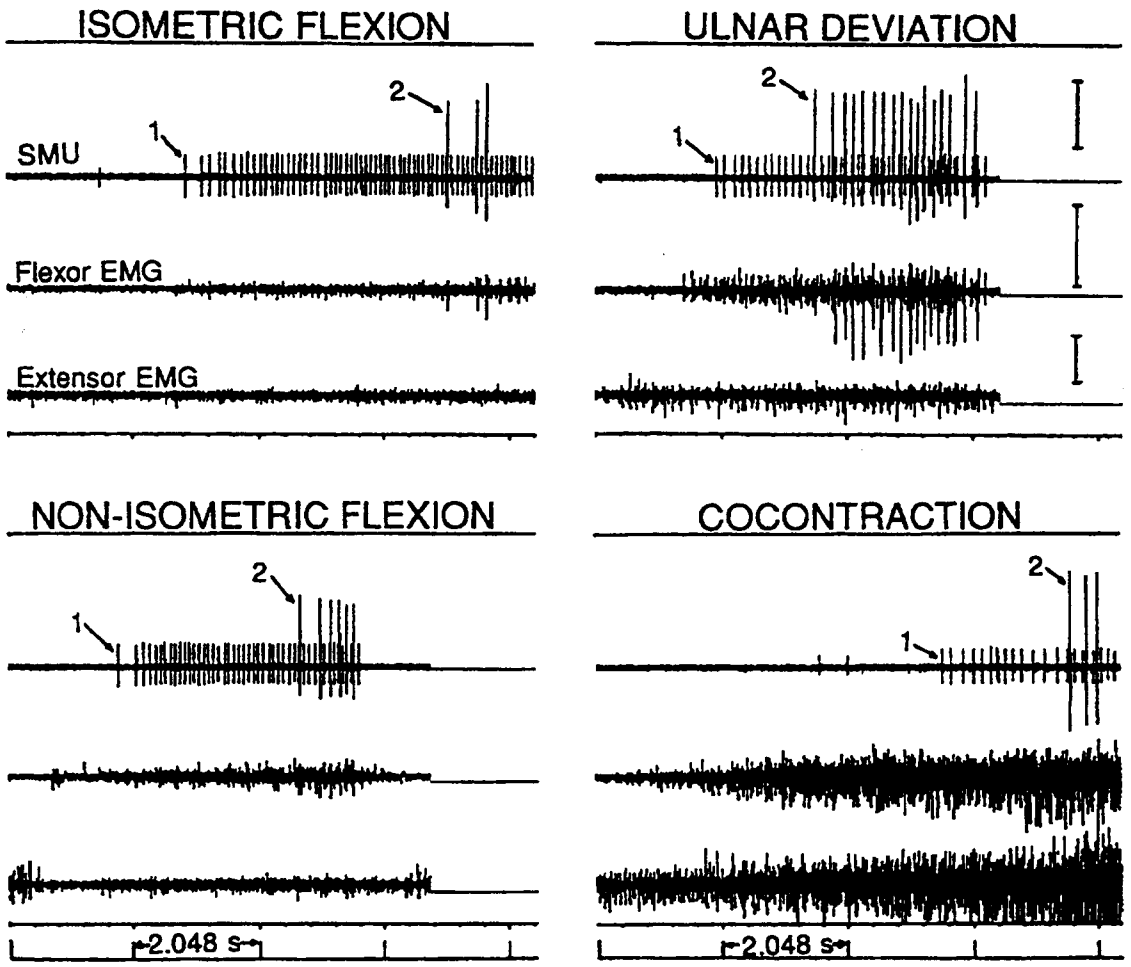

Fig. 2-2 Recruitment order of two FCU SMUs, 1 and 2, for four types of contraction. The top panel in each quadrant shows the two units with concomitantly recorded surface EMG from wrist flexor (middle panels) and wrist extensor (lower panels) muscles. During each task, the smallest unit SMU 1, was recruited before the larger unit, SMU 2. Data were sampled at 40-μs intervals. Each of the calibration bars shown in the second quadrant represent 200 μV for all three panels.

not one of the main fixators of the forearm. The strong effort needed to activate FCU motor units during cocontraction may be explained by the fact that shoulder and upper arm muscles are being activated to fixate the shoulder and elbow joints prior to activation of the wrist flexors. Therefore, the total sense of effort is very high before FCU is activated. The higher magnitudes of the surface EMG may be attributed to cross-talk from surrounding muscles which are coactivated with FCU during cocontraction. The larger magnitude of surface EMG or strong sense of effort needed to recruit the FCU motor units in question, cannot be assumed to reflect activation of a large number of additional FCU motor units not available during other tasks.

TABLE 2-1. Recruitment order with respect to isometric wrist flexion.

Task	Total number	Same order	Reversals	Indistinguishable
Ulnar deviation	143	137	2	4
Co-contraction	91	65	10	16
Non-isometric flexion	49	45	0	4

Table 2-1 summarizes the data for 283 paired comparisons for 216 motor units. The paired data presented in this table were such that their recruitment order for isometric flexion was very stable during repeated contractions. Those motor units which were very close in threshold, and hence interchanged their recruitment order during isometric flexion, were not tested for other tasks. Table 2-1 shows that for 143 motor unit pairs compared between isometric flexion and ulnar deviation, 137 (95.8%) showed the same order of recruitment. For 49 pairs compared between isometric and non-isometric flexion, 45 (91.8%) pairs had the same order of recruitment. During cocontraction, from a total of 91 pairs, 65 (71.4%) showed the same order while for 16 pairs the order of recruitment could not be distinguished. The recruitment of FCU motor units during cocontraction was difficult and generally abrupt, the pattern being similar to that observed

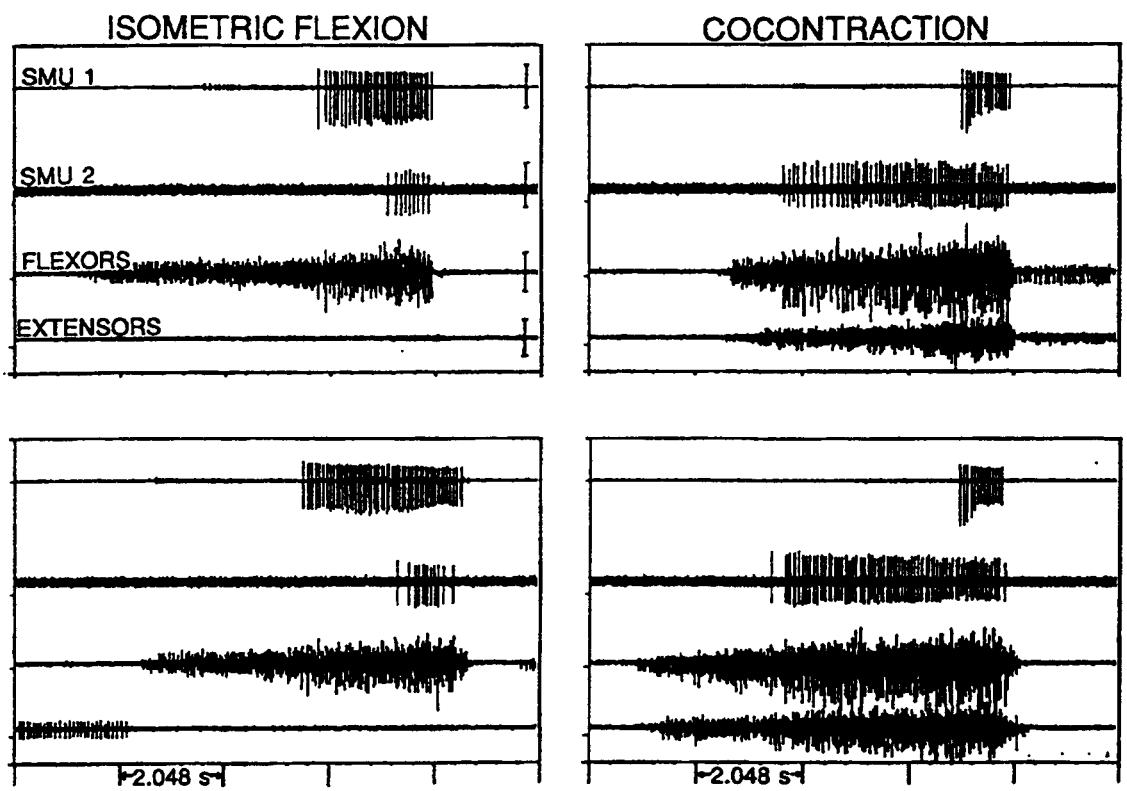

Fig. 2-3 Reversal of recruitment order during the cocontraction task.
A pair of FCU motor units recorded from separate electrodes, top two traces in each panel, are shown after repeated testing with isometric flexion, left panels, and cocontraction, right panels. Surface EMG from wrist flexors and extensors is shown to illustrate the relative activation of the muscles during the two tasks. The motor units were tested for recruitment order during isometric flexion, top left, followed by cocontraction, top right. To check for stability of recruitment order the pair was retested during isometric flexion, bottom left, then cocontraction again, bottom right. The recruitment order was repeatedly reversed during the cocontraction paradigm when compared with the order during isometric flexion.

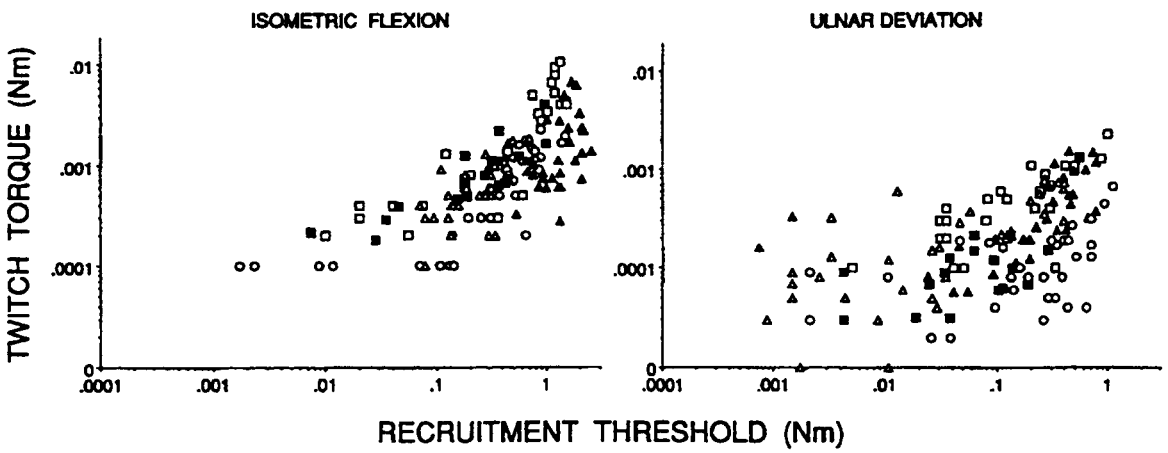

Fig. 2-4 Relationship between twitch torque and recruitment threshold for motor units recruited during isometric flexion and ulnar deviation.
Twitch torque versus recruitment threshold for five subjects (different symbols) are shown for isometric flexion and ulnar deviation contractions. In spite of the scatter, these data show a monotonic increase in twitch torque with increasing recruitment threshold.

for ballistic contraction. Such recruitment patterns made it difficult to discern recruitment order. It may be noted that cocontraction also exhibited reversals for 10 pairs. One such pair is illustrated in Fig. 2-3 for the tasks of isometric flexion and cocontraction. For this pair of SMUs the recruitment order was stable, from SMU 1 to SMU 2, during repeated trials with the isometric flexion task. However, the recruitment order repeatedly reversed upon cocontraction.

The above mentioned observations made on motor unit action potentials reflect the recruitment order of motoneurons in the spinal cord. These do not yield any information on size-related recruitment. Even if they did, size related recruitment in the spinal cord would not necessarily indicate orderly recruitment in terms of force output. The reason being that the force vectors of different muscle units may contribute different proportions of force components in various directions. In other words, some muscle units may be dominant in one direction while others may contribute predominantly to another. Hence, for two distinct directions of contraction, isometric wrist flexion and ulnar deviation, we studied the order of recruitment in terms of force output. In each of the two directions, the twitch tension of the recorded motor units was computed by spike triggered averaging technique (Milner-Brown et al., 1973a; Riek and Bawa, 1992). For all subjects, graphs of twitch torque versus recruitment threshold of FCU motor units were plotted for each of the two isometric contractions and are illustrated in Fig. 2-4. These data clearly demonstrate a monotonic increase in recruitment threshold with increasing twitch torque for both directions of contraction. This monotonic relationship suggests an orderly recruitment, from small to large, of the representative population of FCU motor units. (Motor units were sampled up to approximately 75% of the maximum voluntary force of wrist flexion.)

Discussion

The above observations indicate that FCU motoneurons in man are not fractionated into subpopulations for the four tasks examined here. Rather, the whole pool contributes to each of the contractions. Furthermore, the order of recruitment is according to size principle (Henneman et al., 1965) for each of the contractions tested. The difference in our observations from those of

Denny-Brown (1949) may be due to the fact that the FCU muscle is a very thin muscle surrounded by very large finger flexors, FDP and FDS. When recording from FCU, it is important to ensure that the indwelling electrodes are not recording activity from the surrounding muscles. It is suggested that the separate subpopulations mentioned by Denny-Brown (1949) were not FCU motor units, but possibly belonged to the neighboring muscles.

Chapter 3
RECRUITMENT ORDER OF MOTONEURONS DURING FUNCTIONAL TASKS

Introduction

Recruitment of limb motoneurons in mammals has been studied extensively for the last 35 years using both reflexive and descending excitatory inputs to the motoneuron pools (Henneman, 1957; Milner-Brown et al., 1973; Buller et al., 1980; Desmedt and Godaux, 1978, 1981; Calancie and Bawa, 1985b; Thomas et al., 1986; Bawa and Lemon, 1993). The main observation of these studies has been the stereotyped orderly recruitment of motor units. However, the contractions examined have generally been isometric and carried out in anatomically defined directions. There have been few studies that have examined recruitment of motor units during functional tasks.

The first dorsal interosseous (1DI) has been the most extensively studied muscle for investigation of recruitment of motor units by voluntary excitatory inputs (Milner-Brown et al., 1973; Buller et al., 1980; Desmedt and Godaux, 1981; Thomas et al., 1987). During abduction or flexion of the index finger at the metacarpophalangeal joint, a highly ordered size related recruitment was observed. However, with an everyday functional task in which a subject performed the non-isometric task of using a pair of scissors, a large number of recruitment reversals were reported in the same muscle (Thomas et al., 1987). Therefore, it is important to study the recruitment of motor units during functional tasks, and to explain the implications of any reversals, should they be observed.

Recently, Flament et al. (1993) studied five different tasks all of which involved contractions of the 1DI, as well as other muscles. We examined recruitment of 1DI motoneurons during three of these tasks. Isometric abduction of the index finger was used as the control for recruitment order of pairs of 1DI motoneurons, and the recruitment order of these motoneurons was then examined during the functional tasks of rotation and pincer grip (Flament et al., 1993).

The other two tasks studied by Flament et. al. (power and 'petri' grips) involve larger movements would have led to unstable recordings and, therefore, were not employed for single motor unit studies.[1]

Methods

Experiments were carried out with the right hand of three right-handed subjects ranging in age from 28 to 50 years (2 female, 1 male). Experiments were approved by the Ethics Committee for human experiments at Simon Fraser University. All subjects were free of neuromuscular disorders.

Recording

Surface electromyographic (EMG) and single motor unit (SMU) activity were recorded from 1DI muscle (see Chapter 2 for details).

SMU activity was recorded during three tasks as illustrated in Figure 3-1. The first task was isometric abduction of the index finger while the hand was pronated; contraction of the other intrinsic hand muscles was kept to a minimum. The second task was rotation during which the subject tried to loosen a threaded knob by exerting a rotational torque in an anti-clockwise direction, gripping the knob between the thumb and the index finger of the right hand. Lastly, the pincer task was performed by pressing a spring-loaded staple remover between the tips of the thumb and the index finger. Abduction, as a control, was performed under strictly isometric conditions. The other two tasks were performed against a high resistance, which did not result in strictly isometric conditions. The purpose during the functional tasks was not to produce an

[1] This work has been published in Experimental Brain Research, Jones et al, 1994. I did all the data collection and analysis at Simon Fraser University under the supervision of Dr. Bawa. M. Lyons was an undergraduate student in Dr. Lemon's lab during preliminary experiments. Dr. Lemon continued his collaboration at a distance by reviewing the manuscript and discussing the data.

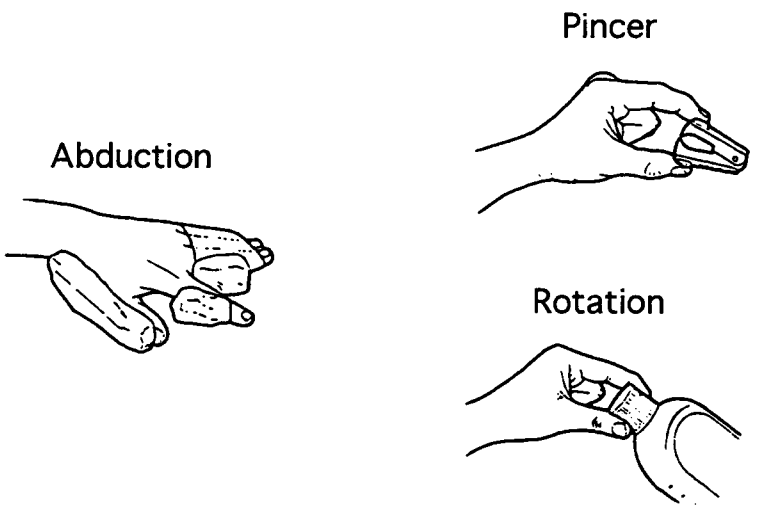

Fig. 3-1 Diagrams of the three tasks in which 1DI recruitment was tested. The task of isometric abduction of the index finger was compared with the more functional tasks of pincer and rotation. It was necessary for the subject to remain in a relatively constant posture when switching between the three tasks to ensure continued recording from the same SMU. The figure has been adapted from Flament et al., 1993.

isometric contraction; instead, we sought to maintain tonic recruitment of the motor units for 1--2 minutes and a high resistance was needed to accomplish this.

After insertion of the SMU recording electrodes, the subject was asked to make an isometric abduction of the index finger. With the help of audio and visual feedback, the subject was asked to increase the amount of contraction in a ramp-like fashion until the first identifiable unit was recorded. By performing a fairly constant contraction, the subject maintained a steady discharge rate with this unit for up to 1 minute and then increased the force of contraction to recruit another clearly identifiable unit. The subject maintained discharge of the second unit for up to one minute. Invariably, more than two (up to four) clearly identifiable units were recorded with the electrodes in one position. Then the subject gently transferred the grip to the rotation device, and performed the rotation task, exerting sufficient force to recruit the same units (if possible) that were recruited for abduction. Next, the subject performed the pincer grip task between the tips of the thumb and the index finger, again exerting sufficient force to recruit the same units as were recruited for abduction. For the functional tasks of rotation and pincer, the instructions to the subject were to increase the force slowly as was done in abduction. However, whether it was the nonisometric nature of the contractions, or the postural setting of the fingers, very slow and smooth contractions were not always possible. Each task was performed 2--3 times to ensure repeatability of the observation. The intramuscular electrodes were then moved slightly to record the next set of SMUs.

Each SMU was identified from the shape and size of the intramuscularly recorded potential. In order to compare the order of recruitment during functional tasks with that during abduction, the contractions were repeated several times for all tasks. Since the order of recruitment for abduction was considered as a control, only those SMU pairs for which the recruitment order was the same during all repetitions of the abduction task were included in the study. For such pairs, consistent reversal of recruitment order during rotation or pincer tasks were considered to be a genuine task dependent reversal.

At the end of the experiment, the intramuscular electrode was removed and the subject was asked to abduct the index finger with maximal force and hold it for 10--20 seconds. This was repeated three times. This allowed an estimate of the surface EMG from 1DI during a maximal voluntary contraction (MVC).

EMG and SMU data were stored on a four channel setting of a Vetter PCM recorder for off-line analysis (rise time for SMU channel was 25 μs {14 kHz}, and for other channels 100 μs {3.5 kHz}).

Analysis

Data were analyzed on a 486 personal computer using Cambridge Electronics Design 1401 interface, with SPIKE2 and SIGAVG software. Well identified SMUs were discriminated with the help of a BAK time-amplitude window discriminator. The resulting TTL pulse was used to trigger the SIGAVG averaging program to produce the motor unit triggered average (MU-TA, Palmer and Fetz, 1985; Lemon et al., 1990) response from surface EMG. Surface EMG was acquired at a rate of 10 kHz. The peak-to-peak amplitude of MU-TA was measured for each SMU.

For 1DI muscle, rectified or integrated surface EMG is linearly related to the total force (Milner-Brown and Stein, 1975; Lawrence and DeLuca, 1983). To compute recruitment threshold of a unit from surface EMG, surface EMG and SMU raw data were acquired with the SPIKE2 program both with a sampling rate of 10 kHz. When an SMU was just recruited, the mean amplitude of the rectified surface EMG, averaged over the first 2 seconds of the contraction, was taken as the recruitment threshold.

Results

Data are presented for 58 SMUs with 41 paired comparisons for abduction, 39 for pincer and 41 for rotation. All recruitment thresholds were less than 10% of MVC. The ability to record from high threshold motor units is dependent upon the stability of the electrode position. The

high contraction levels needed to recruit high threshold motor units often results in the displacement of the electrode and, therefore, the termination of recording from that unit. This, coupled with the fact that subjects were required to move their hand to switch from one task to another, resulted in recording from SMUs of low threshold. For a given pair of units, the lower and higher threshold units were defined according to their recruitment order during the isometric abduction task, with the lower threshold unit being reproducibly activated before the higher threshold one.

Figure 3-2 shows the recruitment order of three SMUs for all three tasks. Each task was tested 2--3 times. The mean amplitude of the rectified EMG at the time of the onset of tonic firing for a unit was taken as its recruitment threshold. Thresholds of units 1 and 2 were very close (10.00 μV, 10.79 μV) while that of unit 3 was quite different (27.10 μV). The peak-to-peak amplitudes of MU-TA were 43, 70, and 217 μV suggesting recruitment in order of size (Milner-Brown and Stein, 1975; Lemon et al., 1990).

Of the 41 pairs which showed consistent recruitment order during the abduction task, 39 were tested for pincer and 41 for the rotation tasks. There were no clear reversals for the pincer task, but two pairs showed inconsistent recruitment order on repeated testing. Out of the 41 pairs for the rotation task, 4 pairs showed inconsistent recruitment order, while one pair showed recruitment reversals on repeated contractions. Thus less than 10% of the pairs were inconsistent in recruitment order for pincer and rotation tasks, and one pair (<2%) showed a reversal for rotation. These data are summarized in Table 3-1.

TABLE 3-1 Summary of the recruitment order of motoneurons during various tasks.

Task	Total number	Same order	Reversals	Interchangeable
Abduction	41	41	0	0
Pincer	39	37	0	2
Rotation	41	36	1	4

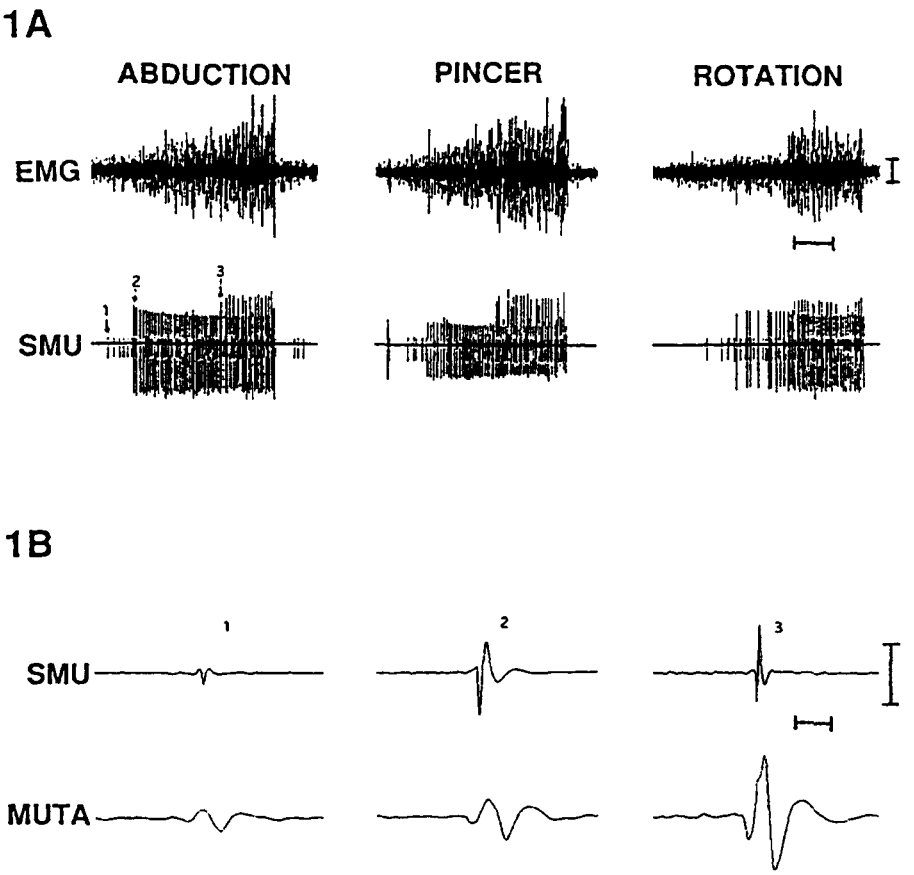

Fig. 3-2 Recruitment order of 3 1DI SMUs during anatomical versus functional tasks. **A**. The order of recruitment of three motor units (SMU), 1, 2 and 3, recorded from first dorsal interosseous (1DI) muscle, are shown for contraction of 1DI during three different tasks: abduction, pincer and rotation. For all three tasks, unit 1 was recruited before 2, and 2 before 3. Increase in the strength of contraction, for each of the three tasks, is indicated by an increase in the magnitude of surface EMG. **B**. The shape of each of the three SMUs is shown on an expanded time scale; the shape and magnitude of each motor unit triggered average (MU-TA) is also shown. *Calibration bars* (EMG and MU-TA) 100 μV. *Time scale*: **A** 1 s, **B** 5 ms.

A comparison of the recruitment threshold for all pairs of motor units is presented graphically in Figure 3-3. Recruitment threshold of the *low threshold unit during abduction* is plotted along the abscissa and that of the *higher threshold unit for abduction* is plotted along the ordinate for all three tasks. All points above the line of identity indicate that the higher threshold unit had the higher EMG value as would be expected if recruitment proceeded from small-to-large motor units. The 39 pairs for pincer were tested 86 times, only 5 points (6%) lie below the line of identity. For rotation, 41 pairs were tested 101 times. Only 10 points (10%) lie below the line of identity. These data show that for low threshold units (<10% MVC), the order of recruitment for the functional tasks of pincer and rotation is the same as that for abduction. The absolute value of recruitment threshold for a pair of motor units during the three tasks was not the same. This may be due in part to difference in the rates of contraction for the three tasks; surface EMG can differ with different rates of contraction (Bigland and Lippold, 1954; Brown and Cooke, 1981). Also, the firing rate upon recruitment was not always the minimal rhythmic firing rate for the motor unit (which is ideally the correct measurement for recruitment threshold). Because of the nature of the experimental paradigm and the nature of the functional contractions, maintenance of minimal rhythmic firing rates was not always possible. For that reason, all repetitions rather than the mean values have been plotted in Figure 3-3.

In most cases, the subject could easily separate the recruitment of the two units in a given pair during abduction but found it harder to do so during the other two tasks. The contractions in the other two tasks were more abrupt, faster contractions, and as a result the recruitment threshold was slightly higher. There are four groups of data plotted in Figure 3-4; abduction versus rotation for the low and the high threshold units and abduction versus pincer for the low and the high threshold units. A two tailed paired t-test showed that in each series abduction, on average, had the lower recruitment threshold at the level of $p \leq 0.01$.

The size of a SMU potential as recorded by intramuscular electrodes was not highly correlated with the size of the motor unit (Henneman et al., 1974). The size of the motor unit

Fig. 3-3 Relationship between the recruitment threshold of pairs of SMUs during various tasks.
For a pair of units, the lower and higher threshold SMUs were identified from the order of recruitment in the abduction task. This definition was used for pincer and rotation irrespective of the order of recruitment for these two tasks. The mean amplitude of rectified EMG (averaged over 2 seconds) at which the lower threshold unit was recruited is plotted along the X-axis; the corresponding value for the higher threshold is plotted along the Y-axis for abduction. For 41 pairs tested for abduction, there is a total of 96 points since each pair was tested 2--3 times. For abduction, all points lie above the line of identity as would be expected. For pincer, for 39 pairs of units, there are 86 points; with only 5 points showing reversals. For rotation, there were 41 pairs with a total of 101 points. There was a total of 10 points showing reversals.

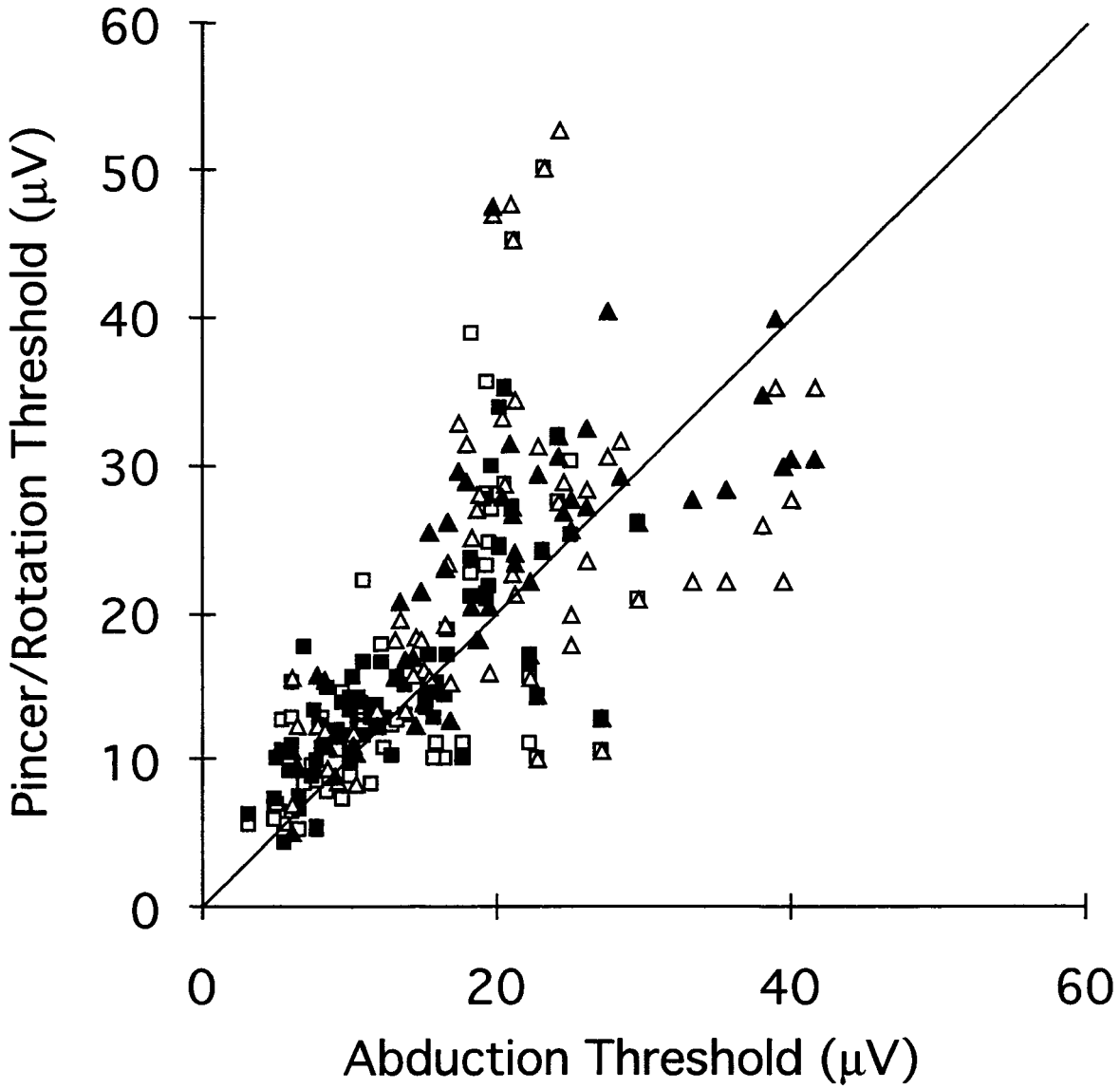

Fig. 3-4 Comparison of the recruitment threshold of functional tasks with respect to abduction.
Recruitment threshold of all paired comparisons are plotted with the threshold for abduction along the abscissa and those for pincer and rotation along the ordinate. The different symbols represent: □ abduction versus pincer of the low threshold unit, △ abduction versus pincer for the higher threshold unit; ■ abduction versus rotation for the low threshold unit and ▲ abduction versus rotation for the higher threshold unit. One tailed paired t-test showed that abduction had the lower recruitment threshold ($p \leq 0.01$) for all comparisons.

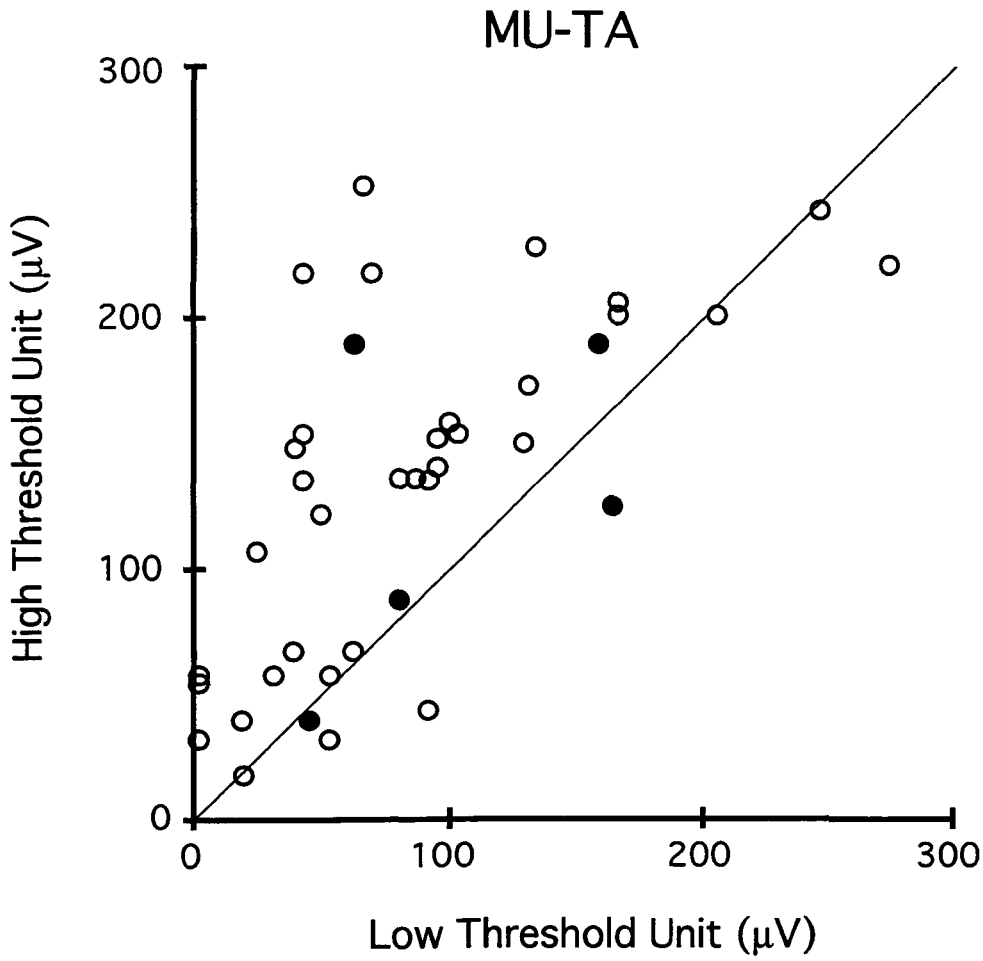

Fig. 3-5 Relationship between size of MU-TA for the low and high threshold motor units of a recruitment pair.
Motor unit triggered average (MU-TA) was computed by spike triggered averaging of surface EMG using intramuscularly recorded SMU potential as the trigger. Peak-to-peak amplitude of the resulting average (MU-TA) was measured for each unit. Amplitude of the MU-TA for lower threshold unit (along the X-axis) was compared with the amplitude of the MU-TA for the higher threshold unit (along the Y-axis) in a pair. Comparison of 41 pairs is shown above. The filled circles show values for units showing reversal or interchange of recruitment order. It may be clearly seen that in general, MU-TA for the higher threshold unit was larger than for the MU-TA for the lower threshold SMU. One-tailed paired t-test showed this result to be significant at the level of $p \leq 0.01$.

triggered average, MU-TA, obtained from surface EMG, has a stronger correlation to the size of the motor unit (Milner-Brown and Stein, 1975; Monster and Chan, 1977; Lemon et al., 1990). After having determined that the order of recruitment of a pair of motor units was the same for all three tasks, we wanted to ascertain whether the lower threshold motor unit was the smaller of the two units. Comparison of 41 MU-TA amplitudes is shown in Figure 3-5. Most of the points lie above the line of identity indicating that the higher threshold unit was larger in size as estimated from the size of its MU-TA. A one tailed paired t-test showed the result to be significant at the level of $p \leq 0.01$.

The filled circles are values from pairs which showed recruitment reversal or inconsistency during the pincer and rotation tasks.

Discussion

Previous studies on motor unit recruitment (see Calancie and Bawa, 1990 for review) have demonstrated that recruitment proceeds in an orderly fashion according to the size principle first enunciated by Henneman (1957). Many of the instances where preferential recruitment within a motoneuron pool has been shown were due to the presence of task groups where different parts of the muscle are activated during different tasks. It has been argued previously that the presence of task groups within a muscle cannot be interpreted as a violation of the size principle (Riek and Bawa, 1992). First dorsal interosseous is not partitioned into task groups (Thomas et al., 1986), and this conclusion is supported by the present study. However, an important difference between Thomas et al. (1987) and the present study is that the former reported a very high percentage of reversals in their functional 'scissors' task, whereas we have observed less than 10% reversals between units whose thresholds ranged within narrow limits (<10% MVC). Except for one pair, these pairs of units did not show reversed recruitment on repeated functional contractions. Since in the present experiments functional task contractions were carried out against fairly high resistance, the units were recruited tonically over relatively longer periods, allowing the recruitment order to be determined with more certainty, as for maintained isometric contractions.

During phasic, dynamic contractions (Thomas et al., 1987) which require the discharge of only few action potentials, reversals are possible. For example with two motoneurons which are different but close in size, one expects, according to the size principle, that the smaller motoneuron will discharge before the larger one. However, with a phasic input, when the motoneurons discharge only a few action potentials, recruitment reversals can be observed. A small percentage of reversals seen under such conditions is not a contradiction of the size principle but may rather be a reflection of the noise inherent in the motoneurons or in the input to the motoneurons. The greater the difference between the sizes of the two motoneurons, the less effect this synaptic noise will have.

Such reversals do not have serious functional consequences. For phasic contractions, one deals with forces of the order of twitch amplitudes rather than tetanic contractions. Twitch contractions do not differ much in sizes between motor units close in threshold. Therefore, a reversal of recruitment between neighboring motor units will not cause any unforeseen jerky contraction. If the reversal was between a very high threshold and a low threshold unit, it would lead to instability. Such reversals have not been reported.

Desmedt and Godaux (1977) examined recruitment order at different contraction speeds of 1DI muscle. At the fastest speeds, when motor units discharged only 1--2 action potentials, i.e. the contractions were phasic, the authors reported that the order of recruitment was unchanged. The reversals observed in the muscle were attributed to conduction velocities of motoneurons. That may be one of the factors but we suggest that synaptic noise is a dominant factor.

Another observation is that some SMUs which showed a consistent recruitment order for abduction, showed inconsistency during the functional tasks of pincer and rotation. This may be explained by the nature of the descending commands for the three tasks. Suppose that the intramuscular electrode records from motor units of the rank 7 and 10 within the 1DI pool. If the command is restricted to only one muscle, in this case 1DI for abduction, there is a certain amount of descending activity converging on the 1DI motoneuron pool to activate motoneurons 7 and 10. During rotation (or pincer task), many more synergists are involved (Flament et al., 1993). Even

though the portion of the descending command to 1DI may be the same, the total descending command is much larger in order to activate the first 10 motoneurons of the 1DI pool as well as the other synergistic motoneurons. With a descending input for abduction alone, 100% of the command is responsible for discharging only 10 motoneurons, and separation of recruitment of the 7th and 10th motoneurons is then very easy. On the other hand, for rotation, the total descending command is much larger, only a percentage of it is going to discharge 1DI motoneurons. This may lead to a lack of precision voluntary control of 1DI motoneurons in the functional tasks.

Despite the very considerable differences in the three tasks performed by our subjects, the order of recruitment of motor units is invariant. Thus, although there is indirect evidence for task-related changes in the central commands used to activate the 1DI (Flament et al., 1992), these commands do not appear to have at their disposal different task groups within this muscle. The command results in an orderly recruitment which is the same for all three tasks, which suggests that this order is intrinsic to the motoneuron pool. The precise action of the 1DI muscle is determined not by the command to 1DI but to the entire hand, and especially to the long finger extensors and flexors, (Schieber, 1993).

Chapter 4

RESPONSES OF HUMAN MOTONEURONS TO Ia INPUTS: EFFECTS OF BACKGROUND FIRING RATE.

Introduction

Synchronous activation of a population of Ia afferents elicits a composite excitatory postsynaptic potential (EPSP) in the motoneurons upon which they converge. The effects of this input on the ongoing activity of the postsynaptic neuron may be quantified by cross-correlating the output spike train of the motoneuron with the stimuli that give rise to the composite EPSP. The results appear as a peak in the peri-stimulus time histogram (PSTH; Fetz and Gustafsson, 1983) which may be quantified in terms of response probability (number of events in the peak / number of stimuli applied).

The magnitude and the shape of the PSTH peak depends upon the shape and amplitude of the composite EPSP (Ashby and Zilm, 1982a; Fetz and Gustaffson, 1983). The characteristics of the composite EPSP, produced by the input volley depend in turn, on both the active and the passive properties of the motoneuron (Rall, 1977; Schwindt and Calvin, 1973). Since many active parameters of a repetitively firing motoneuron vary with firing rate (Schwindt and Calvin, 1972, 1973; Calvin, 1974), it is expected that the characteristics of the composite EPSP, and hence the peak of the PSTH will also vary with the firing rate of the motoneuron.

Human studies of the Ia-to-motoneuron synaptic system have not supported such a relationship between response probability and the firing rate of the motoneuron (Ashby and Zilm, 1982b; Miles et al., 1989). On the other hand, human studies using complex EPSPs generated by transcranial magnetic stimulation (TMS) of the motor cortex have suggested a dependence of response probability on the background firing rate of the motoneuron (Brouwer et al., 1989; Olivier et al., 1995). The interpretations of the results from these two studies differ considerably.

There may be many reasons why the results obtained with TMS may differ from those obtained using peripheral Ia stimulation. Firstly, the descending volley produced by TMS consists of a series of wavelets producing a complex EPSP in the motoneuron (Edgley et al., 1990). This complex EPSP produces a complex excitatory peak in the PSTH which is difficult to interpret in terms of the underlying EPSP. Secondly, a voluntary increase in the firing rate of the motoneuron may alter the excitability of the motor cortex to the TMS (Brouwer et al., 1989). Thus the descending volley generated by the same stimulus at the motor cortex may differ at the two different rates. However, Olivier et al. (1995) attribute the rate effect on response probability using TMS to the properties of the motoneuron as opposed to the motor cortex. If the effect of firing rate on response probability to TMS is mediated by the motoneuron the question arises why a cortical input produces a different effect than a Ia inputs? Or, could the complex EPSP associated with TMS produce results which are different from those produced by the simpler Ia composite EPSPs?

The following study undertook a systematic examination of the effects of Ia EPSPs on the response probability of motoneurons firing at different rates. During this examination stimuli to Ia afferents were applied in two different modes. In the *random* mode of stimulation, stimuli were applied at random with respect to the times of occurrence of motoneuron spikes. In the "*triggered-delay*" mode the stimuli were applied at specific phases of the ISI (Olivier et al., 1995). To ensure that the results are not specific to motoneuron type, we have examined the effect of firing rate on response probability in two populations of motoneurons those innervating the fast flexor carpi radialis (FCR) and those innervating the slow soleus muscle. The observations are explained in terms of the biophysical properties of repetitively firing motoneurons in the cat.[1]

---

[1] This work has been published as an abstract (Jones and Bawa, 1993) and is in press in the Canadian Journal of Physiology and Pharmacology (Jones and Bawa, 1995). I did all experiments and analysis at Simon Fraser University under the supervision of Dr. Bawa.

Methods

Eight neurologically normal subjects (2 female, 6 male) between the ages of 26-50 yrs were recruited for these experiments. All of the subjects were right handed. The experimental procedures were approved by the Ethics Committee on Human Experiments at Simon Fraser University.

Single motor unit (SMU) activity was recorded from the right flexor carpi radialis (FCR) or the right soleus muscle using bipolar intramuscular electrodes. Differential surface electromyographic (EMG) recordings were made with Ag/AgCl disc electrodes (Grass; Quincy, MA) fixed to the skin overlying the FCR or soleus muscles. Other details are given in Chapter 2.

Composite Ia EPSPs were produced in either FCR or soleus motoneurons by delivering constant current stimuli to the median nerve at the cubital fossa or the posterior tibial nerve at the popliteal fossa, respectively. A bipolar felt electrode was used for stimulation and was oriented with the cathode placed proximally and a ground electrode attached to the upper arm or thigh. The stimuli were applied with a Grass S88 stimulator via a SIU5 stimulus isolation unit and CCU1A constant current unit with a pulse duration of 0.3-0.5 ms for median nerve stimulation and 1.0 ms for tibial nerve stimulation. The shorter duration stimulus was used in the upper limb to reduce the stimulus artifact produced even though a 0.5 ms pulse is slightly less efficient in producing pure H-reflexes (Panizza et al., 1989). The stimulating electrode was carefully positioned to obtain an H-reflex response at the lowest stimulus intensity with little or no M wave. Once in a satisfactory position the electrode was secured with Velcro straps.

SMUs recorded in these experiments were of the lowest threshold for voluntary recruitment (<10% maximal voluntary contraction). Since the order of recruitment of motoneurons with a Ia volley is the same as that with voluntary input (Desmedt and Godaux, 1978), one is able to use low intensity stimuli to generate large changes in firing probability of the motoneurons. In trying to extend these observations to higher threshold units, the magnitude of

the stimulus had to increase to the point where there was an unacceptable amount of superposition of SMU responses following the stimulus and large M waves which contaminated the results.

Procedure

Subjects were asked to voluntarily recruit an SMU and maintain a tonic discharge at a constant firing rate using audio and visual feedback. Initially, the subject was required to maintain the repetitive discharge of the SMU at a rate that was as slow as possible and yet rhythmic. These slow firing rates were noticeably different for soleus and FCR motoneurons (see Results). While the subject maintained tonic discharge of the SMU, stimuli were delivered to the nerve in one of two different modes: *random* or *triggered-delay* (Olivier et al., 1995). In the *random* mode of stimulation, the stimulus was given irrespective of the times of discharge of the SMUs. That is, the stimulus could induce an EPSP with equal probability during all phases of the ISI.

In the *triggered-delay* mode, the stimulus was applied at a particular delay, d, with respect to the SMU spike in order to induce composite EPSPs at a specific phase of the ISI. This was accomplished by online discrimination (BAK window discriminator; Clarksburg, MA) of SMU spikes and using the output TTL (transistor-transistor logic) pulses to trigger the stimulator at a fixed delay, d, following the SMU spike, i.e. the spike-to-stimulus delay as illustrated in Fig. 4-1. These delays ranged from 1-60 ms for FCR and 1-80 ms for soleus SMUs. The upper limit of these delay ranges were set so that the composite EPSP would be induced prior to the next naturally occurring action potential when the motoneuron was firing at the faster of the two rates being compared.

In either mode of stimulation the minimum time between two stimuli was 4-5 seconds so that after a response the subject could recover the normal background firing rate. After at least 40 stimuli were given at the slow firing rate the subject was asked to voluntarily increase the firing rate of the SMU and maintain tonic firing at this new elevated rate. The degree to which the subject increased their firing rate was not controlled but generally the average ISI was reduced by 30 ms. Responses to approximately 40 stimuli were then collected at the faster firing rate.

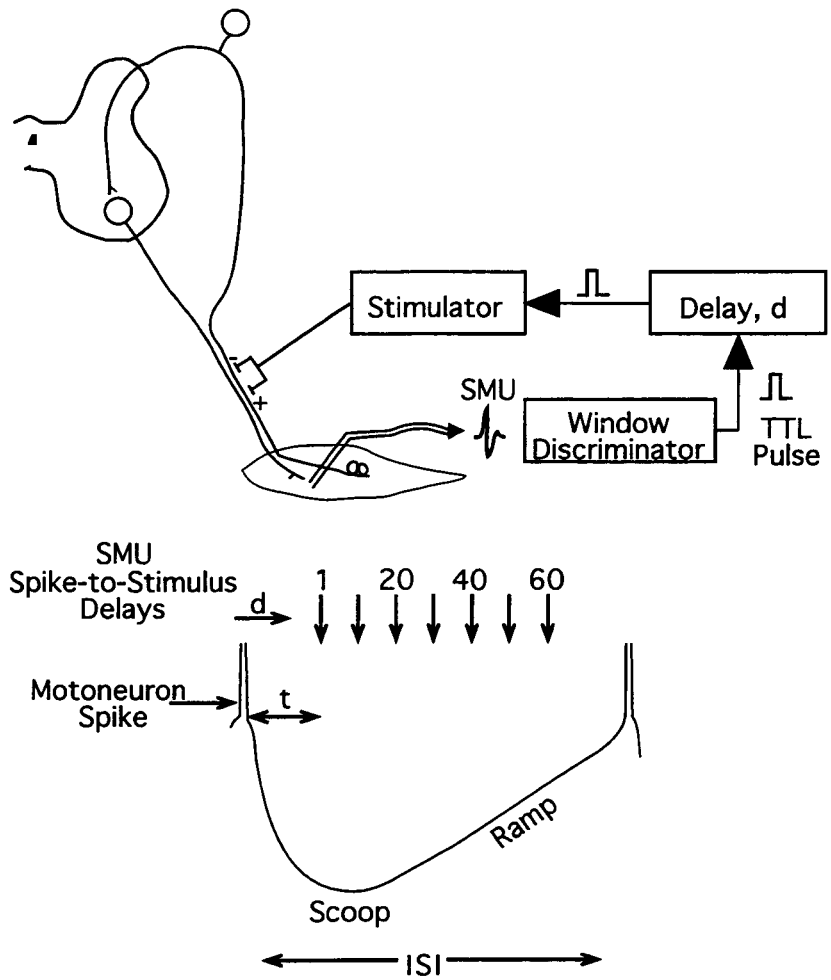

Fig. 4-1 Schematic of experimental set-up.
Top: Activity of a motoneuron is recorded as single motor unit (SMU) activity in the muscle. During the *triggered-delay* mode, the stimulator was triggered at a known delay, d, by a discriminated SMU spike. During the *random* mode, the stimulator output was independent of the SMU firing times. Bottom: During *triggered-delay* stimulation composite EPSPs were induced in the motoneuron at known spike-to-stimulus delays following the motoneuron spike. The dead time, t, represents the transmission times in the reflex pathway and indicates the earliest time a triggered stimulus may be applied following the motoneuron spike.

The parameters that were adjusted for various experiments included: (1) the spike-to-stimulus delay, d; (2) the firing rate of the motoneuron and (3) the mode of stimulation. For a given condition, approximately 40 - 50 stimuli were applied, then a change would be made to either parameter (1) or (2) and a subsequent 40 stimuli would be applied. During *random* stimulation we found that it was necessary to collect responses to a larger number of stimuli, therefore, typically 70 stimuli were given at each rate. During the course of long experiments subjects were allowed to rest between collection periods. To ensure recording from the same SMU, spike triggered averaging was carried out during the experiment on the raw EMG with respect to the occurrence of the SMU spikes. The resulting motor unit triggered average (MU-TA; Palmer and Fetz, 1985) was used to fingerprint the SMU under study.

The stimulus triggers, SMU activity and surface EMG were recorded on a PCM recorder (Vetter instruments; Rebersburg, PA) for off-line analysis.

Analysis

Data were analyzed off-line using a 486 personal computer and a 1401*plus* computer interface from Cambridge Electronic Design (CED; Cambridge, U.K.). MU-TAs were computed, both on- and off-line, and H-reflex responses from surface EMG were averaged using the SIGAVG software (CED), acquiring raw surface EMG at a sampling rate of 10 kHz. For spike train analysis, SMU activity was sampled at 10 kHz and acquired along with the associated TTL pulses, after discrimination with two in-series BAK (Clarksburg, MA) time-window discriminators, and the stimulus triggers. The advantage of acquiring both raw SMU data as well as the equivalent TTL pulses was that the experiment could be checked off-line for correct discrimination of SMUs before constructing histograms (Bawa and Lemon, 1993).

The firing rate of a motoneuron was computed by constructing first order interval histograms, using the SPIKE2 software (CED), for each SMU, for each experimental condition. To assess response probability of the motoneuron in response to the Ia composite EPSP, peri-stimulus time histograms (PSTHs) were constructed between SMU spikes and stimuli using the

SPIKE2 (CED) software. For the *triggered-delay* mode of stimulation, the response probability at time T, P(T), was calculated by dividing the total number of spikes in the short latency peak of the PSTH by the total number of stimuli applied. Due to variation in the ISI naturally occurring spikes may arise between the triggering spike and the response peak at the longest values of T. In these cases the stimulus is discarded and not used in calculating P(T). For the *random* mode of stimulation response probability, P_r, was calculated after subtracting the mean background firing probability from the peak (Bawa and Lemon, 1993). The resulting value is a measure of the probability of response to a single stimulus, so that a P(T) (or P_r) of 0.5 is equivalent to saying that there is a 50% chance that the composite Ia EPSP will directly evoke an action potential in the motoneuron. In the *triggered-delay* mode we also need to consider the time at which the EPSP is produced during the ISI.

Statistics: Response probabilities computed for the same motoneuron at two firing rates were tested for significant difference using paired t-tests and significant differences are reported at the level of $p \leq 0.02$.

Results

Data were obtained from 44 FCR motoneurons and 15 soleus motoneurons by recording of SMUs in the target muscles. In response to a Ia input volley, the motoneurons showed an increased firing probability as evidenced by a peak in the PSTH. The onset of the peak of the PSTH during the *random* mode of stimulation ranged from 15.8 - 25.0 ms (mean ± sd = 19.1±2.9 ms) for FCR and from 36.7 - 45.8 (40.9±3.4 ms) for soleus motoneurons. The onset latencies of the peaks provide an estimate of the dead time arising from the efferent and afferent conduction times. The dead time values, t, were then added to the spike-to-stimulus delays, d, during the *triggered-delay* mode of stimulation to obtain the total delay, T=t+d, at which the EPSP was produced in the motoneuron following the previous action potential.

Firing rate

Firing rate and its inverse equivalent, ISI, will be used interchangeably throughout the text as contextually appropriate. The ISIs reported in Table 4-1 were calculated from the mean of the first order interval histograms. For the faster firing rates in FCR, mean ISIs ranged from 67 - 118 ms (8.5 - 15 imp/s) and for slow firing rates mean ISIs ranged from 95 - 175 ms (5.7 - 10.5 imp/s). For soleus the mean ISIs ranged from 114 - 162 ms (6.2 - 8.8 imp/s) for the fast firing rates and 157 - 303 ms (3.3 - 6.4 imp/s) for the slow rates. While there is some overlap in the ranges representing fast and slow firing rates, the majority of the rates considered fast were greater than 10 imp/s (ISI=100ms) in FCR and greater than 6 imp/s (ISI=166 ms) in soleus. In calculating the mean ISI from the first order histograms it was observed that the variability of the ISIs decreased at the faster rates. This is shown in Table 4-1 as the peak width of ISIs. Peak width represents the width of the interval histogram at ± one standard deviation from the mean value of ISI. This decrease in peak width with an increase in firing rate is a well documented observation (Person and Kudina, 1972; Matthews, 1995) and may have implications for response probability at different firing rates.

TABLE 4-1. Comparison of the ISIs and their variability at the fast and slow rates.

		FCR		SOLEUS	
		ISI (ms)	**Peak width*** (ms)	**ISI** (ms)	**Peak width** (ms)
Fast	**Mean±s.d.**	89±13	28±5	136±14	42±12
	Range	67 - 118	18 - 38	114 - 162	24 - 62
Slow	**Mean±s.d.**	133±20	80±12	201±38	110±59
	Range	95 - 175	48 - 102	157-303	62 - 236

* Width of first order interval histogram at one standard deviation of the mean ISI

Effects of baseline firing rate on response probability using random stimulation.

The effects of motoneuron firing rate on response probability to a Ia input volley were evaluated for 15 motoneurons (8 FCR; 7 soleus) using *random* stimulation. Contrary to our expectations as based on the literature (Ashby & Zilm, 1982b; Miles et al., 1989), firing rate had a clear effect on response probability. Figure 4-2A shows PSTHs for an FCR and a soleus motoneuron at fast and slow firing rates. Values for firing rate, response probability (P_r) and number of stimuli (N) are shown with the respective PSTH. The FCR motoneuron shows a 46 % decrease in response probability at the fast rate compared to the slow. Similarly, the soleus motoneurons response probability is 45% lower at the faster firing rate. Both motoneurons show a decreased response probability at the fast firing rate.

Data for all 15 motoneurons tested with *random* stimulation is summarized in the bar diagrams of Figure 4-2B. The mean percent decrease in response probability at the fast firing rate is 58% for FCR and 44% for soleus. Paired t-tests suggested that there was a significant difference in response probability of a motoneuron at fast and slow rates.

Response probabilities at different delays with triggered-delay stimulation.

Random stimulation induces EPSPs at all phases of the ISI with equal probability, therefore, P_r measures an averaged response probability over the whole ISI. In order to understand the properties of human motoneurons at specific times during the ISI, the *triggered-delay* mode of stimulation was employed. The *triggered-delay* mode of stimulation confined the EPSP to being produced at a set delay, d, following an SMU spike and hence the equivalent total delay, T, following the motoneuron spike. Figure 4-3 shows the results of *triggered-delay* stimulation at four different delays during the ISI for an FCR and a soleus motoneuron. In both cases the motoneuron was being voluntarily driven at a constant firing rate of 8.3 imp/s for the FCR motoneuron and 6.8 imp/s for the soleus motoneuron. The total delay (T) at which the EPSP was produced following the motoneuron spike was estimated from the onset latency of the

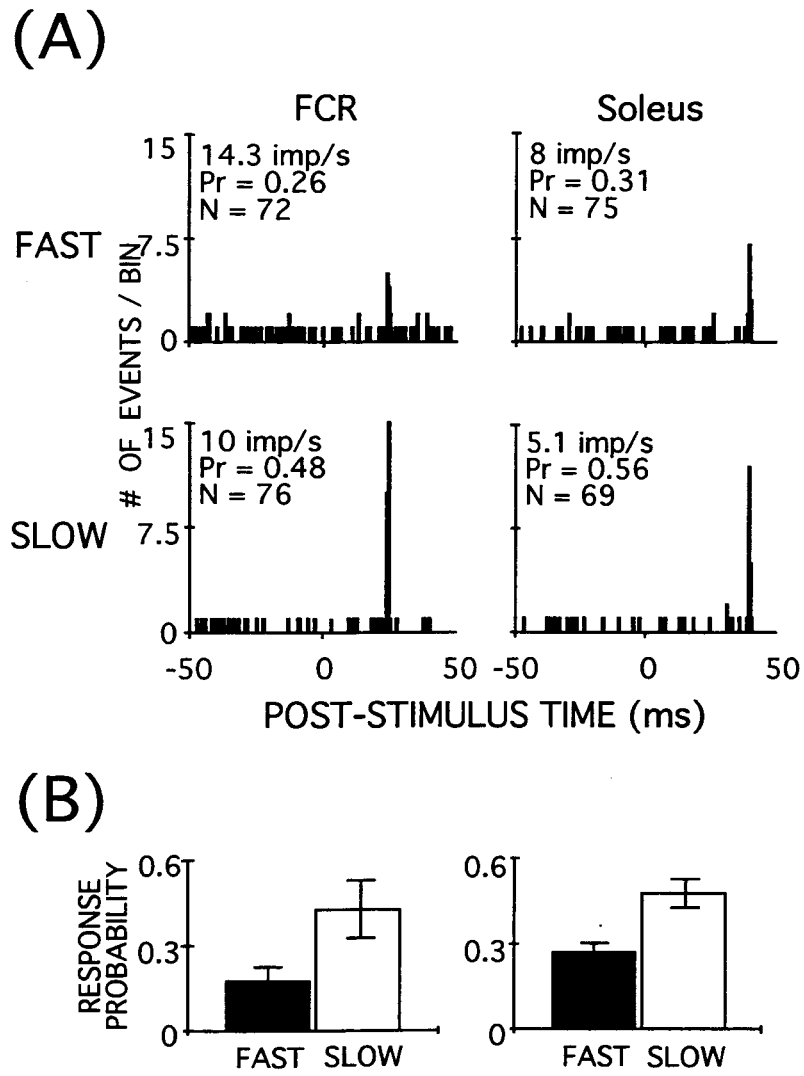

Fig. 4-2. Effects of firing rate on the response probabilities of motoneurons during *random* stimulation.
(A) Peri stimulus time histograms: In the FCR motoneuron the response probability increased from $P_r = 0.26$ at the fast firing rate (14.3 imp/s, top left) to $P_r = 0.48$ when the firing rate decreased (10 imp/s, middle left). In the soleus motoneuron the response probability increased from $P_r = 0.31$ at the fast firing rate (8 imp/s, top right) to $P_r = 0.56$ at the slower rate (5.1 imp/s, middle right). (B) Bar diagrams: The bottom part of the figure summarizes the results from the two muscles. In FCR the mean response probability at fast rate was $P_r = 0.18 \pm 0.09$ ($\pm$ sd; n = 6) while at the slow rate $P_r = 0.43 \pm 0.21$. In soleus, at the fast rate $P_r = 0.27 \pm 0.05$ (n = 7) and at the slow rate $P_r = 0.48 \pm 0.10$. The difference in P_r values at the two rates is significant in both muscles (FCR: $p = 0.013$; soleus: $p = 0.002$).

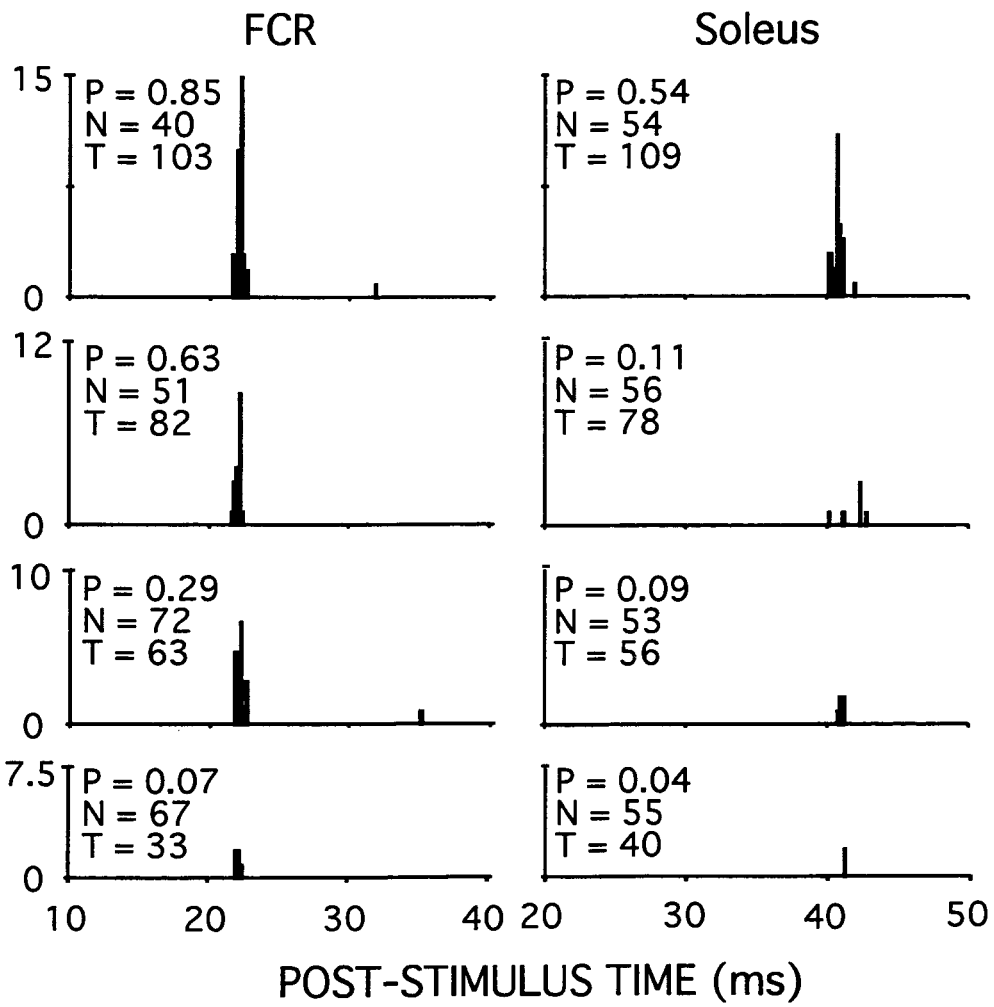

Fig. 4-3. Peri stimulus time histograms (PSTHs) with the *triggered-delay* mode of stimulation.
Response probabilities for an FCR motoneuron and a soleus motoneuron from the same subject are shown for four different motoneuron spike-to-stimulus delays. As the motoneuron spike-to-stimulus delay, T, was decreased, the response probability decreased. The mean firing rate for the FCR motoneuron was 8.3 imp/s and the mean firing rate for the soleus motoneuron was 6.8 imp/s.

peak during *random* stimulation plus the SMU spike-to-stimulus delay, d. For both motoneurons the response probability was the greatest at the longest delay and decreased as the EPSP was produced progressively at shorter delays during the ISI.

The response probabilities at various delays are plotted graphically in Figure 4-4 for the two motoneurons shown in Figure 4-3. The curve formed by joining the consecutive response probability values will be referred to as a *"response trajectory"* in contrast to the membrane voltage trajectory which is expected to constitute an important parameter affecting the response trajectory. From Fig. 4-4 it may be seen that the response probability increases in a monotonic fashion with increases in the total delay. The regions of the ISI that were not tested include both early and later phases. In the initial phase of the ISI the earliest delay testable with *triggered-delay* stimulation is equivalent to a SMU spike-to-stimulus delay of 1 ms plus the dead time, t. In the FCR motoneuron this is approximately 10 ms shorter than in the soleus motoneuron because of differences in the monosynaptic reflex times. To test for repeatability of the response probabilities, we obtained repeat measures at some delays for the FCR motoneuron. Data points in Fig. 4-4 with error bars show the mean and standard deviation for 3 measures of response probability. The data illustrate that response probability values were repeatable over a range of delays and that the profile of the response trajectory was not noticeably altered by variations in response probability.

It may be noted that the shapes of response trajectories depend on the stimulus intensity, in addition to the motoneuron properties. At a given firing rate, the stimulus may be strong enough to produce a response probability of 1 at most of the delays. At the other extreme, stimuli may be weak such that response probability remains 0 during most of the ISI. To avoid these two extremes we tried to adjust the stimulus strength so that response probability was approximately 0.5 at SMU spike-to-stimulus delays of 30-40 ms.

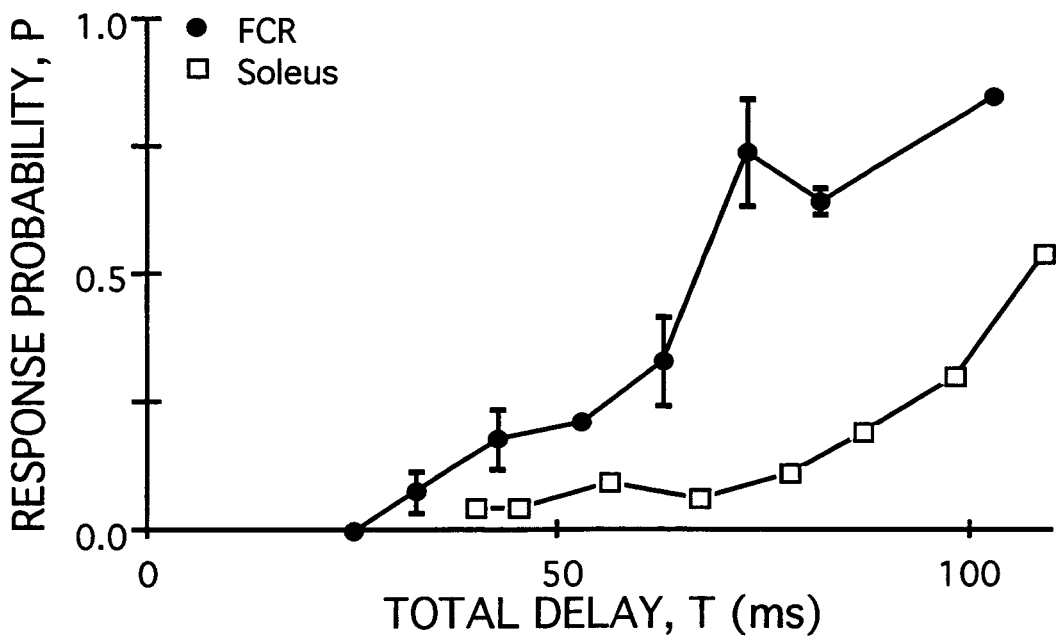

Fig. 4-4. Response trajectories for FCR and soleus motoneurons.
The two response trajectories shown above for the FCR (●) and soleus (□)motoneurons are plotted with data obtained from the same motoneurons presented in Fig. 3. The total delay along the abscissa comprises the onset time of the peak for the motor unit (i.e. dead time) plus the motor unit spike-to-stimulus delay, d. The firing rates were 8.3 imp/s for FCR and 6.8 imp/s for soleus. In the FCR response trajectory, data points represent the mean of three trials with standard deviation bars to indicate the variability in the values.

Effect of baseline firing rate on response probability using triggered-delay stimulation

Having established the relative response probabilities at various delays we proceeded to examine the effect of firing rate on the response probability at these specific delays. Figure 4-5 shows PSTHs from an FCR and a soleus motoneuron during *triggered-delay* stimulation at two different firing rates. The EPSP was induced in the FCR motoneuron approximately 53 ms following the motoneuron spike and resulted in a response probability of 0.49 at the slow rate (11.8 imp/s) which increased to 0.77 at the faster rate (13.3 imp/s). The effect of firing rate is similar for the soleus motoneuron where the EPSP was induced approximately 86 ms following the motoneuron spike resulting in a response probability of 0.12 at the slow rate (4.9 imp/s) which increased to 0.47 at the fast rate (7.1 imp/s).

Figure 4-6 shows data recorded from 28 FCR motoneurons (filled circles) and 10 soleus motoneurons (open squares) during *triggered-delay* stimulation at various delays, T. For some FCR motoneurons we were able to record at multiple delays resulting in a total of 41 paired comparisons of response probability at fast and slow firing rates. The change in response probability is plotted along the ordinate such that positive values reflect an increase in response probability at the faster firing rate. The horizontal line drawn across the figure at zero indicates no change in response probability between the two rates. The majority of the points lie above this line indicating an increase in response probability with increase in firing rate irrespective of the delay. A paired t-test showed these differences in response probability to be significant for both FCR and soleus motoneurons. The introduction of a third axis in Fig. 4-6 (not shown for simplicity) to show dependence on the differences in firing rates (Δ firing rate) for each of the points did not provide any additional information. The reason for this may be that although two points may have had the same difference in firing rate, the absolute values of the fast and slow firing rates were not the same for each motoneuron. It is possible that even if this were controlled that absolute values would have different effects in different subjects.

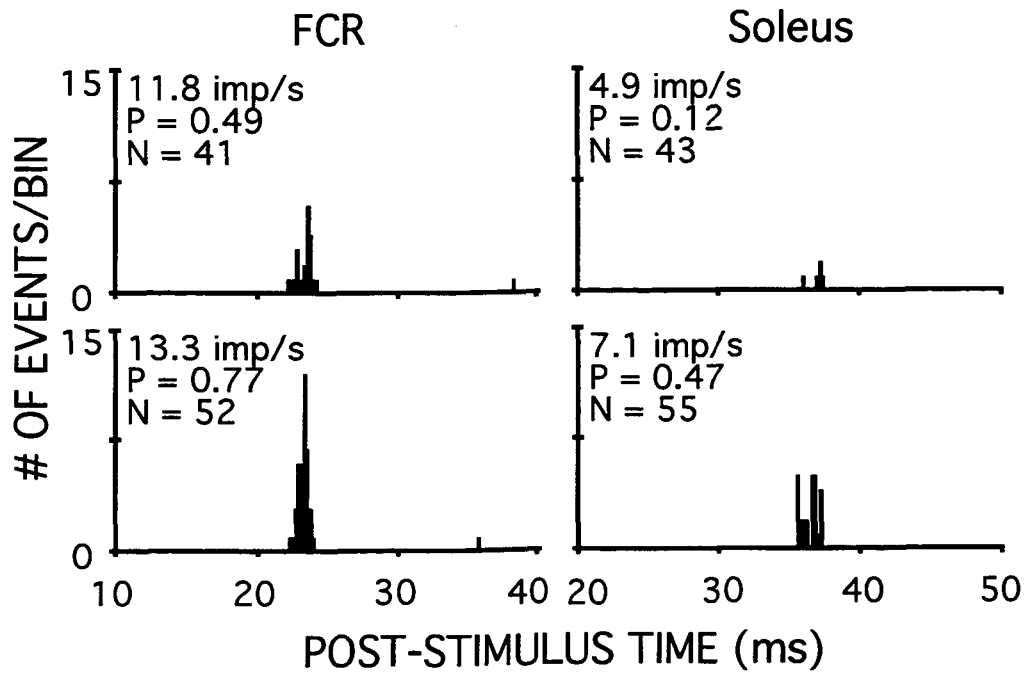

Fig. 4-5. PSTHs illustrating the effect of firing rate on two motoneurons.
The figure shows the effect of firing rate on the response probability during the *triggered-delay* mode. For FCR, the spike-to-stimulus delay, d, was 30 ms (T=53ms) and for soleus it was 50 ms (T=86 ms). The response probabilities are P=0.49 (N=41, number of stimuli) at the slow rate of 11.8 imp/s which increased to P=0.77 (N=52) at the fast rate of 13.3 imp/s in FCR. In soleus, at the slow rate of 4.9 imp/s the response probability was P= 0.12 (N=43). At the fast rate of 7.1 imp/s, response probability increases to P=0.47 (n=55).

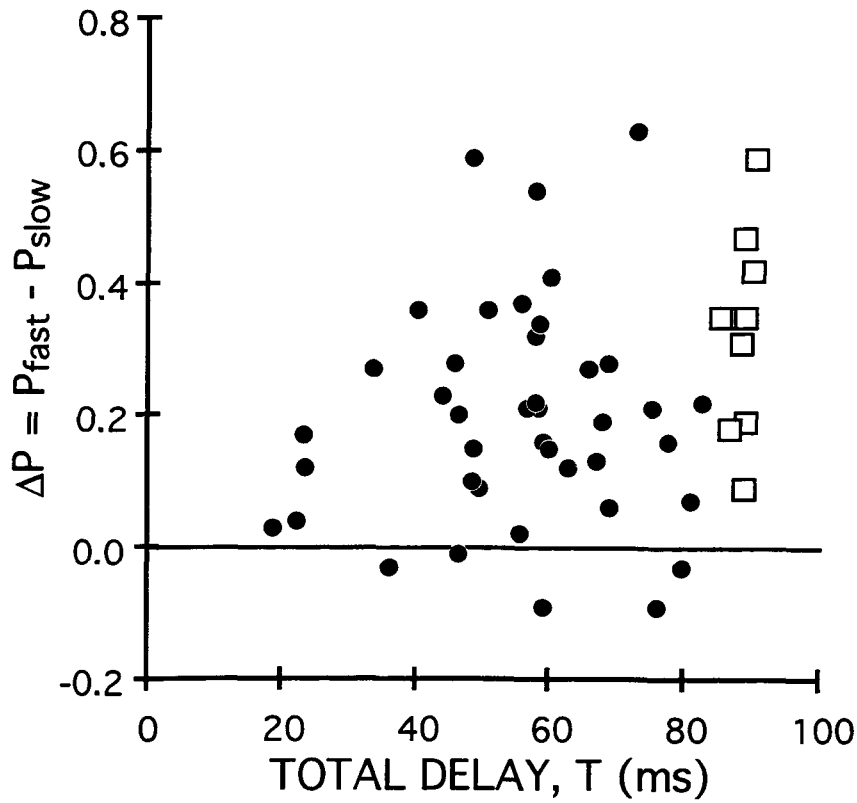

Fig. 4-6. Summary of the data to show the effect of firing rate on response probabilities. Data are presented for 41 paired comparisons from 28 FCR motoneurons (●) and 10 paired comparisons from 10 soleus motoneurons (□). The data illustrate that for the *triggered-delay* mode of Ia stimulation, the response probability is higher at the faster firing rate. In FCR the points were separated into 3 groups based on total delay, T: 1) 18-45 ms, 2) 45.1-60 ms, and 3) $\geq$ 60.1 ms. A Paired t-test for each group showed a significant difference at $p \leq 0.01$. For soleus the paired t-test also shows that the change in P with an increase in firing rate is significant at $p \leq 0.01$. The large scatter in the data is accounted for by differences in the firing rates and stimulus intensities used for different paired comparisons.

Sorting of randomly applied stimuli into sequential time intervals

An increase in the background firing rate of a motoneuron decreases its response probability to *random* stimulation and yet increases the response probability to triggered stimulation at a given delay. In an evaluation of the relationship between results with *triggered-delay* stimulation and *random* stimulation, data were recorded from two FCR motoneurons at both slow and fast rates in response to 274-343 *random* stimuli for each condition. The results are summarized in Table 4-2.

TABLE 4-2. Comparing response probabilities of two motoneurons to *random* stimulation when stimuli are sorted with respect to their occurrence during the ISI.

	1		2	
	Slow	**Fast**	**Slow**	**Fast**
ISI (ms)	135	90	105	75
$\mathbf{P_r}$	0.72	0.47	0.65	0.51
$\mathbf{P_{1\text{-}60}}$	0.59	0.64	0.59	0.74
$\mathbf{P_{rem}}$	0.78	0.24	0.72	0.10
$\mathbf{P_{20}}$	0.11	0.51	0.38	0.68

The response probability to *random* stimulation (P_r) was higher at the slow firing rate for both motoneurons. From the same data the response probability was measured again but only to stimuli which fell within the range of 1-60 ms following the last rhythmically firing SMU spike ($P_{1\text{-}60}$). This computation is similar to that with the *triggered-delay* mode but covers a range of spike-to-stimulus delays rather than a specific delay. Overall, within this range of delays, response probability was higher at the faster firing rate supporting the results obtained with the *triggered-delay* mode of stimulation. This would suggest that the remaining stimuli which fall outside the spike-to-stimulus range of 1-60 ms must elicit a greater response probability at the

slow firing rate. This is the case and these values are reported in Table 4-2 as P_{rem}. Triggered responses at a delay of 20 ms were also examined separately for these two motoneurons to confirm our general finding of the effect of firing rate on response probability at a given delay. Again, we see an increase in response probability at the faster firing rate at a delay of 20 ms (P_{20}).

Response trajectories at two firing rates

The comparison of P(T) values at single points of the ISIs does not necessarily reflect the same trend during all phases of the ISI. In order to compare all successive points for the same motoneuron firing at two different rates we obtained response trajectories for 3 FCR motoneurons at fast and slow firing rates. The resulting profiles of the trajectories are illustrated for 2 motoneurons in Figure 4-7. Response trajectories 1 and 2 were obtained with the *triggered-delay* mode of stimulation and show response probability values that are higher at the faster firing rate (open circles) within the range of delays tested.

Response trajectories 3 and 4 were obtained from motoneuron 2 of Table 4-2. In generating these response trajectories the stimuli were sorted into 10 ms bins with respect to their spike-to-stimulus delay thus producing pseudo-triggered response probabilities. The average values are plotted at the midpoint of the 10 ms bin. The resulting response trajectories support those obtained with *triggered-delay* stimulation showing response probability to be higher at the faster firing rate (open squares) at all delays greater than the dead time of 25 ms.

The differences in the two pairs of response trajectories (1&2 versus 3&4) may be attributed to at least three factors. Firstly, the absolute firing rates are different in the two motoneurons at the fast and slow firing rates. Secondly, the stimulus intensities, and therefore the composite EPSPs induced in the two motoneurons may be of different amplitudes (i.e. larger amplitude EPSP for trajectories 3&4). The third factor contributing to the differences in the two pairs of response trajectories is the method of stimulation. Over the long period of recording there may be a large variability in the composite EPSPs evoked by the stimulation. By using the pseudo-triggered method of generating a response trajectory, the variability in composite EPSP

size is distributed equally to all delays. The question then arises why use the *triggered-delay* mode at all? The main reason is that with *random* stimulation it is difficult to keep the same motoneuron firing repetitively at two different firing rates for long enough periods of time to obtain enough stimuli at each delay range. Whereas with *triggered-delay* stimulation one can compare response probability at fast and slow firing rates at particular delays without having to sample throughout the entire ISI.

Using the pseudo-triggered method of generating response probabilities we were also able to compute responses at delays within the dead time. It may be noted that for the motoneuron shown in Fig. 4-7 the response probability increased at shorter intervals during the slow firing rate (filled squares). The other motoneuron of Table 4-2 did not show this increase in response probability at delays which were less than the dead time. Instead, the response probabilities for this motoneuron were equal (almost zero) at both rates during the dead time.

Discussion

The aim of the present study was to understand the properties of human motoneurons during repetitive firing. This was done by examining the effects of the background firing rate of a human motoneuron on its response probability to homonymous Ia volleys. This rate effect was examined during *random* and *triggered-delay* modes of stimulation. We found that the overall response probability determined during *random* stimulation decreased with an increase in background firing rate. However, if the EPSP was produced at a fixed delay following the spike, the response probability increased with an increase in background firing rate. By using the two methods of stimulation, *random* and *triggered-delay*, we were able to measure two indices of motoneuronal excitability. During *random* stimulation, response probability provides an index of the overall excitability, or the input/output gain of a repetitively firing motoneuron. While during *triggered-delay* stimulation, response probability provides an index of membrane excitability at

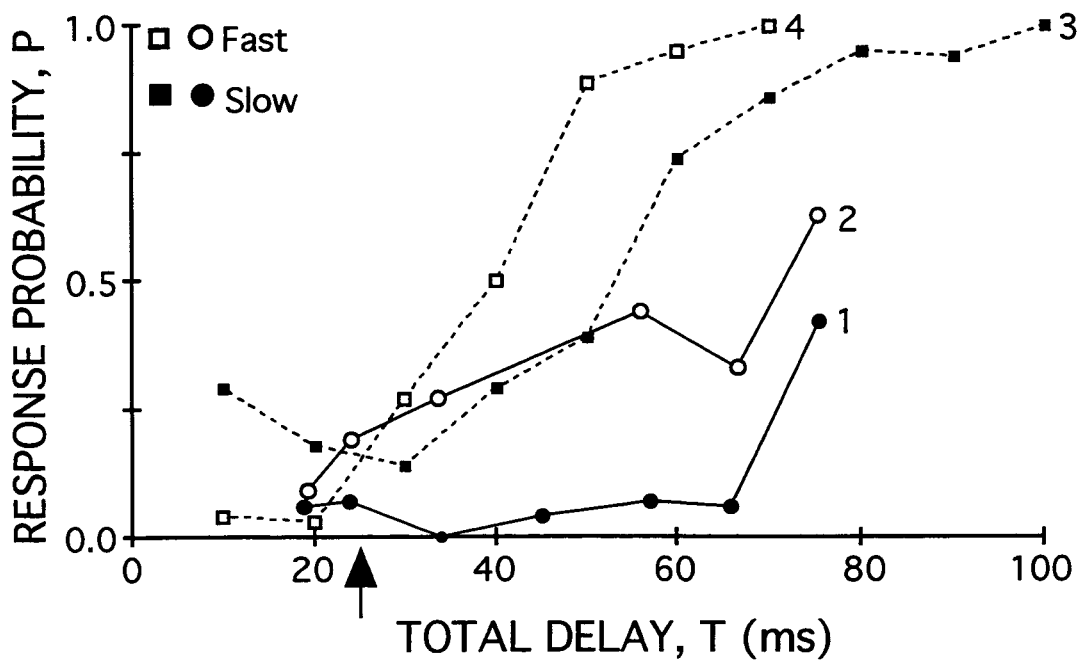

Fig. 4-7. Response trajectories for two FCR motoneurons at fast and slow firing rates. Response trajectories 1 and 2 were obtained with *triggered-delay* mode while the unit was firing at slow (●, 7.7 imp/s) and fast (○ 10.5 imp/s) firing rates. The curves 3 and 4 were obtained from an FCR motoneuron of another subject (■, slow rate = 9.5 imp/s; □fast rate = 13.3 imp/s). The data from this motoneuron were collected with the *random* mode of stimulation and during analysis the stimuli were sorted into 10 ms bins with respect to the timing of the last rhythmically firing spike. The arrow indicates 25 ms dead time for this response peak; with this pseudo triggered method we were able to test times shorter than the dead time.

specific times during the ISI. Results from both methods of stimulation may be explained on the basis of the biophysical properties of repetitively firing cat motoneurons.

The response probability of a repetitively firing cat motoneuron to an input volley has been suggested to depend on the membrane potential and its rate of change, the firing threshold, the membrane conductance, noise in the presynaptic-motoneuron system and the size and shape of the EPSP (Fetz and Gustafsson, 1983; Gustafsson and McCrea, 1984; Cope et al., 1987). In the repetitively firing cat motoneuron many of these factors change with the firing rate. For example AHP trajectories during the ISI show characteristic decreases in scoop depth as firing rate increases (Schwindt and Calvin, 1972; Baldissera and Gustafsson, 1974; Heyer and Llinás, 1977). The voltage threshold for action potential generation varies throughout the ISI (Calvin, 1974) and shows a correlated increase with increasing firing rates (Schwindt and Crill, 1982; Powers, 1993). Membrane conductance during the latter part of the ISI also varies with firing rate where motoneurons firing at a faster rate exhibit a lower conductance at a given delay following the spike (Schwindt and Calvin, 1973; Mauritz et al., 1974). How do all these factors combine to produce changes in response probability with respect to rate?

Consider two membrane voltage trajectories during the ISI of a motoneuron firing at two different firing rates (solid lines, Fig. 4-8) as observed in the cat (Schwindt and Calvin, 1972). In the presence of noise, probing the entire ISI with a composite EPSP will result in response trajectories depicted by the dashed lines in Fig. 4-8. In the *random* mode, the test volley has equal probability of arriving at all phases of the ISI. Hence the response probability is given by

$$P_r = \frac{1}{ISI}\int_0^{ISI} P(T)dT$$

where P(T) is the response probability obtained with the *triggered-delay* mode at a given time T following the spike. The average response probability over the complete ISI, P_r, can be divided into responses over three regions of the ISI. The region of the ISI probed with our *triggered-delay* mode of stimulation is represented by region II on the abscissa which is marked by the

boundaries of the dead time (t) and a spike-to-stimulus delay of 60 ms. Within this region our results show that response probability at any time is greater at the faster firing rate. This was supported by the *random* stimulation results which confined response probability calculations to stimuli which fell within this range ($P_{1\text{-}60}$, Table 4-2). This may be accounted for by the biophysical factors mentioned above. Firstly, if we assume that the same amount of excitatory synaptic current is generated by the stimulus at the slow and fast firing rates, then the lower membrane conductance at the faster firing rate will result in a larger EPSP (Schwindt and Calvin, 1973). Within the range of firing rates tested the increment in firing threshold may be insignificant. This leads to a second factor affecting the results in which the distance between the membrane voltage trajectory and the firing threshold is decreased at the faster firing rate. Both of these factors would lead to a higher response probability at the faster firing rate. On the other hand a factor which may lead to a decreased response probability at the faster firing rate is the increased slope of the ramp phase of the AHP. Such increases in ramp slope, which have been analytically modeled in the cat Ia to motoneuron system (Fetz and Gustafsson, 1983), would tend to decrease the response probability at the faster firing rate..

How does the response probability compare in the regions not probed with the *triggered-delay* stimulation? In the region of the dead time (region I, Fig. 4-8) the conductance of the membrane is very high at both rates and may result in near total shunting of the input current resulting in a negligible EPSP. This combined with the distance of the membrane potential from firing threshold results in negligible response probabilities which are not different at the two firing rates. The remaining region is that following the spike-to-stimulus delay of 60 ms plus the dead time. Since P_r is higher at the slower firing rate yet the summation of response probabilities in regions I and II is greater for the faster firing rate, one can infer that the response probability in region III must be much higher at the slower firing rate and this has been experimentally confirmed (P_{rem}, Table 4-2).

Why is response probability so much higher at the slower firing rate in the latter region of the ISI? This may be explained by using the observations reported by Person and Kudina (1972)

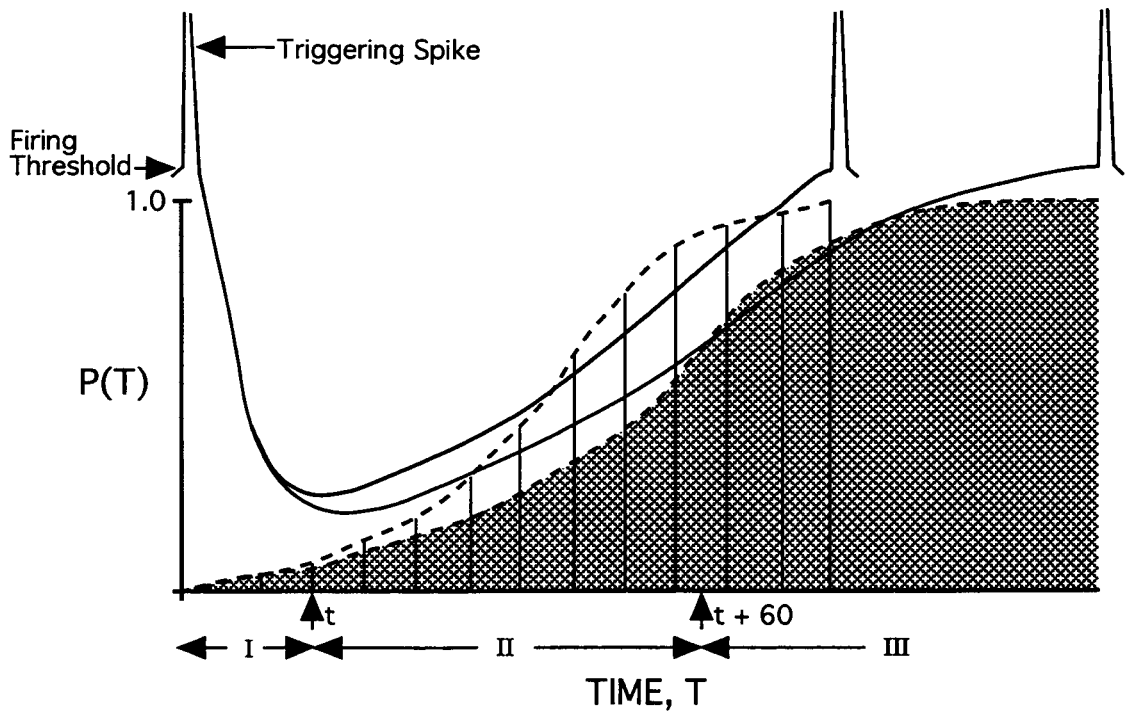

Fig. 4-8. The qualitative explanation of results based on observations from intracellular recordings of repetitively firing cat motoneurons.
Two AHP membrane voltage trajectories (solid lines) are illustrated representing fast and slow firing rates, assuming a decrease in scoop depth at the faster firing rate. The corresponding response trajectories are shown by the dashed lines with response probabilities of zero at the time of the spike. Phase I depicts the dead time, phase II depicts the interval of ISI examined with the *triggered-delay* mode of stimulation. During phase II, response probability, P(T), is higher at the faster firing rate. The response probability for the *random* mode of stimulation, P_r, is given by the cumulative probability over the entire ISI which is represented by the shaded area for the slower rate and area marked with vertical lines for the faster rate.

on human motoneurons. For the rectus femoris motoneurons, the authors showed that for ISIs > 80 ms, the standard deviation of the ISI was linearly related to the ISI, i.e. the slower the firing rate, the higher was the variability in firing rate. This was attributed to an asymptotic shape of the trajectory. The slower the firing rate, the longer the asymptotic region thus the higher the response probability at the slower firing rate. Both Matthews (1995) and Piotrkiewicz and colleagues (1992) support such an idea with computer simulations which take into account firing probability from first order interval histograms, noise and membrane potential.

The above arguments can be supported by the shapes of the membrane voltage trajectories in the cat. It has been demonstrated that at slow firing rates, the membrane potential does not approach threshold with a constant slope, but rather the approach to the next spike is asymptotic (Schwindt and Calvin, 1972, Fig. 6C1; Baldissera and Gustafsson, 1974, Fig. 3). The slower the firing rate, the longer the asymptotic region. This prolonged asymptotic region of the AHP would give rise to the large variability in ISIs and a high response probability to an experimental input. For the data reported in our own work (Table 4-1), ISIs showed a considerably higher variability at the slower firing rates resulting in a much longer period of high response probability towards the end of the ISI. On the other hand, the ISIs at fast rates had very small variability resulting in a very short period of very high response probability.

The other factor which may contribute to a higher response probability at the slower rate in the *random* mode is the presence of delayed depolarization. It has been shown previously that motor units can fire doublets at the minimal rhythmic firing rate (Bawa and Calancie, 1983). As the firing rate is increased the tendency to fire doublets decreased. The tendency to fire doublets has been attributed to the presence of delayed depolarization (Calvin, 1974). Comparison of trajectories 3 and 4 in Figure 4-7 at intervals less than 25 ms may be explained by delayed depolarization. At the slower firing rate (trajectory 3), the increase in response probability at very short post-spike intervals may be attributed to the presence of delayed depolarization (also Kudina and Alexeeva, 1992), while at the faster firing rate (trajectory 4) the delayed depolarization may be absent resulting in a lower response probability.

Thus the results of the human experiments can be explained qualitatively using biophysical properties of repetitively firing motoneurons in the cat discharging in response to intracellular injections of current. However, cat motoneurons may exhibit very different membrane voltage trajectories such as those described for fictive locomotion (Brownstone et al., 1992) or for axotomized motoneurons (Heyer and Llinás, 1977). In these cases the membrane potential is quite shallow over the course of the ISI. If the depth of the afterhyperpolarization (AHP) was the main factor in determining the response probability to an input volley, we would expect to see little change in response probability with respect to the delay following the action potential with such trajectories. It may also be pointed out that our own results can be explained using the properties of cat motoneurons and the explanation does not require a separate hypothetical AHP trajectory model for human motoneurons (Ashby and Zilm, 1982b).

The literature is divided on the question of the effects of firing rate on the response probability of motoneurons to Ia inputs. On the one hand some authors suggest that firing rate does have an effect on response probability (Kudina, 1988; Kudina and Alexeeva, 1992; Piotrkiewicz et al., 1992). While on the other hand, some authors report that baseline firing rate has no effect on response probability (Ashby and Zilm, 1982b; Miles et al., 1989; Brouwer et al., 1989; Nordstrom et al., 1992; Poliakov et al., 1994; Turker and Cheng, 1994). Kudina (1988) reports a decrease in response probability with *random* stimulation and also shows results using *triggered-delay* stimulation which are comparable to the present results. The differences between Kudina's results and our own are in the early region of the ISI where Kudina reports that for the first 60-100 ms, the motoneurons were inexcitable and that this period of inexcitability did not change with an increase in firing rate. Our results show that for delays as short as 16 ms following the spike in an FCR motoneuron the response probability increased with an increase in firing rate. These differences may be due to a variance in upper and lower limb motoneurons and stimulus intensities.

The studies which assume no effect of background firing rate on the motoneuron response to Ia input cite the results of primarily two papers. In the first paper (Ashby and Zilm, 1982b) the

authors originally report that following an increase in firing rate the response probability of a motoneuron to Ia input was the same or decreased slightly compared to that when the same unit was discharging slowly. The authors settle on the former conclusion as the theoretical model (Ashby and Zilm, 1982a) predicted no effect of firing rate on the response probability of a motoneuron. Ashby and coworkers have reiterated the lack of effect of background firing rate on Ia responses in a more recent study (Brouwer et al., 1989). A comparison of the response probabilities to Ia input in this later study (Brouwer et al., 1989; Fig. 2) with the present results shown in Fig. 2 suggests that their sensitivity for detecting an effect is low due to the extremely low response probability values used.

The second frequently cited paper suggesting no effect of background firing rate on response probability is that of Miles et al. (1989). However, the observations of Miles et al. (1989) are equivalent to our results with *random* stimulation although they are not reported as such. These authors report that firing rate has no effect on response probability of soleus motoneurons to Ia inputs when firing at background rates of 6, 8 and 10 imp/s. They, however, show a significant increase in response probability at a firing rate of 4 imp/s. The apparent lack of a rate effect is probably due to the normalization procedure used in these studies in which response probabilities are normalized to 166 stimuli. For example, with the motoneuron firing at 6 imp/s, 166 stimuli are given and there are 80 responses to the stimuli. This would result in a response probability of 0.48. If the normalized response probabilities at 8 and 10 imp/s are the same then we may assume them to be 0.48. Removing the effect of their normalization of response probability to 166 stimuli results in response probability per stimulus (equivalent to the present results) of 0.36 and 0.28 for firing rates of 8 and 10 imp/s respectively. Thus their results also show a decrease in response probability with an increase in firing rate.

The present results obtained with Ia inputs are consistent with those obtained with cortical inputs to motoneurons (Brouwer et al., 1989; Bawa and Lemon, 1993; Olivier et al, 1995). The cortical volleys were produced using transcranial magnetic stimulation (TMS). Even though qualitatively the effects of the two inputs are the same, quantitatively they may be different.

Firstly, because the composite EPSP produced by the Ia volley is different from the complex EPSP produced by a series of descending cortical volleys which result from TMS (Edgley et al., 1990). Secondly, there is a possibility of an increase in the descending volley with voluntary increases in firing rate because of a greater background excitability of the motor cortex. This would be in direct contradiction of the interpretation posed by Brouwer et al. (1989) in which the corticospinal neurons are considered less excitable at faster firing rates. In spite of these differences, similar quantitative trends support the fact that these rate effects are attributed to the motoneuron properties rather than to changes in the input volleys.

It may be pointed out that with voluntary increases in firing rate, there may be a decrease in presynaptic inhibition of homonymous Ia afferent terminals, which in turn would increase the magnitude of the Ia volley impinging on the motoneurons. This may partly contribute to our results in the *triggered-delay* mode. However, this effect can not be large otherwise the reverse effect in the *random* mode of stimulation would not be observed.

Main Conclusions

In summary the results of the current study present two main points. Firstly, in combination with the results of Olivier et al. (1995), this study demonstrates that the effect of motoneuron firing rate on response probability is qualitatively the same with Ia and corticomotoneuronal input. This finding does not support the observations of Brouwer et al. (1989) or their conclusions that decreased response probability to TMS at fast rates is a result of decreased motor cortex excitability. Instead these results suggest that the intrinsic properties of the motoneuron result in the rate effects described in the current study. Furthermore, it is important to note that these results may be explained with reference to the biophysical properties of cat motoneurons. Secondly, and most importantly, is the consequence these results have for the current model of human motoneuron trajectories now considered axiomatic in the literature (Ashby and Zilm, 1982b; Miles et al., 1989; Brouwer et al., 1989; Nordstrom et al., 1992; Poliakov et al., 1994; Turker and Cheng, 1994). The essential feature of this model is that a

motoneuron's response probability to a Ia input is independent of discharge rate. This essential feature is clearly challenged by the present results and a need for redressing human motoneuron properties revealed. In light of the need to develop a new model for human motoneurons and the results of the present study, it seems appropriate that this be done in the context of known properties of cat motoneurons.

Physiological relevance

Functionally, the peripheral, the descending and the interneuronal inputs to motoneurons are generally not time locked to the motoneurons action potentials, but arrive randomly. This is equivalent to the *random* mode of stimulation used in this study. Hence the input will be less effective in modulating the discharge of the motoneuron at a higher firing rate unless the intensity of the input increased *pari passu* with the firing rate of the motoneuron. This rate effect on response probability is not due to a busy-line phenomenon but depends on the post-spike membrane properties which vary between the different types of neurons. Another implication of these results, both for experimental results and functional effects is that for two simultaneously firing motoneurons, the slower firing motoneuron (therefore, generally the higher threshold one) will be more responsive to the same input (Bawa and Lemon, 1993).

Chapter 5

EXCITABILITY OF FAST AND SLOW HUMAN MOTONEURONS DURING REGULAR REPETITIVE FIRING AND FOLLOWING DOUBLETS.

Introduction

In cat spinal motoneurons, intracellular recordings have revealed that the soma-dendritic spike is followed by a period of afterhyperpolarization (AHP; Brock et al., 1952). For the duration of the AHP, the relative excitability of the membrane is decreased to transient inputs due to inactivation of fast sodium channels and activation of potassium conductances (Barrett and Crill, 1980; Barrett et al., 1980). The duration and depth of the AHP varies throughout a motoneuron pool in such a way that the motoneurons with the lowest rheobase, exhibit the longest and deepest AHP (Gustaffson and Pinter, 1984; Zengel et al., 1985). The duration of the AHP is correlated to the repetitive firing properties of the cell with minimum repetitive discharge rates being inversely related to the duration of the AHP (Kernell, 1965). This would imply that the lowest threshold motoneurons with the longest duration and deepest AHP, will fire at relatively slow rates and exhibit long periods of depressed excitability following a spike.

Depth and duration of an AHP not only vary with the recruitment threshold of a motoneuron but also with its pattern of activation. The depth and duration of an AHP are significantly augmented when two spikes are fired in succession (Ito and Oshima, 1962) such as following a doublet discharge (Calvin, 1974). This augmentation is due to the algebraic addition of the conductances underlying the AHP (Baldissera and Gustafsson, 1971; 1974b). Thus post-spike excitability of a motoneuron may be significantly affected following a doublet discharge due to an increase in the depth, duration and conductance of the membrane during the AHP.

The objectives of this study were firstly, to systematically investigate the post-spike excitability of the faster firing flexor carpi radialis (FCR) and slow soleus human motoneurons by

measuring their response probability to Ia input volleys at various times during the ISI. The second objective was to compare the changes in post-spike excitability of FCR motoneurons following single spikes and doublet discharges. It is hoped that these data will contribute to a better understanding of the membrane properties of repetitively firing human motoneurons.[1]

Methods

Experiments were performed on nine subjects ranging in age from 26 - 51 years (2 females and 7 males) including all authors. The experimental protocols were approved by Ethics Committees on Human Experiments at Simon Fraser University and the University of Miami, and all subjects gave their informed consent.

Surface EMG and intramuscular single motor unit (SMU) recordings were taken from the right flexor carpi radialis (FCR) and soleus muscles of all subjects. H-reflexes were elicited in FCR by stimulation of Ia afferents in the medial nerve at the cubital fossa, and, in soleus by stimulation of the posterior tibial nerve at the popliteal fossa. For details of recording and stimulation see Jones and Bawa (1995).

Stimuli were delivered in one of two modes: 1) *random* mode in which the stimulus arrived randomly with respect to the discharge of SMU spikes; or 2) *triggered-delay* mode where the stimulus was triggered by an SMU spike to occur at a fixed delay following the SMU spike. In the latter mode the triggered delays varied between 1 - 80 ms for FCR and 1 - 100 ms for soleus during regular repetitive firing. During doublet firing in FCR the delay was varied from 50 - 200 ms.

---

[1] A portion of this study has been presented as an abstract (Jones et al., 1995). I collected the data with either Drs. Bawa or Calancie both at the University of Miami and Simon Fraser University. I did all the analysis at Simon Fraser University under the supervision of Dr. Bawa.

Procedure

The procedures were essentially the same as those outlined in Chapter 4. Briefly, subjects were asked to recruit a low threshold SMU from either FCR or soleus by making a weak isometric contraction, and then maintain the unit's discharge at a relatively slow but steady rate using visual and auditory feedback. Each SMU was then studied with *random* and/or *triggered-delay* modes of stimulation during regular single spike firing or following doublet discharge in FCR.

Data Analysis

Data were analyzed off-line using a 486 personal computer and a 1401plus computer interface from Cambridge Electronic Design (CED; Cambridge, U.K.) as in Chapter 4. Response probability was computed from peri-stimulus time histograms (PSTHs; 0.1 ms binwidth) constructed between stimuli and SMU spikes. A motor unit's response probability at sequential total delays was plotted and the resulting curve was termed the 'response trajectory'. This was done using either *triggered-delay* stimulation or sorting the data acquired during *random* stimulation into 10 ms bins at sequential delays following the spike (see Chapter 4 for details). A smooth curve was approximated to the response trajectory data using the optimal segments technique (Finegood et al., 1988). For noisy data, each data point may be connected to the subsequent point by a straight line, the resulting zig-zag curve provides a rough trend in the data. The method of smoothing for such curves used by Finegood et al. (1988) involves minimizing the differences in the slopes of the sequential line segments joining the data points. The algorithm uses the data values to return a range of possible error values for the data and prompts the user to enter an appropriate error value within that range prior to fitting the smooth curve. Zero % error would produce a curve with more variation in slopes than the original zig-zag curve constructed by joining the data points with a straight line. The larger the error the more closely the resulting smoothed line will resemble a linear fit to the data. We estimated the error for the smoothing

procedure from the standard error of the response trajectory as indicated in the RESULTS (Fig. 5-1).

Results

Data are presented from 39 FCR SMUs, 9 of which exhibited doublet firing, and 6 soleus SMUs. The number of SMUs and observations will be mentioned for each condition separately.

Response trajectories and their variability

Using triggered stimulation we were able to measure response probability at various times following the motoneuron spike. Figure 5-1 illustrates the response trajectory of a single FCR motoneuron and the 95% confidence intervals (broken lines) for response probability at each delay. For five of the eight delays shown in Fig. 5-1 we were able to repeat the measure of response probability at least three times. The average number of stimuli given to estimate the response probability was 40 at any given delay. In the case of the other three delays we did not acquire more than one observation of response probability. For these delays we have used the average standard deviation of 0.05 obtained from the other five delays to estimate the confidence intervals at these points.

The solid line in Fig. 5-1 has been drawn through the data points using the optimal segments method (Finegood et al., 1988). For each delay with multiple observations, mean ± S.E.M. were calculated, and S.E.M. was expressed as a percentage of its mean value (termed S.E.M.%). An average of all S.E.M.% values was calculated. This value fell one quarter of the way through the range of errors returned for our data by the algorithm and was used to smooth the response trajectory curve in Fig. 5-1 and all subsequent figures. The response trajectory illustrated by the solid line shows a monotonic increase in response probability with increasing delay following the motoneuron spike. While there is variability in the estimate of response probability at a given delay, this variability is low and does not critically affect the shape of the response trajectory.

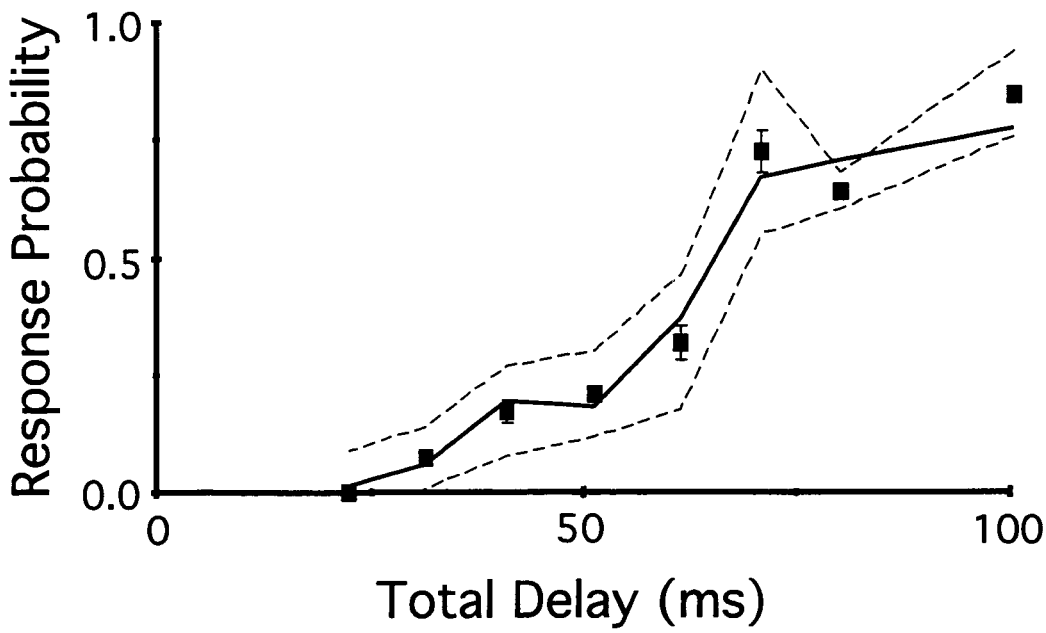

Fig. 5-1. Variability of response probability during the ISI.
Response probability in an FCR motoneuron was measured using *triggered-delay* stimulation at various times following the spike while the unit was firing repetitively with a mean ISI of 113 ms (i.e 8.8 imp/s). Multiple measures of response probability were computed at total delays of approximately 30, 40, 60, 70, and 80 ms. The mean values are plotted with their respective standard error bars (errors at some delays are smaller than the data point). The solid line represents the smoothed response trajectory obtained using the optimal segments technique while the broken line represents the 95% confidence intervals about the mean values of response probability. The probability of the motoneuron responding to the Ia input volley increases in a monotonic fashion throughout the ISI and reaches values near 1.0 at a total delay close to the mean ISI.

Repeated measures of response probability were acquired from two other FCR motoneurons from two separate subjects. In considering all three FCR motoneurons in which we were able to acquire repeated measures for response probability at various delays, we found that the estimate of response probability at a given delay had an average standard deviation of 0.05 with a range from 0.01 to 0.09. The average number of stimuli given at each delay for all three motoneurons was 49. This suggests that our estimates of response probability with approximately 50 stimuli are reliable.

Response trajectories from FCR and Soleus

Figure 5-2A shows 6 of the 37 response trajectories recorded from 32 FCR motoneurons. The average ISI for the tonically firing FCR motoneurons was 112 ± 10 ms (i.e. approximately 9 imp/s)which is in the slow firing range for FCR (Chapter 4). Response probabilities at sequential delays have been connected by thin lines to illustrate the individual response trajectories of the motoneurons. The thin solid lines illustrate responses recorded during triggered delay stimulation while the two broken lines illustrate response trajectories acquired by sorting responses obtained during random stimulation. The thick solid line represents the response trajectory produced by connecting the mean values of response probability from all 37 SMUs. Figure 5-2B shows 6 response trajectories recorded during triggered stimulation of 6 soleus motoneurons. The average ISI for the tonically firing soleus motoneurons was 154 ± 9 ms (i.e. 6.5 imp/s). Again the mean response trajectory calculated from all 6 SMUs is plotted as a thick line. The mean response trajectories in Fig. 5-2A & B were smoothed using the optimal segments technique and the resulting curves are illustrated in Fig. 5-2C. The data symbols represent the mean and standard error bars for response probability at different total delays for the two populations of motoneurons tested.

For both the fast FCR motoneurons and the slow soleus motoneurons the shape of the smoothed mean response trajectory in Fig. 5-2C is similar to the shapes of the individual response trajectories showing a monotonic increase in response probability with increasing delay following

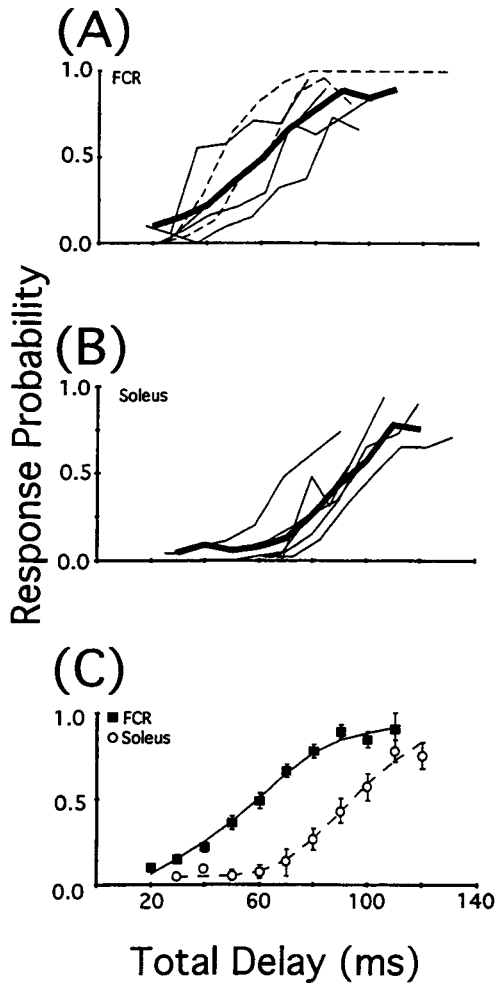

Fig. 5-2. Comparison of FCR and soleus response trajectories.

A. Response trajectories from 6 FCR motoneurons are shown, 4 of which were obtained using *triggered-delay* stimulation (thin solid lines) and 2 obtained by sorting responses during *random* stimulation (thin broken lines). Similar individual response trajectories from another 26 FCR motoneurons were obtained (with a minimum of 4 points per trajectory) and the average response probability at sequential values of total delay (10 ms bins) was calculated from the 32 motoneurons. These values are connected by the thick solid line. **B.** Response trajectories were acquired from 6 soleus motoneurons (thin solid lines) and response probability values were averaged (thick line). **C.** Mean values of response probability at sequential values of total delay are shown (error bars are S.E.M.). A smooth line was drawn through the data points collected from each muscle to represent the smoothed mean response trajectory. The response trajectories differ in both duration (time to reach response probability values of 1.0) and depth (value of response probability at a given value of total delay). Mean firing rates: 9 imp/s (FCR) and 6.5 imp/s (soleus).

the motoneuron spike. The time course of the mean response trajectory in FCR returns to response probability values near 1.0 at a shorter delay following the motoneuron spike than does the response trajectory for the soleus motoneurons. Also the soleus response trajectory seems to have a longer period of low response probability during the first 60 ms following the motoneuron spike.

Response trajectories from FCR during regular repetitive firing and following doublets.

The firing of a doublet greatly affected the response probability of a motoneuron to a Ia volley. Figure 5-3 illustrates the response trajectories from 9 FCR motoneurons during repetitive single spike firing, Fig. 5-3A, and following doublet firing, Fig. 5-3B. Four of the response trajectories for singles and doublets were acquired during random stimulation. During regular repetitive firing the motoneurons had an average ISI of 96 ± 8 ms (i.e. 10.4 imp/s). During doublet firing, the average intradoublet interval was 6 ms with a range between 5 and 15 ms. Values for interdoublet intervals were not assessed as often the motoneurons were not firing doublets in a repetitive fashion (however see Bawa and Calancie, 1983; Kudina and Alexeeva, 1992).

That the firing of a doublet has a significant effect on the response probability of a motoneuron may be illustrated by considering the motoneuron marked by the asterisks in Fig. 5-3A & B. During single spike firing with a mean ISI of 110 ms the motoneuron had a response probability of 1.0 at a delay of 90 ms. Following a doublet the response probability at a delay of 90 ms dropped to a value less than 0.2 with the same stimulus intensity. This represents an 80% reduction in the effectiveness of the Ia volley or post-spike excitability following a doublet.

Figure 5-3C shows the smoothed response trajectory drawn through the mean response probability values obtained during single spike firing and following doublet discharge at various delays. The response trajectory following doublet discharge has zero values for the first 60 ms following the first spike of the motoneuron doublet after which it slowly increases. The mean response trajectory during regular single spike firing reaches a response probability of 0.5 near a

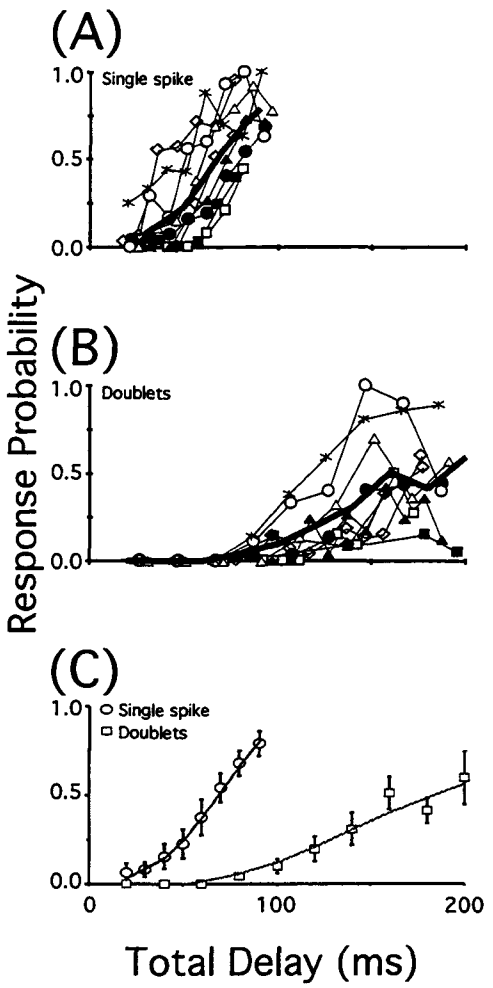

Fig. 5-3. Effect of doublet discharge on response trajectory of FCR motoneurons. **A.** Response trajectories are shown for 9 SMUs which were firing with mean values of ISI = 96 ± 8 ms during regular single spike firing. The resulting average response trajectory (thick line) was not significantly different from that shown in Fig. 2A. **B.** These same 9 SMUs were capable of firing doublet discharges with an intradoublet interval between 5-15 ms. The response probability of a motoneuron was significantly reduced following the discharge of a doublet. The mean value of response probability at a given delay was calculated and the resulting curve is represented by the thick line. **C.** The mean values of response probability at sequential total delays were fitted by a smooth line to give the smoothed mean response trajectories during regular repetitive firing and following doublets. The time course of the response trajectory is markedly slower following a doublet discharge.

delay of 70 ms whereas following a doublet, the delay must be approximately 200 ms to reach the same value of response probability.

Effect of stimulus intensity on response trajectories

The size of the composite EPSP generated by the Ia volley is a significant factor contributing to response probability and hence the shape of the response trajectory. Response trajectories were collected from 3 FCR motoneurons and 1 soleus motoneuron with at least two different stimulus intensities while the motoneurons were firing at constant firing rates. Figure 5-4 shows response trajectories from an FCR motoneuron (mean ISI = 110 ± 6 ms) at three different stimulus intensities. The response probability increased with increased stimulus intensity, making the response trajectories shallower and shorter in duration. It is of interest that at the shortest delay of approximately 18 ms (Fig. 5-4), response probabilities converged at the three levels of stimulus intensity.

In another FCR motoneuron, firing at a faster rate with an ISI of 80 ms, response probability was evaluated for four different stimulus intensities at a delay of 22 ms (the shortest delay testable in this unit with triggered stimulation). At the lowest stimulus intensity used the response probability was 0.29 which increased to 0.45 then to 0.80. The value for response probability seemed to saturate around this level as the highest level of stimulus intensity resulted in only a small increment in response probability to 0.84.

Discussion

The primary aim of this study was to add further experimental results in order to understand the biophysics governing the repetitive firing of human motoneurons (Olivier et al., 1995; Jones and Bawa, In press). In the previous chapter we examined the post-spike responses of repetitively firing motoneurons to peripheral Ia volleys. Those results suggested that the responses of human motoneurons could be qualitatively explained with reference to the properties of repetitively firing cat motoneurons. Encouraged by these initial suggestions, we wanted to

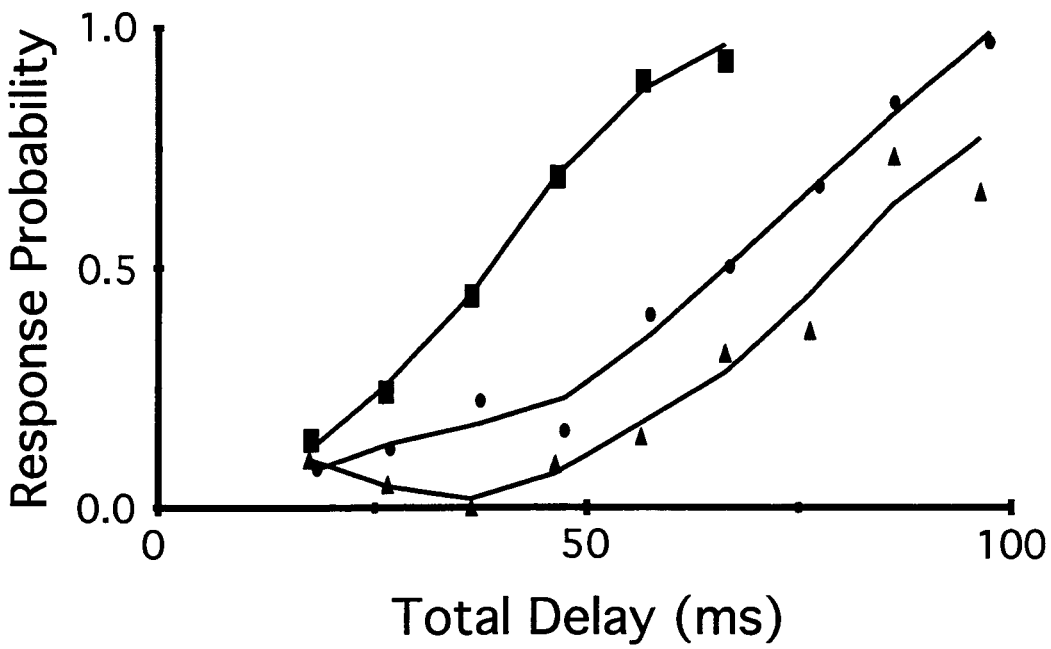

Fig. 5-4. Effect of stimulus intensity on the response trajectory of a motoneuron. Using *triggered-delay* stimulation the response trajectory of an FCR motoneuron was computed for three different stimulus intensities (low ▲; medium ●; and high ■). The mean ISI (110 ms) was similar during testing with all three stimulus intensities. The response trajectories have been drawn as smooth lines through the data points. As the stimulus intensity increased both the depth of the response trajectory, relative to 1.0, and the duration (from earliest delay to delay at which response probability reached 1.0) decreased. The responses trajectories at all stimulus intensities converged at the shortest delay of 18 ms.

explore further the equivalence of human and cat motoneurons. The present study compared response trajectories of: 1) motoneurons innervating fast and slow muscles; 2) a motoneuron during normal rhythmic firing and after a doublet; and 3) the effects of the intensity of input volley on the shape of the response trajectory.

In comparing FCR and soleus motoneurons, there were differences in the durations and shapes of the mean response trajectories. The differences in duration of the response trajectory, the time to return to response probability values near 1.0, are due in part to differences in the firing rates of the two populations of motoneurons, 9 imp/s in FCR and 6.5 imp/s in soleus. However, the differences in firing rates of FCR and soleus SMUs at these relatively low rates are presumed to be primarily due to inherent differences in the depth and duration of their AHPs. The two motoneuron populations have different minimal rhythmic firing rates upon recruitment during weak isometric contraction which is strongly correlated in cat motoneurons, recruited by current injection, with the duration of the AHP (Kernell, 1965b). Therefore, the differences in duration of the response trajectories reflect this underlying difference in the two populations of motoneurons tested.

It is not only the durations, but the general shapes of response trajectories from the two motoneuron populations that were different. Firstly, in the slower firing soleus motoneurons the response probability at a given delay is less than that of the FCR motoneurons. This results in a deeper response trajectory for the soleus motoneurons suggesting a difference in the underlying AHP trajectory near the minimal rhythmic firing rate of the two populations of motoneurons. However, other factors such as input conductance may also contribute to this apparent difference in depth. In repetitively firing cat motoneurons, input conductance at a particular delay following a spike depends on the firing rate of the cell (Schwindt and Calvin, 1973). In the slower firing soleus motoneurons then, the input conductance may be higher at sequential delays than that in the faster firing FCR motoneurons which would result in a lower response probability.

In the above comparisons, the question of similarity of input currents to the two populations of motoneurons is raised. This factor was eliminated when the response trajectories

were compared for single spike and doublet firings. Since the single spikes and doublets were firing randomly, equal input currents were guaranteed under both firing modes and the response trajectories would reflect only the differences in the membrane voltage trajectories and the magnitude of the input conductances.

Intracellular recordings have revealed increases in the depth of the AHP following doublet up to two fold compared to that during regular single spike firing (Calvin, 1974). The response probability at any phase of ISI, if it were dependent only on the membrane trajectory, would be reduced to, at the most, half following a doublet. But our experimental data shows that it was reduced considerably more. For example when the mean value of response probability was 0.81 at a total delay of 90 ms during normal firing, it decreased to a mean value <0.2 after a doublet (Fig. 5-3C). This suggested that the shunting of the input current affects the response probability considerably. Ito and Oshima (1962) report an increase in the peak membrane potential of the AHP of 49 % following two closely spaced spikes, however, the input conductance at the peak of the AHP is 100% higher than that following a single spike. Such high values for input conductance following a doublet may tend to shunt a great majority of the current arising from the input volley and thus result in a much greater decrease in response probability than could be attributed to differences in membrane potential alone.

Shunting of input current may also have resulted in the convergence of response trajectories elicited with different stimulus intensities (Fig. 5-4). In this case the motoneuron was firing at the same slow firing rate and therefore the membrane voltage trajectory during the ISI would have been consistent throughout. The only difference contributing to the three different response trajectories was the size of the input volley. The two response trajectories elicited by the lower stimulus intensities seemed to have parallel time courses throughout most of the ISI which seemed to suggest a simple relationship between the size of the input volley and the resulting response trajectory. The third response trajectory elicited by the highest stimulus intensity did not appear to run parallel to the other two trajectories but instead appeared to have a steeper slope. Further discussion of the effect of EPSP amplitude on the response trajectory is left to Chapter 7.

In spite of the convergence of response trajectories at the shortest delay at slower firing rates, we were able to obtain quite high response probability values at shorter ISIs. When a motoneuron was fired at a faster rate (ISI=80 ms), we were able to obtain response probability values as high as 0.84 at a total delay of 22 ms. This effect could result from a shallower membrane voltage trajectory and lower input conductance at the faster firing rate.

Conclusions

The results of the present study highlight the contribution of membrane conductance in addition to the membrane voltage to the post-spike excitability of human motoneurons. Based on membrane voltage trajectories, the cat data would suggest the response trajectories after doublets to be, at most, twice as deep as those during regular single spike firing at a slow rate. But the present data show that the post-doublet excitability was much lower than predicted by membrane voltage alone. We attribute this result to the input conductance of the membrane. Another effect attributed to high membrane conductance is the shunting of input currents resulting in convergence of response probabilities at very short post-spike delays acquired at three different stimulus intensities while the motoneuron was firing at a slow rate. The shunting effect of high conductance seems to be quite obvious at this phase of the ISI. None of the previous literature has taken conductance into account when considering response probability of a motoneuron to Ia input.

Functional Significance

Does the response trajectory reflect the recovery phase of the AHP? If AHP alone determined the post-spike excitability, the response trajectory would have the shape of a step function (Chapter 4). However, the synaptic noise (Calvin and Stevens, 1968) converts this step function into a sigmoid. This sigmoid is further affected by the membrane conductance which varies continuously during the duration of the ISI (Baldissera and Gustafsson, 1974; Ito and Oshima, 1962; Schwindt and Calvin, 1973). Judging from the results of Chapters 4 and 5, one

can say that the membrane voltage trajectory has a dominant effect on the shape of the response trajectory. This occurs as a result of the noise in the system. The relative effects of membrane voltage, conductance and noise will be explored further in Chapter 7.

Chapter 6

COMPARISON OF PERIPHERAL IA AND CORTICOMOTONEURONAL COMPOSITE EPSPS IN HUMAN MOTONEURONS.

Introduction

The spindle Ia afferent to α-motoneuron synapse has been studied extensively using anatomical, electrophysiological and modeling techniques. These studies have led to a better understanding of the relationship between Ia inputs, synaptic potentials and the resulting effects on motoneuron discharge (Gustafsson and Pinter, 1984; Walmsley and Stuklis, 1989; Segev, Fleshman and Burke, 1990).

In cases where intracellular recordings are not possible, EPSP parameters (amplitude, rise-time) may be estimated using spike train analysis techniques. When a rhythmically firing motoneuron receives a transient input, the peri-stimulus time histogram (PSTH) shows an excitatory peak. Using composite EPSPs produced by electrical stimulation of homonymous Ia afferents, it has been shown in the cat that the area of the PSTH peak is directly related to the EPSP amplitude, while the duration of the peak is directly related to the rise-time of the EPSP (Fetz and Gustafsson, 1983). Adopting this approach, we compared the characteristics of PSTHs derived from human motoneurons in response to peripheral Ia and descending corticomotoneuronal volleys. From these observations we deduced the shapes of the composite EPSPs, giving insight into the nature of the synaptic inputs from the two sources.[1]

---

[1] A portion of this study has been presented as an abstract (Jones et al., 1995). The data was collected at both Simon Fraser and the University of Miami with Drs. Bawa, Calancie and Hall. I did all the analysis at Simon Fraser University under the supervision of Dr. Bawa.

Methods

Experiments were conducted on 8 right-handed subjects ranging in age from 24 - 51 years. Experimental protocols were approved by the 'Human Ethics' committees at the two institutions, and all subjects gave their informed consent. Single motor unit (SMU) activity was recorded from the right flexor carpi radialis (FCR) muscle with highly-selective, bipolar needle electrodes (Chapter 2) and surface EMG was recorded over the muscle belly using Ag-AgCl disc electrodes (Grass Instrument Co.). A subject was asked to recruit a low threshold SMU by making a weak, isometric contraction, and then maintain the unit's discharge at a relatively slow but steady rate using visual and auditory feedback. The motor unit shape was discriminated to generate a trigger pulse (BAK Electronics, Inc.).

Input Volleys

Ia volleys were produced either by an electrical stimulus applied to the median nerve through a bipolar felt electrode placed at the cubital fossa, or by delivering a tap to the FCR tendon at the wrist via a moving coil linear motor (Model 310, Cambridge Technology, Inc.). Electrical stimuli to elicit the H-reflex were constant-current, 0.5 ms square-wave pulses, of sufficient magnitude to elicit an H-reflex with minimal M-wave. The contact surface of the hammer percussing the FCR tendon was 5 mm wide and consistent positioning throughout the experiment was maintained by clamping the subject's forearm and hand in a fixed position. Taps were elicited in a length controlled fashion with a duration of 3.0 ms and an amplitude adjusted so that the surface EMG reflex response (peak-to-peak) matched that elicited by electrical stimulation during a given experiment. Descending corticomotoneuronal volleys were generated by transcranial magnetic stimulation (TMS) of the motor cortex using a circular coil of 9.5 cm outer diameter (Cadwell MES-10). In all cases the coil was positioned along the midline, with the center approximately 1 cm anterior to the vertex (C_z). For all inputs, the minimal interval between

successive stimuli was never less than 3.5 seconds. Peripheral and TMS inputs were delivered in either *random* or *triggered-delay* mode (see Chapter 4 for details).

Analysis

The sampling rate for data acquisition was 10 kHz while PSTHs were constructed with bin widths of 0.1 ms (*Spike2*; Cambridge Electronics, Inc.). The PSTHs showed periods of increased responses with onsets ranging from 12 - 25 ms (depending on the subject, the stimulus and the motor unit). The total durations of increased response probability above background, termed peak width, was determined and compared for the three excitatory inputs.

To estimate the rising phase of the underlying EPSP, a cumulative bin integration was performed over all the bins of the peak obtained during random stimulation, starting with x=1 as the first bin of the excitatory peak (Homma and Nakajima, 1979). The cumulative values at each bin were normalized with respect to the total area of the peak (number of counts in the peak) and the resulting normalized values were fit, by the method of least mean square, to the following equation (Homma and Nakajima, 1979):

$$Y(x) = x^{s} \cdot \exp\left(\frac{-s \cdot x}{RT}\right), \qquad (1)$$

where x is the bin number (0.1 ms per bin), s represents slope, RT is the time constant and Y(x) is the normalized cumulative value at bin x. The time constant, RT, determines the duration of the rising phase of the function and, therefore, approximates the rise-time of the underlying EPSP. The results of integration of the PSTH peak, and the shape of the response trajectories were used to make conclusions about the rise times of the underlying EPSPs.

Statistical analysis of the data utilized paired t-tests when comparing SMUs receiving excitatory input from two sources, and independent t-tests when comparing the populations of SMUs receiving either H-reflex or TMS input. Significance is reported for values of $p < 0.05$.

Results

Data were obtained from recordings of 31 flexor carpi radialis SMUs. Twelve of these SMUs were studied with the *triggered-delay* mode of stimulation with each motor unit receiving both H-reflex and TMS inputs. Six of these motor units were also studied with *random* stimulation: 2 received both H-reflex and TMS inputs, 3 received TMS only and 1 received H-reflex input alone. Thirteen units were studied with *random* stimulation alone with 11 of those receiving H-reflex and 2 receiving TMS input. An additional 6 SMUs were studied in the *triggered-delay* and *random* mode using both H-reflex and tendon tap input to each motor unit.

The mean interspike interval (ISI) of SMUs receiving H-reflex input was 108.2 ± 3.0 ms (± S.E.M.) while those receiving corticomotoneuronal input had a mean ISI of 105.8 ± 4.0 ms. The ISIs (inverse of firing rate) were not significantly different for the two inputs. The onset latency during random stimulation ranged between 14.3 - 25.5 ms (19.6 ± 1.4 ms) for TMS, 17.4 - 27.9 ms (21.0 ± 0.9 ms) with H-reflex input and 24.1 - 31.5 ms (27.8 ± 3.7 ms) with tendon taps.

Random Stimulation

Random stimulation resulted in short latency excitatory peaks in the PSTHs whose total widths varied between 0.8 - 1.6 ms (1.25 ± 0.06 ms) for H-reflex, and between 3.6 - 5.2 ms (4.43 ± 0.23 ms) for TMS. However, the excitatory peaks resulting from TMS were generally segmented into 2-3 subpeaks: SP_1, SP_2, SP_3 (Olivier et al., 1995). We limited our investigation to the SP_1 response which has been suggested to arise from the D wave (Edgley et al., 1990), in comparing peripheral and corticomotoneuronal inputs. The mean peak width of the SP_1 response was 1.33 ± 0.08 ms and ranged between 1.0 - 1.6 ms. The values for peak widths in response to H-reflex input were not significantly different from those of the SP_1 response.

Figure 6-1 shows PSTHs from a motor unit in response to both H-reflex and TMS input during random stimulation. In the bottom part of Fig. 6-1, the peaks of the PSTHs have been

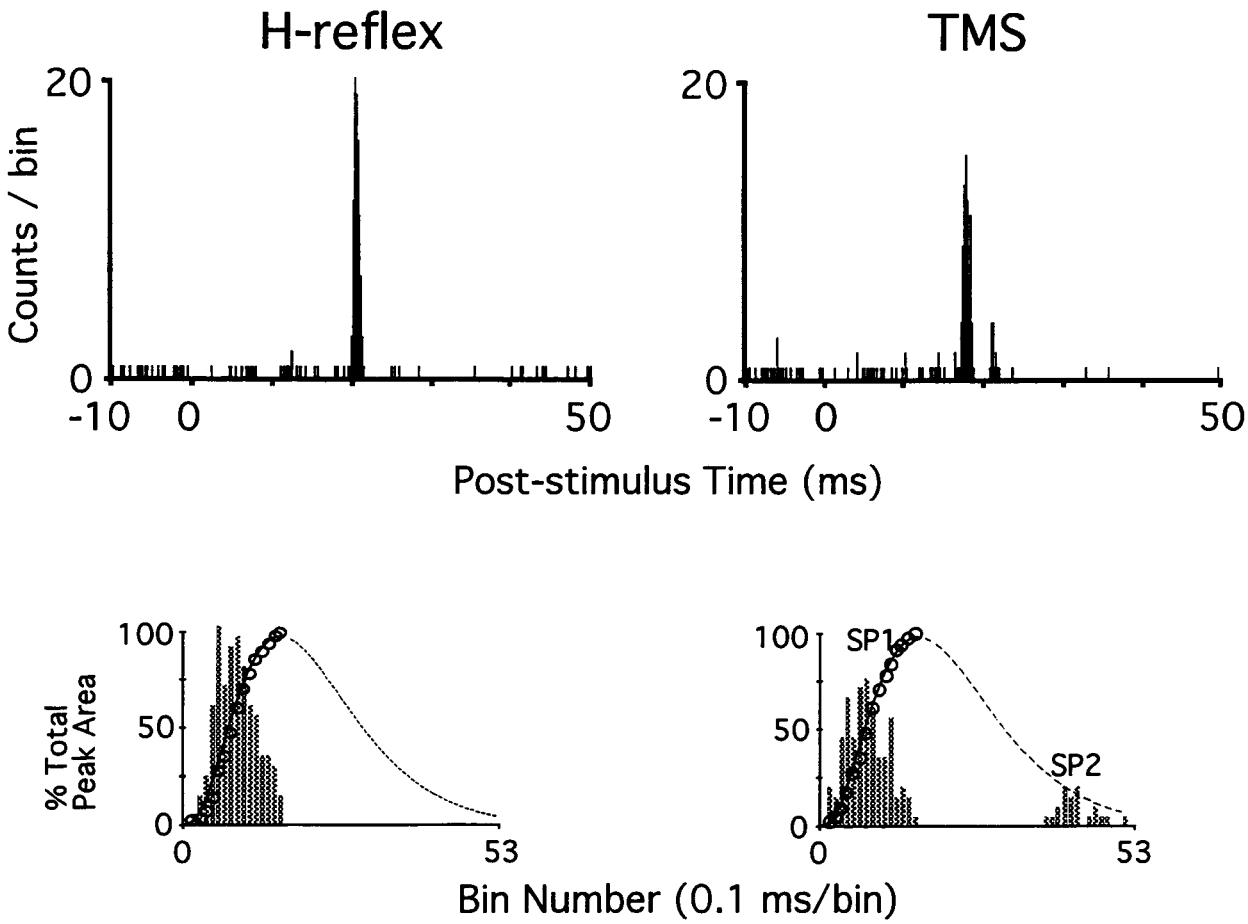

Fig. 6-1. PSTHs of a SMU in response to H-reflex and TMS inputs.

The top part of the figure shows the PSTHs generated by H-reflex (left) with peak onset at 19.4 ms (# of stimuli, n=293) and the TMS-evoked PSTH with peak onset at 16.8 ms (right; n=326) during random stimulation. The SMU was firing with a mean ISI of 100 ms during both conditions. The peaks of the PSTHs are shown on an expanded time scale in the bottom panels of the figure showing the H-reflex peak width of 1.5 ms and the TMS peak width of 5.2 ms. The TMS peak is composed of two subpeaks, SP_1 and SP_2, with the SP_1 peak width of 1.5 ms. The open circles are normalized cumulative bin values for the peaks. The solid lines overlaying the peaks are an estimate of the rising phase of the EPSP obtained by fitting *Eq. 1* to the open circles (see METHODS). The parameters for the equation are: H-reflex, s = 2.85, RT = 13.6 bins; SP_1, s = 2.80, RT = 14.0 bins.

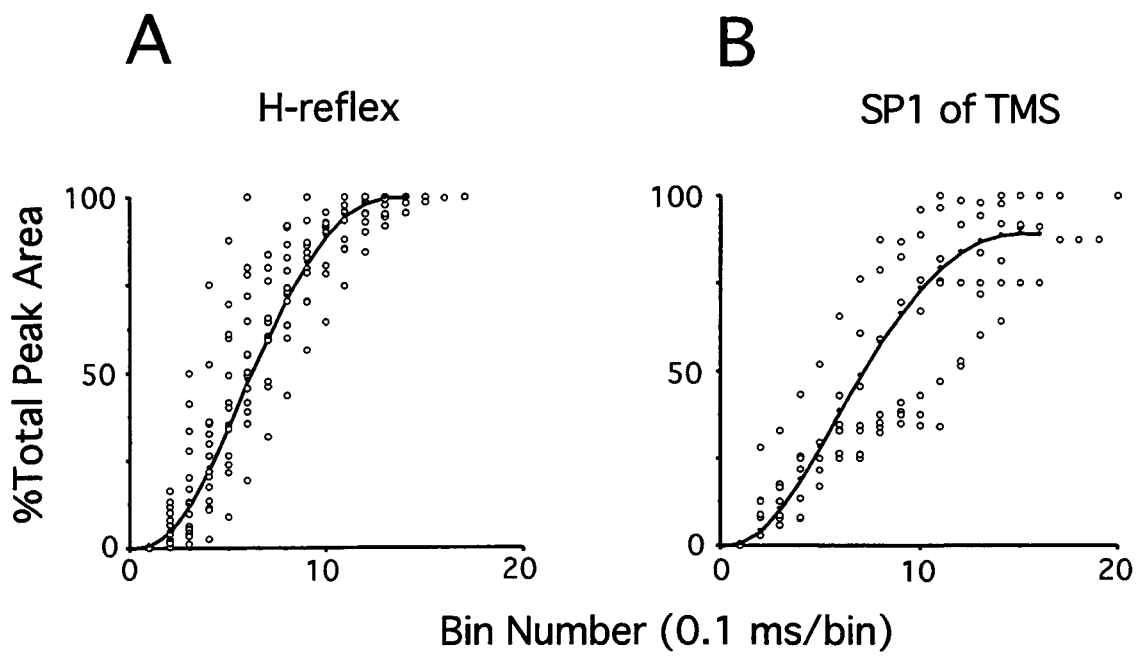

Fig. 6-2. Averaged estimate of the rising phase of the composite EPSP.

Normalized cumulative data points for 14 peaks for H-reflex (A) and 7 peaks for SP1 (B) are shown by the open circles. *Eq. 1* was fitted to these data points to obtain an average rising phase of the respective EPSP. The results of the curve fit are shown by the solid line which is plotted for values up to x = RT. For H-reflex input (A), the resulting fitted curve had the parameters of s = 2.9, RT = 13.5 bins where the curve fit had an r = 0.91 with a standard error of the estimate (SEE) = 14.9 %. For the SP_1 component of the TMS input (B), the resulting fitted curve had the parameters of s = 2.6, RT = 15.1 bins where the curve fit had an r = 0.88 and an SEE = 16.1 %. Therefore, the fitted curves estimate the rise-times of the composite EPSPs to be 1.35 and 1.51 ms for H-reflex and SP_1 respectively.

expanded showing a peak width of 1.5 ms for both the H-reflex and SP_1 of the TMS input. The solid curve overlying the histogram peaks is the best fit of *Eq. 1* to the experimental values (open circles) and represents an estimate of the rising phase of the composite EPSP acting upon this motoneuron. The subsequent broken line represents the solution of *Eq. 1* beyond experimental points and is shown only to facilitate visualization of our data with respect to the profile of an EPSP as recorded in the cat.

Figure 6-2 illustrates the results of integration and curve fitting of *Eq. 1* to all the data collected during random stimulation. The data points (open circles) in Fig. 6-2A represent the cumulative bin integration for 14 SMUs in response to H-reflex stimulation and Fig. 6-2B for 7 SMUs in response to TMS input. The calculated time constant for the curve describing the H-reflex responses is RT = 13.5 bins while that for the curve describing the TMS input is RT = 15.1 bins. The rise-time estimates of 1.35 ms and 1.51 ms for responses to H-reflex and TMS respectively, are slightly higher than the mean peak widths for H-reflex and the SP_1 as reported above, but fall within one standard deviation of the mean.

Triggered Delay Stimulation

At the longest delay tested, response probability and peak width had their greatest values. Comparison of the mean peak widths at this delay revealed no significant differences in a single motor unit's response to H-reflex (1.23 ± 0.09 ms) or TMS (1.20 ± 0.10 ms; SP_1). These values of peak width obtained with *triggered-delay* stimulation were compared to those obtained with the same input during *random* stimulation; no significant differences were found (n=12).

In the *triggered-delay* mode, the response probability of a motor unit decreased for shorter delays, regardless of the source of excitation (TMS, H-reflex or tendon tap; Fig. 6-3). This decrease was accompanied by an increased onset latency and narrowing of the PSTH peak (see Olivier et al., 1995 Fig. 2A). It is suggested that if two inputs result in response peaks of quite different widths, the response probability would fall more sharply at shorter delays for that input producing the narrower peak. That is, the response trajectories resulting from the two inputs

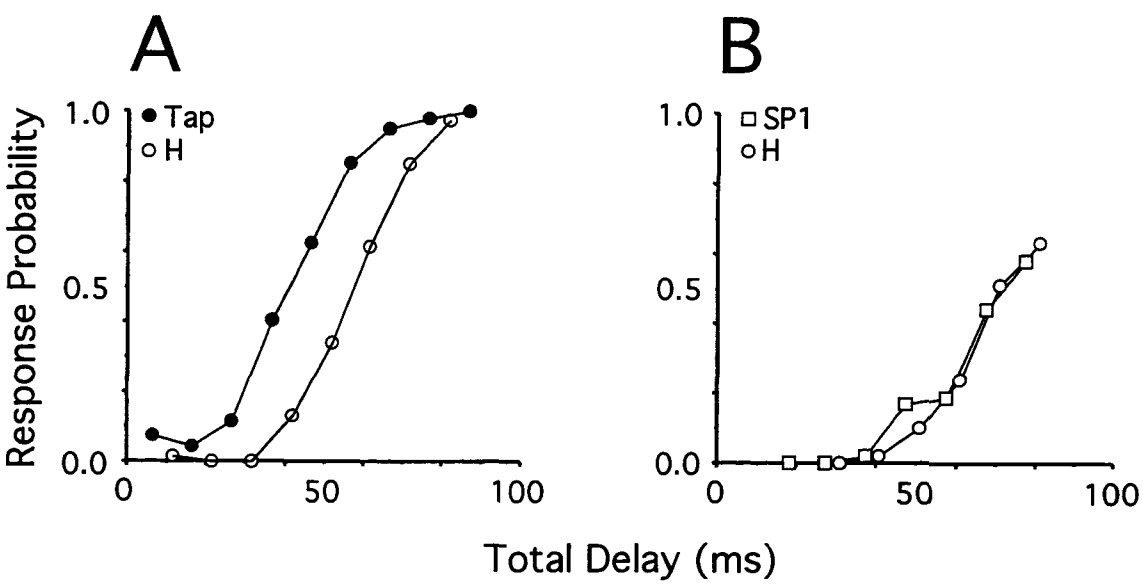

Fig. 6-3. Response trajectories and the influence of peak width.

A: Response trajectories in an SMU are shown for two inputs, tendon tap (•) and H-reflex (**o**). The SMU was firing repetitively with an ISI of 105 ms during taps and 110 ms during H-reflex. The two trajectories started at approximately the same probability values at the longest delay. As the delay was shortened, the trajectories deviated from each other. Response probability fell sharply for the short duration H-reflex peak (1.5 ms) compared to that for the longer duration peak (4.4 ms) with tendon taps. **B**: Response trajectories of an SMU subjected to H-reflex and TMS input during repetitive firing with a mean ISI of 95 ms during both conditions. The trajectories for H-reflex and SP_1 start from a similar response probability at the longest delays and overlap throughout the course of the trajectory suggesting similar rise-times of the EPSPs. Total delay is equal to the *triggered-delay* plus the time to onset of the response peak.

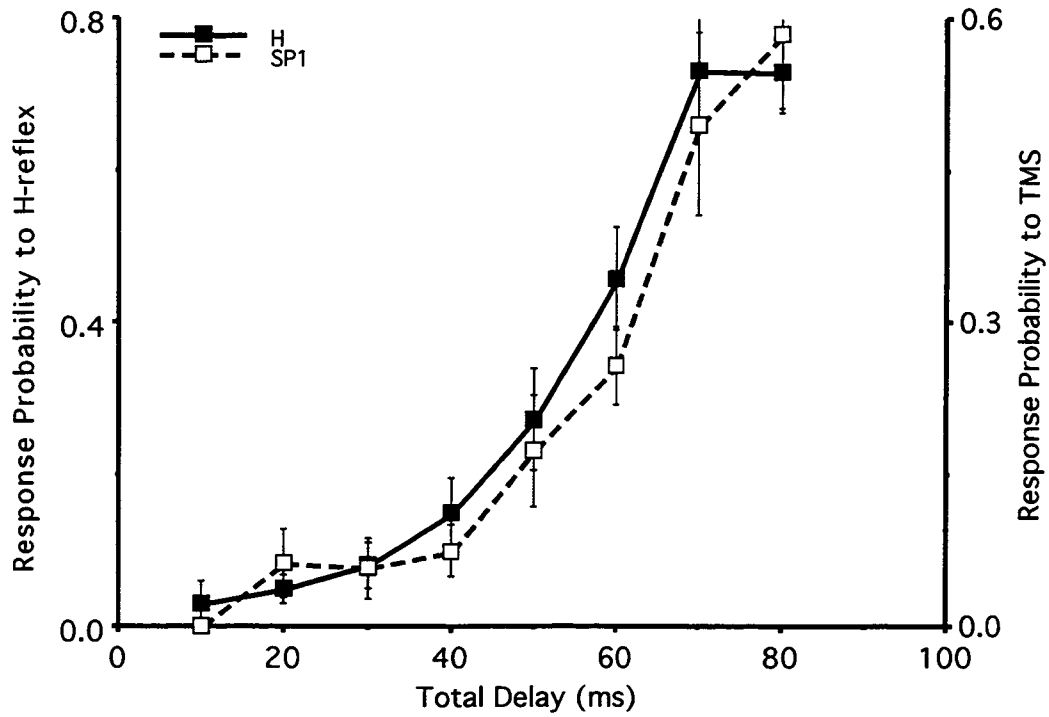

Fig. 6-4. Average response trajectories for H-reflex and SP_1 responses.

The figure shows the mean and standard error from 12 SMUs for response probabilities at different total delays. The response probabilities have been plotted along separate ordinates so that both H-reflex and SP_1 start from a similar position at the longest delay. The shapes of the two response trajectories overlap and suggest no differences between the rising phases of the composite EPSPs underlying the two inputs.

would not overlap. This hypothesis was tested with inputs produced by tendon taps and H-reflex in 6 SMUs. The peak widths with tendon taps were 3.70 ± 0.46 ms and with H-reflexes were 1.25 ± 0.15 ms. Figure 6-3A shows the response trajectories from a SMU to tendon tap and H-reflex inputs. While both inputs result in response probabilities near 1.0 at the longest delay, the response probability falls more sharply for the narrower H-reflex peaks as the delays are shortened. Applying the same logic, we compared the response trajectories for SP_1 and H-reflex inputs. Figure 6-3B shows that the time course of the response trajectories overlap for the SP_1 response to TMS and the electrically induced Ia volley for this motor unit.

Averaged data for 12 SMUs receiving both H-reflex and TMS inputs in the *triggered-delay* mode are illustrated in Figure 6-4. The response probabilities for the two inputs are plotted on separate ordinates so as to overlay response probabilities from the two sources at the longest total delay. This allows for a comparison of the mean response trajectories resulting from the two inputs. This figure illustrates that the rate of change of response probability is similar for both H-reflex and TMS input.

Discussion

The primary aim of this study was to compare the responses of repetitively firing FCR motoneurons to peripheral Ia and corticomotoneuronal inputs. The inputs were delivered randomly with respect to the discharge of the motor units or at a fixed delay following the motor unit discharge. Results of the study suggest that the composite EPSPs which underlie the responses of motoneurons to H-reflex and SP_1 of the TMS input have similar rise-times.

The rise-time of a composite EPSP is governed by many factors including: 1) the passive membrane properties of the motoneuron (Rall, 1967; Gustafsson and Pinter, 1984); 2) the history of synaptic activation (Lüscher et al., 1983); 3) the time course of the post-synaptic conductance (Lev-Tov et al., 1983); 4) the temporal dispersion of synaptic bouton activation (Walmsley and Stuklis, 1989; Segev et al., 1990); and 5) the spatial location of the active synaptic boutons (Rall,

1967; Walmsley and Stuklis, 1989). We will examine each of these factors in turn and their possible contributions to the present results.

The first factor of passive membrane properties was accounted for by recording responses to the two inputs (Ia and corticomotoneuronal) from the same motoneuron or the same population of low threshold motoneurons. The second factor - history of synaptic activation - would have little effect on the present results since the stimuli were delivered at slow rates (< 0.3 stimuli/s). With respect to factor three, there is no evidence as yet which would suggest that the time course of post-synaptic conductance changes associated with Ia or CM input to motoneurons is different. Therefore, the contribution of this factor may be insignificant.

We believe that the last two factors play a significant role in the interpretation of the present results. Different degrees of temporal dispersion of an input, factor four above, are known to cause differences in the rise-times of composite EPSPs (Walmsley and Stuklis, 1989). We have demonstrated this effect by creating different amounts of temporal dispersion in the same pathway to the motoneuron by using two different stimuli to excite Ia afferents. Electrical stimulation of peripheral nerves produces near-synchronous activation of the fast conducting Ia afferents. We expect that the temporal dispersion of this volley would be minimal (Segev et al. 1990). Edgley and coworkers (Edgley et al., 1990) have convincingly argued that SP_1 results from the direct excitation of the CM cells resulting in a D-wave. If the dispersion within the D-wave with TMS was higher than that of the H-reflex we would expect longer rise-time estimates, but this was not the case. It does not, on the other hand, seem that the temporal dispersion within the D-wave would be significantly less than the already minimal values obtained with H-reflex. Therefore, this factor is not likely to play a significant role in the comparison of rise-times computed for H-reflex and the SP_1 response with TMS input.

The fifth factor affecting composite EPSP rise-time is the distribution of the synaptic boutons on the soma-dendritic membrane. This information may be obtained either from anatomical reconstruction or electrophysiological estimates. To date, there have not been detailed anatomical studies on the distribution of synapses from the CM cells to motoneurons, in contrast

to studies of Ia synaptic distribution (Burke et al., 1979). The electrophysiological estimates of the synaptic location rely upon the axiom that the further a current source is from the soma, the longer the rise-time of the resulting voltage transient (Rall, 1967). The earliest work in baboon forearm motoneurons suggested similar time courses for both CM and Ia EPSPs (Clough et al., 1968). A similar conclusion was reached by Jankowska et al. (1975) for hindlimb motoneurons of Macaca irus monkeys. These authors further concluded that there was an overlap in distribution of synapses made by group Ia and CM cells on the soma-dendritic surface of the motoneuron (but cf. Porter and Hore, 1969).

Given the above arguments, the present results are consistent with a similar distribution of synaptic boutons for both Ia and corticomotoneuronal inputs to the upper limb FCR motoneurons in man. The significance of these results to motor control theory is the importance of the interplay between the functional role of an input and its position on the soma-dendritic membrane. Since the CM pathway is the efferent limb of the transcortical servo loop (Phillips, 1969), then it seems reasonable that its synaptic input to the motoneuron overlaps with that of the segmental servo loop. The role of the CM pathway during voluntary contractions implied by the proximal placement of CM synapses in the present results, suggests that this pathway would be effective in directly controlling the discharge rate of the motoneurons. Distally distributed inputs, on the other hand, would be more effective in modulating the integrative properties of the motoneuron.

Chapter 7
COMPUTER SIMULATION OF HUMAN SPINAL MOTONEURONS.

Introduction

The biophysical properties of a motoneuron impart and structure the computational process in which the cell is engaged. These biophysical characteristics include both active and passive parameters resulting from a host of ligand- and voltage-dependent ionic channels, the resistive and capacitive elements of the membrane and the ionic concentration inside and outside the cell. None of these factors can be assessed in human studies and for this reason results from animal studies, especially on cat motoneurons, are cautiously extrapolated to the human spinal cord.

In repetitively firing spinal motoneurons of the cat, intracellularly recorded membrane voltage trajectories between spikes undergo predictable changes with increases in firing rate (Baldissera and Gustafsson, 1974; Schwindt and Calvin, 1972). Within the primary range of firing an increase in firing rate is accompanied by a decrease in the maximum depth of the membrane voltage trajectory (the scoop) following a spike with relatively little change in the latter portion of the trajectory (the ramp) in which the membrane potential approaches threshold in a ramp-like fashion (Schwindt and Calvin, 1972). The changes in membrane voltage at different firing rates are accompanied by firing rate dependent changes in membrane conductance (Schwindt and Calvin, 1973). These changes in membrane voltage and conductance during the ISI are expected to alter the excitability of the motoneuron and because of their rate dependence, motoneuronal excitability is predicted to vary with firing rate. In addition to the effects of membrane voltage and conductance, the excitability of the motoneuron is affected by the level of membrane noise produced by background synaptic input (Calvin and Stevens, 1968).

The aim of the previous studies was to design human experiments that would employ changes in motoneuronal excitability as a means of obtaining information about the intrinsic properties of human motoneurons (Chapters 4 and 5). Having obtained those results, the

objectives of the following simulations were: 1) to begin to develop a model which is capable of describing the responses of repetitively firing human motoneurons to transient input volleys; and 2) to highlight the importance of factors other than membrane voltage trajectory in determining the excitability of repetitively firing motoneurons.

The motoneuron models in the present thesis have been architecturally and electrotonically fashioned after an S and an FR type motoneuron innervating the medial gastrocnemius muscle of the cat (Cullheim et al., 1987; Fleshman et al., 1988). The conductances used included a sodium and fast potassium conductance in the initial segment as well as a sodium, fast potassium and slow potassium conductance in the soma (Dodge and Cooley, 1973; Traub, 1977). The slow potassium conductance was described as a time- and voltage-dependent process rather than a calcium mediated process for simplicity. The results from this preliminary model support the general idea that extrapolation of properties of cat motoneurons to human motoneurons is appropriate for the explanation of the results described in Chapters 4 and 5.

Methods

All simulations were done with the Nodus software (De Schutter, 1989) on a Macintosh Centris 660AV computer. Spike train data resulting from the simulations was analyzed using the SPIKE2 software (Cambridge Electronic Design) as described in Chapters 4, 5 and 6.

Neuron Structure

Motoneurons were modeled in a compartmental fashion with partitions representing the soma, initial segment and equivalent dendrite. The measurements of the compartments were based on the reconstruction of cat lumbosacral motoneurons reported in the literature (Cullheim et al., 1987; Fleshman et al., 1988). The specific cells used from these publications were an S type soleus motoneuron (identified as cell 35/4) and an FR type MG motoneuron (cell 43/5). The structure of the two motoneurons is illustrated in Figure 7-1. The soma is represented by a sphere with a diameter of 50.9 or 48.8 μm for the S and FR motoneuron respectively (Cullheim et el.,

1987). The initial segment compartments are represented by cylinders of the same size in both neurons with a diameter of 10 and length of 100 μm (Traub, 1977). The dendrites for each motoneuron are represented by an equivalent cable whose diameter changes as a function of distance from the soma (Fleshman et al., 1988; Clements and Redman, 1989). Each equivalent dendrite is based on measurements taken from Fleshman et al. (1988; Fig. 9, Step Model). The diameter of the stem compartment of the equivalent dendrite ($d_{eq(stem)}$) was estimated from the equation

$$d_{eq(stem)} = \left[\sum_{j=1}^{n} d_j^{\frac{3}{2}} \right]^{\frac{2}{3}}, \qquad 7\text{-}1$$

where d_j is the mean diameter of the j'th stem dendrite for n number of stem dendrites (Fleshman et al., 1988). Starting with a stem diameter of 25 μm , the equivalent dendrite for the S type motoneuron extended for 17 compartments to a final diameter of 0.63 μm. The FR type motoneuron had an equivalent dendritic stem diameter of 40 μm which gradually narrowed to a diameter of 1 μm in the nineteenth and final compartment. Both dendrites terminated in a closed end. The length of each dendritic compartment was varied so that no compartment had an electrotonic length greater than 0.2 λ (Segev et al., 1985). The total lengths of the equivalent dendrites were 7000 and 6675 μm for the S and FR type motoneurons, respectively.

Passive and Active parameters

The passive parameters determining the cable properties of the neurons were set according to the results of Fleshman et al. (1988) on these two cells. Specific membrane capacitance, C_m, was 1.0 μF/cm^2, specific cytoplasmic resistivity, R_i, was 70 Ω·cm and the specific membrane resistivity, R_m, was set according to the step model of membrane resistivity (Fleshman et al., 1988; Clements and Redman, 1989; Segev et al., 1990). The S type motoneuron had a value of R_m at the soma of 0.7 kΩ·cm^2 which was stepped to a value of 20 kΩ·cm^2 for the dendritic

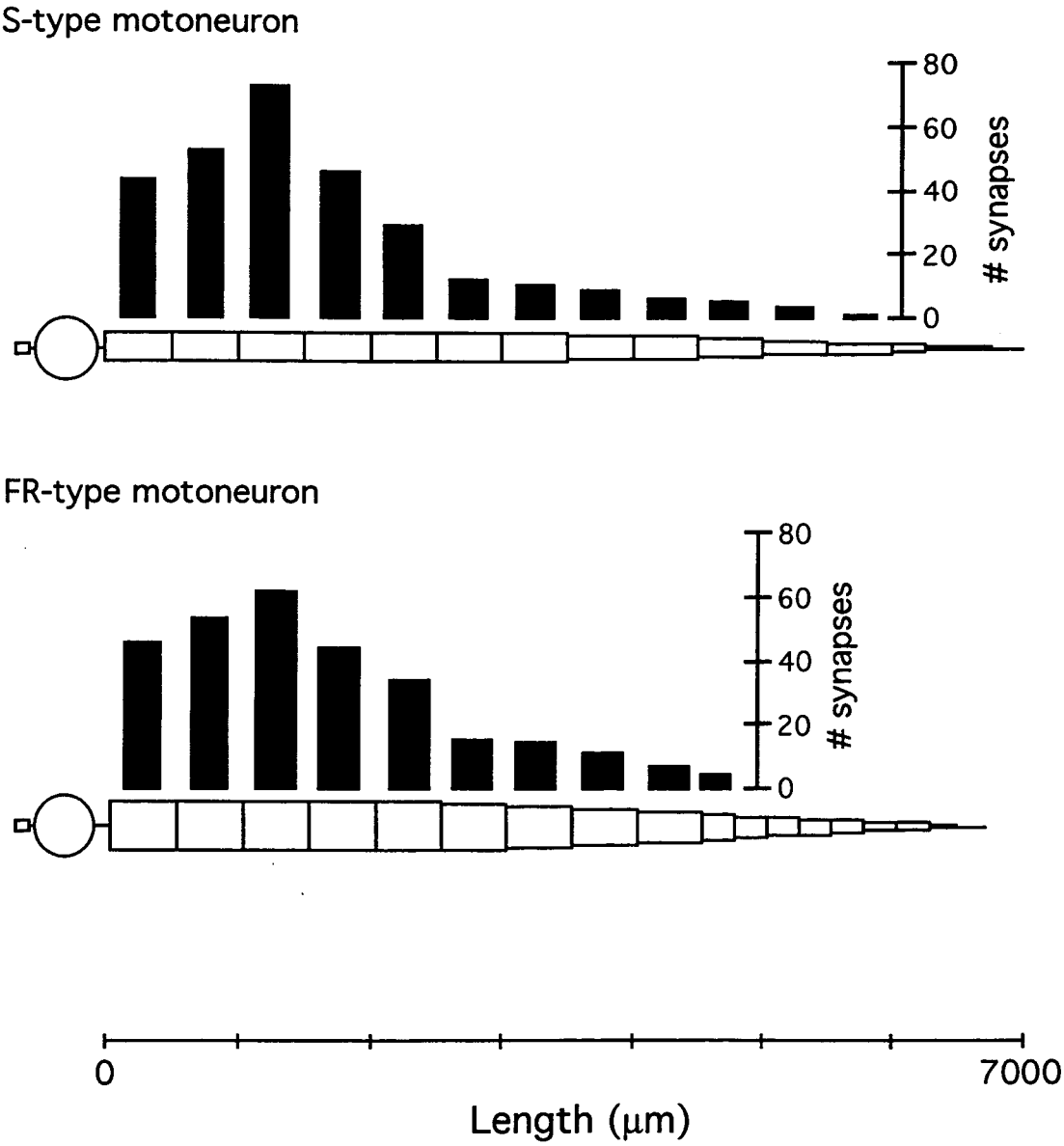

Fig. 7-1 Structure of the S- and FR-type motoneuron models and their associated synapses.

The morphology of the S- and FR-type motoneurons was roughly based on the structure of cells 35/4 (S) and 43/5 (FR) as described by Cullheim et al. (1987) and Fleshman et al. (1988). The dendritic compartments are named as d0, d1, d2, ... etc. with the compartment most proximal to the soma being d0. The specific membrane resistivity has been set according to the step model with values for the soma and dendritic compartments taken from the data of Fleshman et al. (1988) for these two cells. This resulted in a total electrotonic length of 2.29 and 2.45 for the S- and FR-type motoneurons respectively. The size of the initial segments, to the left of the soma, was the same in both models. Synaptic distribution was roughly based on the results of Segev et al. (1990) for these same two motoneurons. Although shown as number of synapses per compartment, synaptic input was actually modeled as a single synapse in each compartment with a peak conductance equal to the number of synapses assigned to the compartment as shown above multiplied by a variable maximum conductance for a single synapse.

compartments. The FR type motoneuron had values for R_m of 0.225 and 11 $k\Omega \cdot cm^2$ for the soma and dendrites respectively. The resulting electrotonic lengths of the equivalent dendrites were 2.29 and 2.448 for the S and FR type neurons respectively. The R_m of the initial segment in both neurons was set equal to that of the soma.

All ionic currents were simulated by standard Hodgkin-Huxley (H-H) equations (Hodgkin and Huxley, 1952) as described and adapted from Traub (1977). Active properties were associated with the initial segment and soma compartments only, and consisted of 5 H-H conductances along with the passive resistive properties mentioned above (equations in APPENDIX). The initial segment contained a sodium conductance giving rise to a fast inward current, $I_{Na(IS)}$ [Eq. A-5] (cf. Barrett and Crill, 1980), and a "fast" potassium conductance giving rise to a delayed rectifier type current, $I_{Kf(IS)}$ [Eq. A-10]. The soma compartment (x) contained a sodium conductance, $I_{Na(x)}$ [Eq. A-13], a "fast" potassium conductance, $I_{Kf(x)}$ [Eq. A-18], and a "slow" potassium conductance, $I_{Ks(x)}$ [Eq. A-21], which gave rise to the afterhyperpolarization. The "fast" and "slow" potassium conductances are analogous with those described by Barrett et al. (1980) for cat motoneurones. The sodium and "fast" potassium conductances in the initial segment are activated at a lower threshold relative to the equivalent conductances in the soma (Dodge and Cooley, 1973). All sodium and "fast" potassium conductances were the same for the two types of motoneurons , however, the "slow" potassium conductance parameters were adjusted differently in each model as described below. The density of sodium and "fast" potassium conductances was set according to previous models of cat spinal motoneurons (Traub, 1977; Traub and Llinás, 1977).

Behavior of the motoneuron models

In order to obtain the input resistance of the two motoneuron models, hyperpolarizing current pulses of 1 nA amplitude and 50 ms duration were applied to the soma compartment and the resulting membrane potentials plotted in Figure 7-2A. This was repeated at three intensities of current for the two motoneurons and resulted in a linear steady state current/voltage relationship

(Fig. 7-2B). Input resistance, R_N, for the two neurons was obtained from the slope of the regression line through the data of Fig. 7-2B. R_N for the S type motoneuron was 3.9 MΩ and 2.0 MΩ for the FR type motoneuron. The time constants for the two motoneurons were obtained by injecting 20 nA, 0.2 ms hyperpolarizing pulses to the soma compartment of the two neurons. The resulting voltage transient was plotted on a semilogarithmic plot and the time constant, τ_0, was computed by curve fitting with the equation

$$V(t) = C_0 \exp^{\left(\frac{-t}{\tau_0}\right)} \qquad 7\text{-}2$$

(Fleshman et al., 1988). The equation was fit to the transient record over a 5 ms period centered at 1.5 times the experimental value of τ_0 reported in Fleshman et al. (1988). The τ_0 values computed in this manner were 16.4 and 8.8 ms for the S and FR type motoneurons respectively.

For the firing behavior of the motoneuron, the following equation was solved for membrane potential, $V_{m[x]}$, at the soma:

$$C_m \frac{\partial V_{m[x]}}{\partial t} = \frac{V_{m[x]} - E_R}{R_{[x]}} + \sum_{ion} g_{ion[x]}\left(V_{m[x]} \cdot t\right)\left(V_{m[x]} - E_{ion}\right) + \sum_{y} \frac{V_{m[x]} - E_{[y]}}{R_{[xy]}} + I_{inj}, \qquad 7\text{-}3$$

where the subscript [x] refers to the soma compartment and [y] to the compartments linked to [x]. The total somatic resistance is given by

$$R_{[x]} = \pi D^2 R_m \quad \Omega,$$

with D = 50.9 μm for the S-type motoneuron and 48.8 μm for the FR-type motoneuron. $R_{[x]}$ is taken to be the inverse of the passive leak conductance g_l in our model. The first term in Eq. 7-3 represents the leak current, the next term represents the sum of the ionic currents located in the soma compartment. The contribution of currents from other compartments is represented in the third term of Eq. 7-3 and the final term is the injected current. To obtain $V_{m[x]}$ as a function of time, Eq. 7-3 was integrated by using the forward Euler method (Moore and Ramon, 1974) according to the equation

$$V_m = V_o + \Delta t \frac{\partial V_o}{\partial t},$$

where V_0 is the initial value of membrane voltage and $\frac{\partial V_0}{\partial t}$ is the initial slope. It is a simple and fast, though unstable, numerical integration method and was suitable for the computing power we had access to.

An action potential was elicited by injecting a 0.5 ms, 10 nA depolarizing current pulse into the initial segment and the resulting AHP recorded from the soma is plotted in Fig. 7-2C for each motoneuron. The parameters describing the AHP of the 2 motoneurons are reported in Table 7-1.. The depth and duration of the AHPs was adjusted to match the values reported by Zengel et al. (1985) for type identified motoneurons in the cat by adjusting parameters of the "slow" potassium conductance. Depth of the AHP was adjusted by changing the density of the slow potassium conductance on the soma and duration was adjusted by changing the numerator in the backward rate function β_q [Eq. A-23, A-26].

TABLE 7-1. Summary of AHP parameters for the two motoneuron models

	S	FR
AHP magnitude, mV	4.8	4.1
AHP duration, ms	160	90
AHP half-decay time, ms	48	23

Following adjustment of conductances to match reported cat spinal motoneuron AHP parameters, repetitive firing was elicited by injecting long duration current pulses into the soma compartments of the two motoneuron models. The interspike intervals (ISIs) were measured

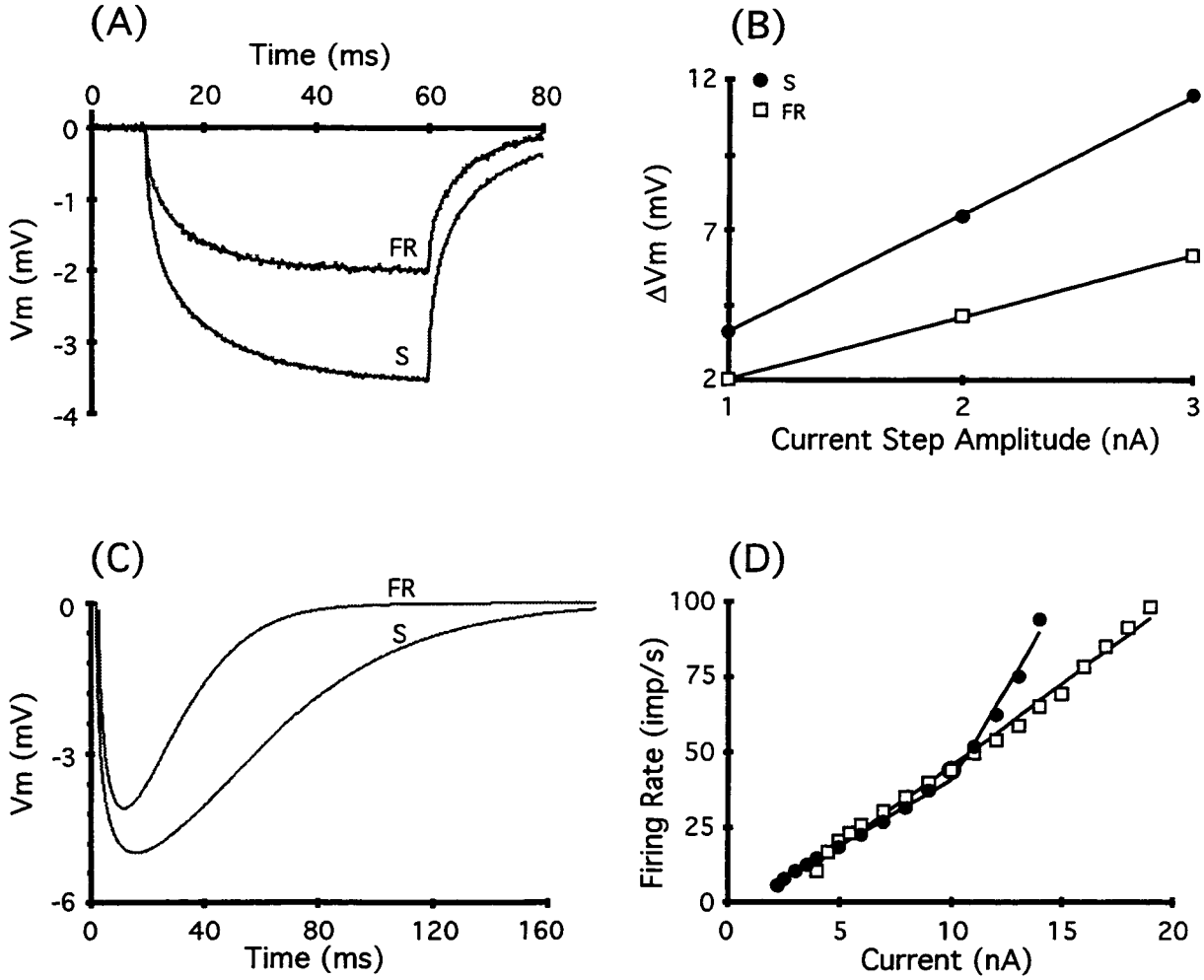

Fig. 7-2 Behavior of the two model motoneurons.
A: Response of the two motoneurons to a 50 ms hyperpolarizing current of 1.0 nA. The time course of the change in membrane potential is slower for the S-type motoneuron. The maximum change in membrane potential was measured just prior to the offset of the current input for use in determining input resistance. B: The maximum change in membrane potential was plotted with respect to the amplitude of the current input for the two motoneurons. Linear regression analysis of the data was used to estimate the input resistance of the motoneurons. The equation of the line fit to the data from the S-type motoneuron was $\Delta V=3.9I-0.33$, and that fit to the data from the FR-type motoneuron was $\Delta V=2.0I-0.033$. C: An action potential was elicited by a 0.5 ms 10 nA current pulse injected into the initial segment. The resulting AHPs for the two motoneurons are shown after the models have been set with AHP parameters according to the cat literature. D: Relationships between firing rate and amplitude of current injected into the soma (the *f/I* curves) during steady state firing are shown for the two motoneurons. The S-type motoneuron begins repetitive firing at a lower value of current and has a lower minimal rhythmic firing rate compared to the FR-type motoneuron. The S-type motoneuron shows a primary and secondary firing range over the values of currents tested and the slope of the line fit to the primary range is less than that fit to the data from the FR-type motoneuron.

following adaptation and the inverse, firing rate, was plotted with respect to the amplitude of current injected into the soma to produce the *f/I* curve plotted in Fig. 7-2D. The S type motoneuron exhibited both a primary and secondary range (Kernell, 1965a) which was fit by regression analysis in two parts. The line fit to the primary range (between 2 - 9 nA) had a slope of 4.4 imp·s^{-1}/nA while that fit to the secondary range had a slope of 12.3 imp·s^{-1}/nA. The FR type motoneuron was characterized by a single linear regression line with a slope of 5.4 imp·s^{-1}/nA. The *f/I* curves in the primary range agree with the data reported by Kernell (1965b) where small (i.e. S type) motoneurons are shown to have a less steep slope and begin repetitive firing at lower values of injected current. The secondary range in the S type motoneuron was unexpected but was not explored further as this range of firing rates is seldom reported in normal human motoneurons. The motoneurons also show an inverse relationship between AHP duration and minimal rhythmic firing rate characteristic of cat motoneurons studied intracellularly (Kernell, 1965b).

Synaptic and current pulse inputs to the motoneurons

Synaptic conductances were added to the equivalent dendrites of the two motoneurons according to Segev et al. (1990; Fig. 4, Step Model). Instead of assigning 300 individual synapses of the same peak conductance to the motoneuron models (Segev et al., 1990), the number of synapses in a particular compartment was determined and modeled as a single equivalent synapse with a peak conductance, g_{max}, equal to

$$g_{max} = n \cdot g_{peak(ss)}$$

where $g_{peak(ss)}$ is the peak conductance of a single synapse (e.g. 5 nS; Finkel and Redman, 1983) and n is the total number of synapses assigned to that compartment. Each equivalent synapse was modeled as a synaptic conductance transient defined by an alpha function with a time to peak conductance of 0.2 ms [Eq. A-27 & A-28]. The distribution of equivalent synaptic input on the equivalent dendrite is shown in Fig. 7-1. Both motoneurons were assigned 300 synapses,

however, these were represented by 12 or 10 equivalent synaptic conductances in the S and FR type motoneurons respectively. The synaptic conductances were activated synchronously to produce a composite EPSP which was larger and slower in the S-type motoneuron. As a means of altering the size of the composite EPSP for a given simulation the value of $g_{peak(ss)}$ was changed, thus maintaining the same relative distribution of synaptic input over the equivalent dendrite. With $g_{peak(ss)}$ set to 1 nS, synchronous activation of the synaptic conductances from resting potential resulted in a composite EPSP with a rise-time of 1.5 ms and an amplitude of 3.4 mV in the S-type motoneuron and a rise-time and amplitude of 1.0 ms and 2.3 mV in the FR-type motoneuron. Injection of a 9.0 nA, 1.0 ms depolarizing current pulse into the third dendritic compartment (d2) of the S-type motoneuron resulted in a voltage transient (pulse potential or PP) that had the same amplitude and rise-time as the composite EPSP (see Walmsley and Stuklis, 1989). Therefore, many of the simulations with the S-type motoneuron were done using a current injection into the dendrite rather than by activation of the synaptic conductances to decrease the duration of the computations. A site for injection of current pulses into the equivalent dendrite of the FR-type motoneuron where the resulting PP matched the composite EPSP was sought. No adequate match was found, therefore, simulations incorporating the FR-type motoneuron were always done with synaptic input.

Results

The majority of the results are given for simulations using the S-type motoneuron model except where stated. Stimuli during a simulation, either a current pulse input or synchronous synaptic input, had a random interstimulus interval between 0.5 and 2 seconds. In the first section the relationship between membrane voltage trajectories, EPSPs and response probabilities are considered for a noiseless membrane. Simulations done in the absence of membrane noise made it easier to assess the contributions of membrane voltage and conductance to motoneuron response, in addition to making computations faster. Later simulations describe the effects of adding noisy current to generate the stochastic firing characteristic of human motoneuron data.

Noiseless membrane

To assess the effect of background firing rate on the response probability of a motoneuron to Ia input, the S type motoneuron was fired at five different rates. The membrane voltage trajectories at these five rates during steady state firing are shown in Figure 7-3. The figure shows changes in the membrane potential trajectories which are similar to those reported in cat motoneurons, namely the maximum depth of the AHP decreases as firing rates increase (Schwindt and Calvin, 1972). At the slowest firing rate of 5.6 imp/s the maximum depth of the AHP, measured from the foot of the preceding spike, was 10.8 mV. The depth of the AHP decreased by 2 mV to 8.8 mV at the fastest firing rate tested (18 imp/s). Figure 7-3 (top) also shows changes in the latter part of the AHPs as the firing rates increased. Initially at the minimal rhythmic firing rate of 5.6 imp/s the recovery of the membrane potential towards threshold showed an asymptotic region. At the faster firing rates this asymptotic region gradually decreased and the membrane potential returned to threshold in a more ramp-like fashion.

During rhythmic firing, a current pulse input was given to the motoneuron. If the resulting voltage transient brought the motoneuron to firing threshold, the ISI was shortened and the subsequent ISI was typically longer. Otherwise, simulations in the absence of noise exhibited a constant ISI. Figure 7-4 (left) illustrates the peri-stimulus time histograms (PSTHs) resulting from simulations using the S-type motoneuron at three firing rates in response to the 9.0 nA current pulse input. The excitatory peak in the PSTH decreased as the firing rate increased. This result is summarized in Fig. 7-4 (right, filled circles) where response probability, P_r, is plotted as a function of background firing rate. In the range of firing rates tested there was a clear effect of background firing rate on the ability of the S-type motoneuron model to respond to the input. As the firing rate of the motoneuron was increased, the response probability to a constant current pulse input decreased.

Simulations using the FR-type motoneuron were done at three different firing rates in response to a synchronous synaptic input rather than a current pulse input. The resulting

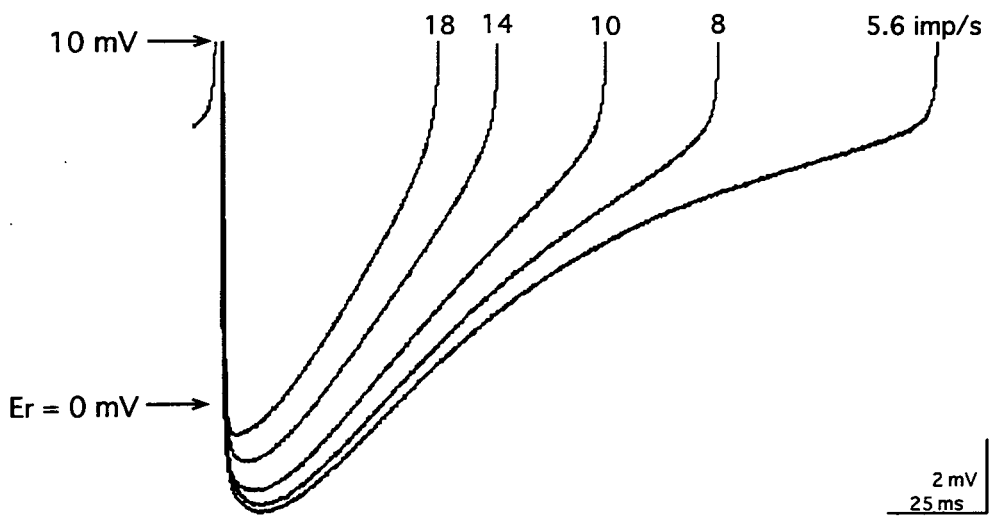

Fig. 7-3 Membrane voltage trajectories of the S-type motoneuron during repetitive firing.

Five different levels of current steps were injected into the soma compartment of the S-type motoneuron model to elicit repetitive firing. The membrane voltage trajectories between spikes at the five different rates are shown following initial adaptation. As the firing rate increases the maximum depth of the AHP decreases. At the slowest firing rate as the membrane voltage returns toward threshold, the model exhibits an asymptotic region which gradually decreases at the faster firing rates. The trajectories are illustrated for voltages up to an absolute value of 10 mV positive to the resting potential of 0 mV. The firing level at all rates was approximately 10 mV.

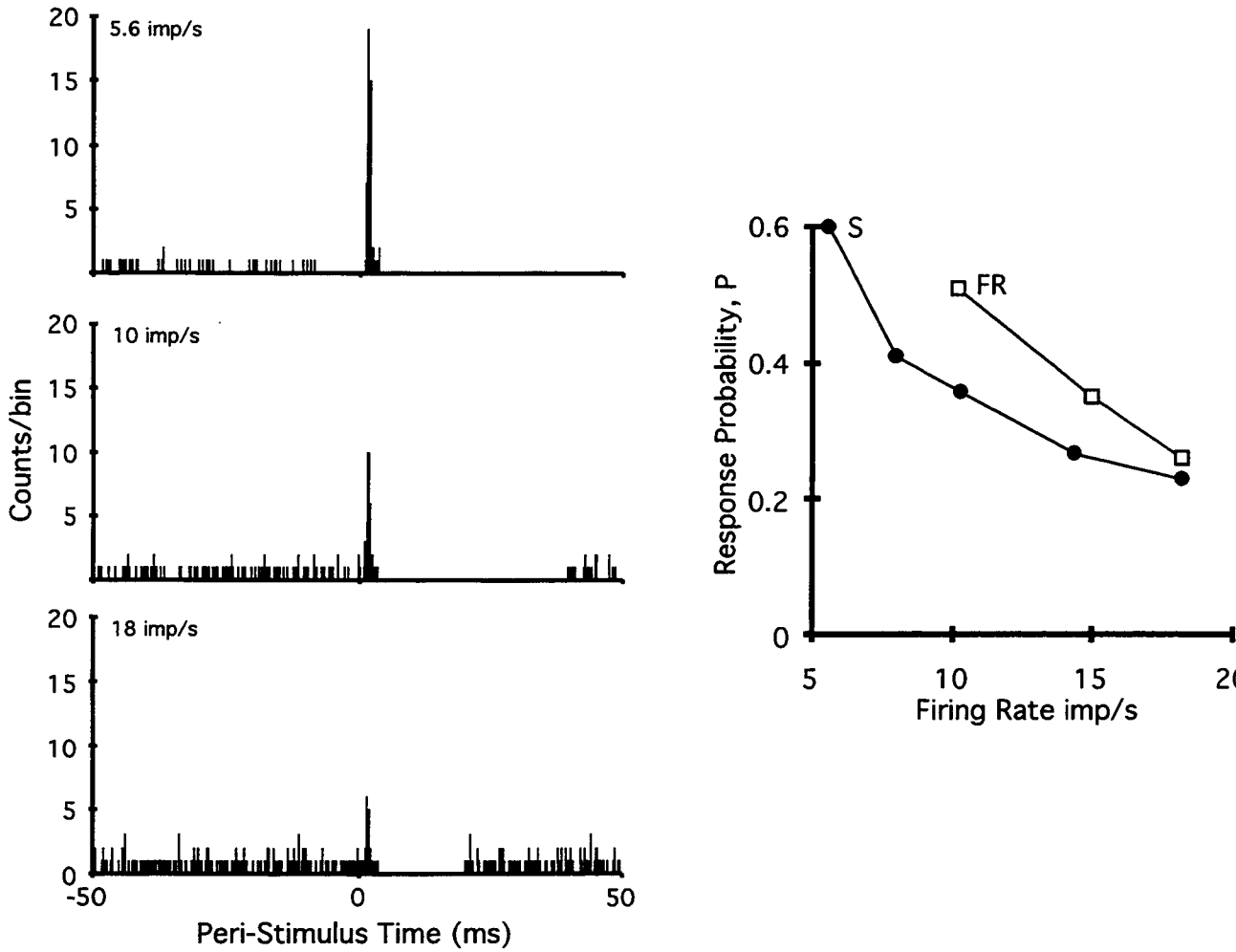

Fig. 7-4 Effect of background firing rate on response probability in a noiseless membrane.

The left side of the figure shows PSTHs from the S-type motoneuron in response to a constant current pulse input at three different firing rates. The same number of stimuli are given to the motoneuron over a period of 4 minutes of simulation time (real computation time averaged 388.5 minutes). As firing rates increased the peak in the PSTH decreased. The right side of the figure shows the effect of firing rate on response probability over 5 different firing rates with the S- and 3 different rates with the FR-type motoneuron. An increased firing rate was clearly related with a decreased response probability in both motoneurons.

composite EPSP was produced by the synchronous activation of the 10 synaptic conductances on the equivalent dendrite (Fig. 7-1). The synapses has a $g_{peak(ss)}$ of 1 nS which resulted in a composite EPSP at resting potential with a rise-time of 1.0 ms and an amplitude of 2.3 mV.[1] The response probability of the FR-type motoneuron to a constant synaptic input decreased as firing rates increased (Fig. 7-4, open squares).

The advantage of using a noiseless motoneuron in these initial simulations was the ability to examine some deterministic values of membrane voltage at which spikes were triggered at different firing rates. The delay following a spike when the input was first able to trigger a spike in the S-type motoneuron was evaluated. This was called the effectual delay, d_e, and a number of parameters were evaluated with respect to this delay which are summarized in Table 7-2. The computations showed that as the firing rate increased the effectual delay decreased. The response probability was zero below d_e and 1.0 for values greater than d_e. The effectual delay was then used to calculate the percentage of the ISI in which the PP was within reach of threshold,

$$\%ISI = \frac{ISI - d_e}{ISI} \times 100.$$

As firing rate increased the percentage of the ISI within reach of threshold to the PP decreased. Therefore, although d_e decreased at the faster firing rates, it did not decrease in proportion to the reduction in ISI at the faster firing rates. This explains why P_r was higher at slower firing rates.

The next question was whether action potential threshold changed with firing rate, and whether the firing threshold varied during the ISI. The membrane potential at which the action potential begins its rapid rise was evaluated at the different firing rates and defined as the firing level (Reyes and Fetz, 1993). Simulation data showed that the firing level over the range of firing rates tested did not vary much and had a mean value of 10.02 ± 0.04 mV ($\pm$ SD). The value of the membrane potential at the effectual delay was measured at the five rates tested. Over the five

[1] the inputs to the S- and FR-type motoneurons are nominally equivalent as both mimick the membrane voltage response in the soma to the synchronous activation of 300 synapses with a $g_{peak(ss)}$=1 nS.

rates tested the average membrane potential at d_e was 3.4 ± 0.25 mV. However, there was a tendency for the membrane potential at the effectual delay to increase with increasing firing rates (Table 7-2). When the peak amplitude of the PP measured at rest (3.4 mV) is added to the membrane potential at the effectual delay the sum falls short of the firing level by 3.22 mV. This would imply that either the PP amplitude was significantly greater during rhythmic firing or that the threshold for an action potential decreased during the ISI.

TABLE 7-2. Evaluation of threshold parameters of the S-type motoneuron at different firing rates.

Firing Rate (imp/s)	ISI (ms)	d_e (ms)	% ISI within threshold	Vm at d_e (mV)*	PP at d_e-1 (mV)
5.6	180	74	58.9	3.2	5.1
8.0	125	66	47.2	3.2	4.7
10.3	97	58	40.2	3.3	4.3
14.3	70	44	37.1	3.5	4.1
18.2	55	35	36.4	3.8	3.8

* All voltage levels are given relative to the resting membrane potential of 0 mV.

To investigate whether the amplitude of the PP elicited by a constant current pulse input varied during rhythmic firing, the size of the PP was measured at sequential times during the ISI at different firing rates and the results are illustrated in Figure 7-5. A 9.0 nA, 1.0 ms current pulse injected into d2 was used to generate a PP (the same as that shown in Fig. 7-3) with an amplitude of 3.4 mV at rest. The S-type model neuron was then fired repetitively at 10.3 imp/s and the PP was induced at sequential 10 ms delays beginning with a delay of 10 ms following the spike, Fig. 7-5 (top). At a post-spike delay of 10 ms the amplitude of the PP was reduced with respect to that at rest and progressively increased in size at longer delays following the

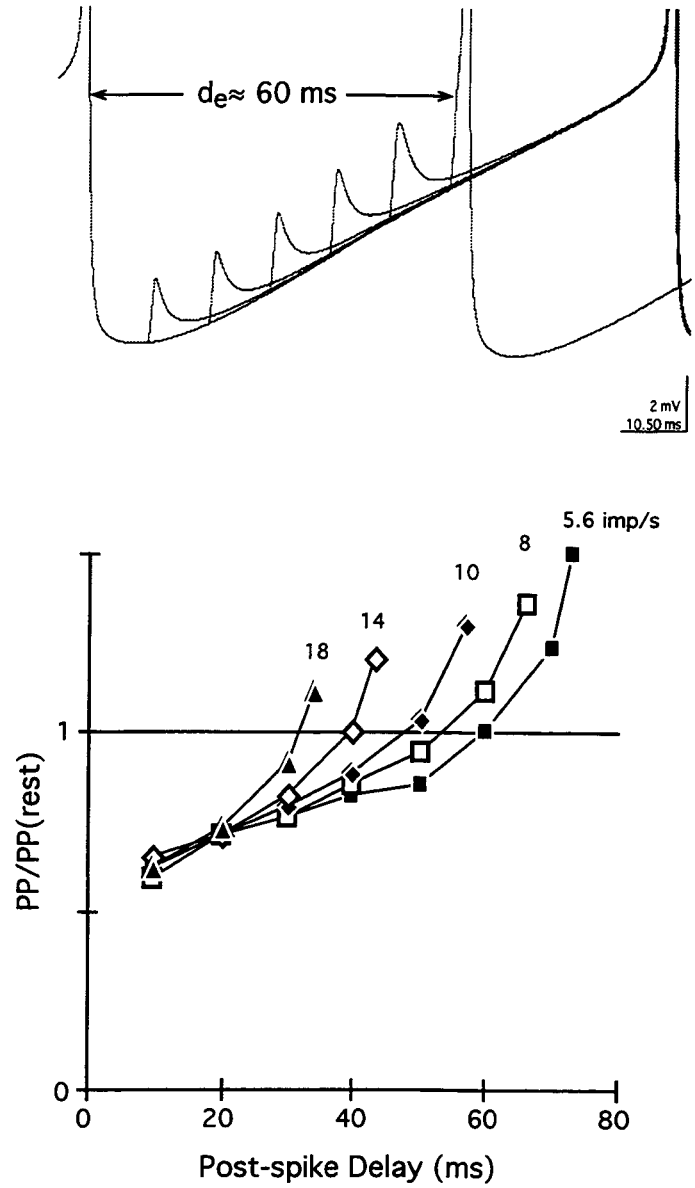

Fig. 7-5 Change in amplitude of the PP during repetitive firing compared to that at rest.

Top: ISI membrane voltage trajectory when the S-type motoneuron was firing at approximately 10 imp/s and the PP is induced at various post-spike delays. At short post-spike delays the amplitude of the PP was reduced with respect to that at rest. As the post-spike delay was increased the amplitude of the PP increased until the effectual delay at which the PP triggered a spike. Bottom: The change in PP amplitude with respect to that measured at rest as a function of post-spike delay at 5 different firing rates. At a post-spike delay of 10 ms the PP is the same size at all firing rates. The rate of change of PP amplitude varies with firing rate as does the maximum value of the PP 1 ms prior to the effectual delay which is represented by the data point at the longest post-spike delay for each firing rate.

motoneuron spike until a post-spike delay of 50 ms at which the amplitude of the PP had returned to resting values. At a delay of 60 ms the PP was of sufficient magnitude to bring the motoneuron to threshold eliciting an action potential.

This procedure was repeated for a number of different firing rates using the same current pulse input to the S-type motoneuron. The data are plotted in Fig. 7-5 (bottom) where the ordinate scale is a measure of the PP amplitude with respect to that obtained at rest. The figure shows that PP amplitude is approximately equal for all firing rates at the shortest delay evaluated (10 ms) and reduced considerably as compared to that at rest. As the post-spike delay increased, the rate of change of PP amplitude varied with firing rate in such a way that the faster the firing rate of the motoneuron, the earlier the PP amplitude returned to resting values. The final values for relative PP amplitude were evaluated at a post-spike delay 1 ms prior to the effectual delay (absolute values given in Table 7-2). The slower the firing rate the greater the relative amplitude of the PP prior to the effectual delay. If the amplitude of the PP immediately prior to the effectual delay is added to the membrane potential at the effectual delay, the average sum over all rates is 7.8 ± 0.3 mV. This value is still, on the average, more than 2 mV shy of the firing level (10.02 mV) during repetitive firing.

Noisy membrane

During voluntary isometric contractions in which human subjects are asked to maintain a constant firing rate, the motor unit fires not with a constant ISI as above but exhibits some level of variability (Clamann, 1969; Person and Kudina, 1972). The source of this variability is the ongoing bombardment of the motoneuron by post-synaptic conductances resulting in fluctuation of the motoneuron membrane potential (Calvin and Stevens, 1968). Variability in the ISIs was incorporated into the simulations in order to determine whether the behavior of the model motoneurons approximated the human experimental data (Jones and Bawa, 1995; Chapter 4 and 5). This was accomplished by injecting noisy current into the second dendritic compartment (d1) of the S type motoneuron model. White noise current with a Gaussian distribution of amplitudes

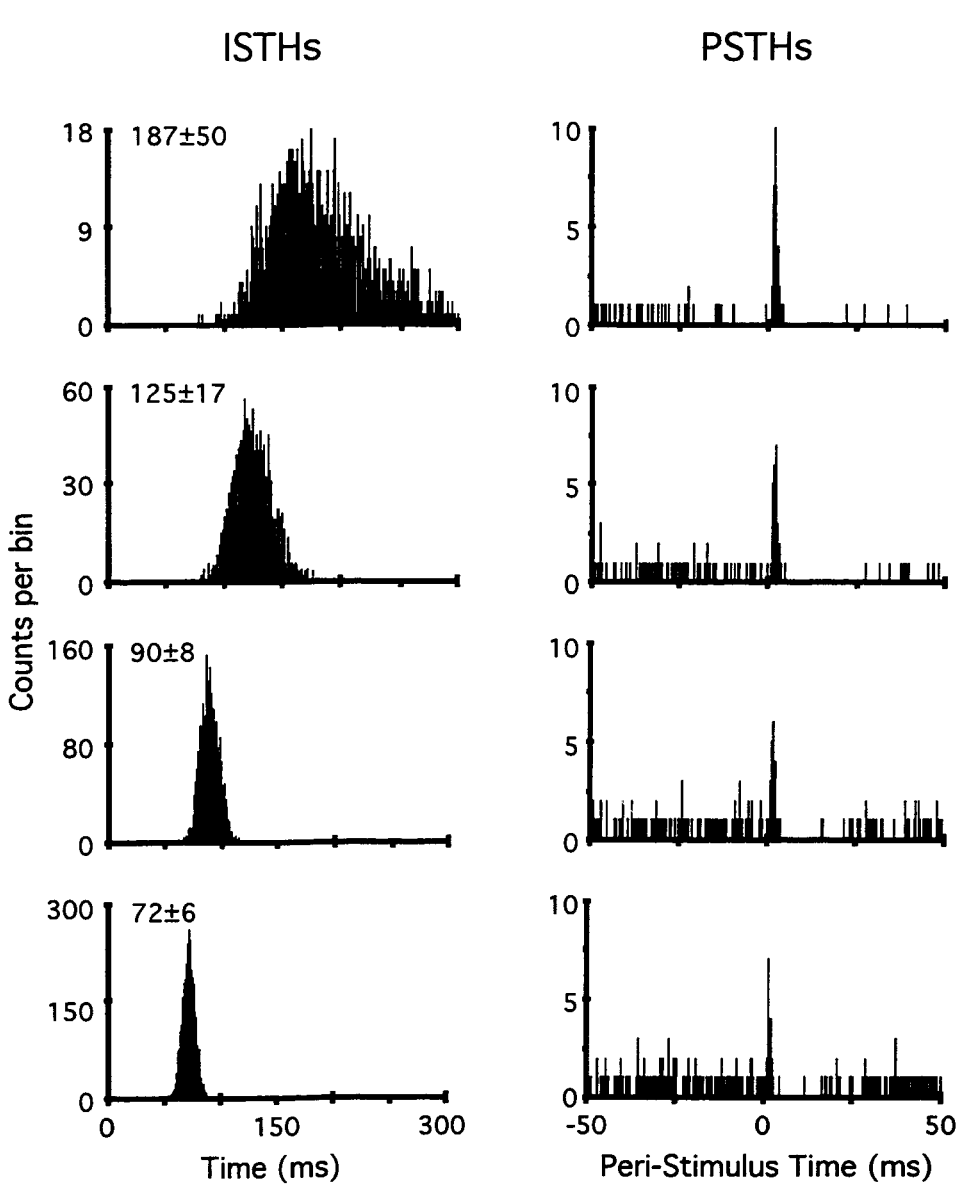

Fig. 7-6 Effect of background firing rate on the peak of the PSTH during stochastic firing.

The S-type motoneuron was fired in a stochastic manner by injecting noisy current into d1 as well as the current injected into the soma to elicit repetitive firing. The left side of the figure illustrates the resulting variation in ISIs represented by the first order interval histograms (ISTHs). The mean and standard deviation of the ISIs are given with each ISTH. The level of noisy current was the same at each rate. The right side of the figure shows the PSTHs resulting from a 9.0 nA current pulse input to d2. The same number of stimuli are given over a 4 minute simulation period (average computation time 2826.5 min.). The response probability measured from the peak of the PSTH was reduced as firing rates increased.

was used which had a mean of 0.0 nA and a variable standard deviation. Figure 7-6 (left) illustrates the resulting interspike interval histograms when noisy current with a constant standard deviation of ± 20 nA was added to the current necessary to elicit repetitive firing at different rates. The histograms show the characteristic reduction in ISI variability with an increase in mean firing rate. Using a 9.0 nA, 1.0 ms current pulse input into d2, response probability was computed from the PSTHs shown in Fig. 7-6 (right) for the equivalent ISI distributions. As with the noiseless simulations, the response probability to this input was greatest when the motoneuron was firing at the slowest rate with the greatest ISI variability. As the firing rates increased there was a tendency for the response probability to decrease as illustrated by the reduction in the number of counts in the excitatory response peaks of the PSTHs. This was similar to the results obtained when there was no variability in the ISIs, Fig. 7-4, except that overall response probability values to the same input were lower when the noisy current was introduced. The relationship between response probability and firing rate during stochastic firing is plotted in Fig. 7-7 for two different current pulse inputs (9.0 nA, open circles and 20 nA, open squares) to the S-type motoneuron. Each input results in a response probability which is greatest at the slowest firing rate and declines as firing rates increase.[2] The response probability at various firing rates during noiseless simulations with a 9.0 nA current pulse is plotted for comparison. The reduction in response probability to the same input by the addition of noise is clear until the higher rates.

Response trajectories: S type model motoneuron

Response trajectories were plotted as a means of comparing the post-spike excitability of the S-type model motoneuron to the results obtained in human studies (Chapter 5). Figure 7-8

---

[2] The larger input (20 nA, 1.0 ms) resulted in a PP that had an amplitude of 7.0 mV, 1.4 ms rise-time and 3.2 ms half-width at resting potential. The $Na_{(IS)}$ conductance had to be blocked to make this measurement otherwise a spike was initiated. At rest without block of the $Na_{(IS)}$ conductance, various amplitudes of 1.0 ms current pulses were injected into d2 and the resulting voltage transient measured. A pulse of 17.85 nA was the largest amplitude that could be given at resting potential without triggering a spike. This current pulse resulted in a PP of 8.6 mV with a 2.4 ms time to peak. Obviously the input triggered some inward IS current but it wasn't of a sufficient ampitude to trigger a spike.

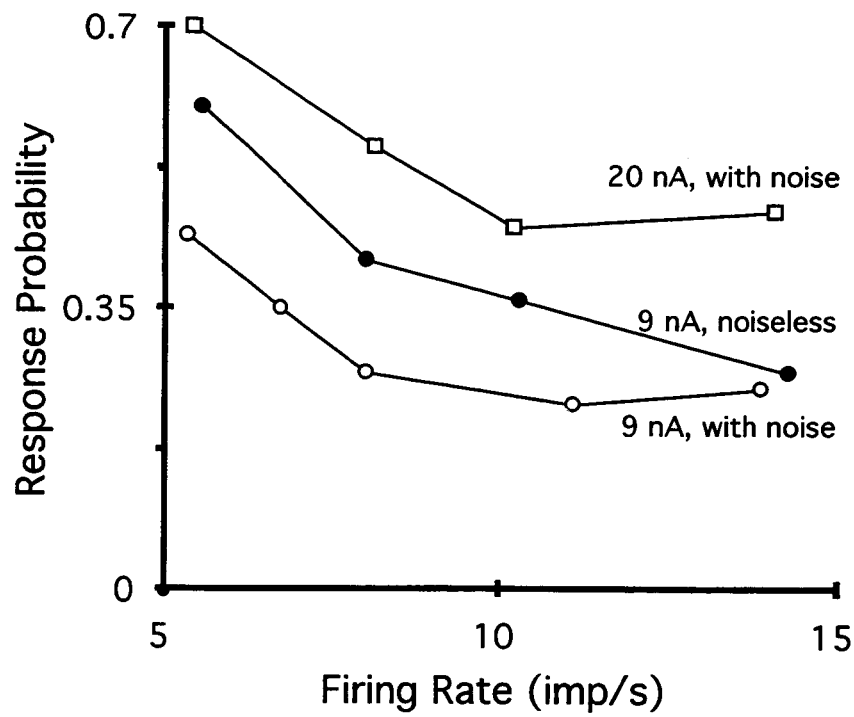

Fig. 7-7 Effect of background firing rate on response probability during stochastic firing with two different amplitude current pulse inputs.

During stochastic firing, as firing rates increased the response probability of the S-type motoneuron decreased. This is shown for two current input pulses, 9 nA (open circles) and 20 nA (open squares). The response probability in the absence of noise with a 9.0 nA current pulse input is shown for comparison. The maximum difference in response probability with the two inputs over the rates tested was 0.21 (9.0 nA) and 0.25 (20.0 nA). The apparent plateau of the firing rate effect on response probability may be a result of a lack of sufficient noise at high firing rates. This is suggested by the similar response probabilities near 14 imp/s regardless of the presence of noise.

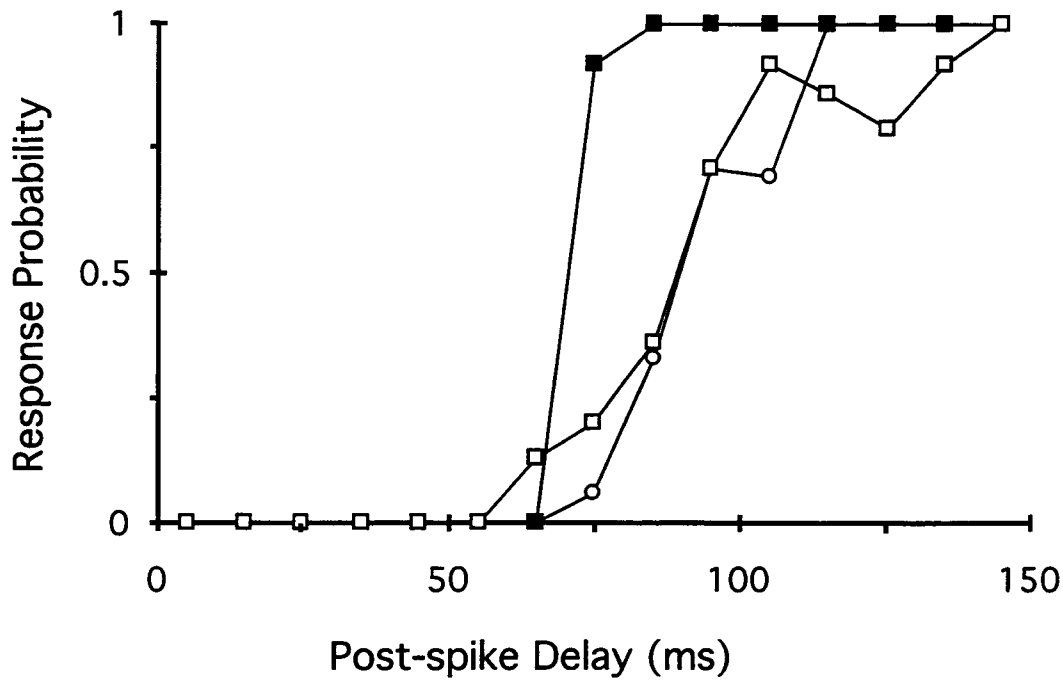

Fig. 7-8 Response trajectories of the S- and S_{sh}-type motoneuron models.

The response trajectories acquired by stimulation with a 9.0 nA, 1.0 ms current pulse are shown for the S-type motoneuron with no noise added (solid squares), with added noise (open squares) and the S_{sh}-type motoneuron with noise (open circles). During the simulations the firing rates were approximately 6.6 imp/s. Without noise the response trajectory resembles a step function. By adding noise the latter portion of the response trajectory shows a reduced slope. The S_{sh}-type motoneuron has a shallower AHP than the S-type which results in a further reduction in the slope of the response trajectory.

shows the response trajectories from the model motoneuron under three different conditions when tested with a 9.0 nA, 1.0 ms current pulse input. The first condition (solid squares) illustrates the response trajectory of the model firing at a rate of 6.6 imp/s (ISI = 151 ms) in the absence of membrane noise. The response probability in each 10 ms bin has a value of zero until a post-spike delay between 70-80 ms when response probability rises immediately to a value of 0.92. At any delays greater than 80 ms the response probability is 1.0, that is, the stimulus is effective 100 percent of the time. The shape of the response trajectory resembles a step function which would be predicted from studies done on cat motoneurons (Fetz and Gustafsson, 1983). In the second condition (open circles) ± 20 nA of noisy current was injected into d1 resulting in variation about the mean ISI of 149 ± 27 ms (6.7 imp/s). The effect of the noise was a reduction in value of response probability at post-spikes delays from 75-105 ms, thus reducing the slope of the response trajectory. This change in the response trajectory accounts for the difference in total response probability between condition 1, Pr = 0.46, and condition 2, Pr = 0.35. Although the slope of the response trajectory was reduced by the addition of noise, it remained steeper than the slope of the response trajectory from human soleus motoneurons firing at similar rates (Chapter 5).

One of the means of approaching the slope of response trajectories in human motoneurons was to reduce the maximum value of the "slow" potassium conductance from 12 to 5 mS/cm^2 and to adjust the numerator of β_q [Eq. A-23] to a value of 0.012 from 0.015. This resulted in an AHP depth of 2.9 mV instead of 4.8 mV, a half-decay time of 47 ms and duration of 160 ms following an antidromically elicited spike (this model neuron with the shallower AHP will be referred to as S_{sh}). The third condition in Fig. 7-8 (open squares) shows the response trajectory computed from the S_{sh} neuron while firing at a rate of 6.4 imp/s (ISI = 157±33). The trajectory showed a reduced slope and was shallower at post-spike delays between 85 and 55 ms. The overall excitability of the S_{sh} motoneuron, assessed by a total response probability value of $P_r = 0.44$, was increased over that of the S-type motoneuron in condition 2. The response trajectory from the S_{sh} model motoneuron was a better approximation of a response trajectory from a soleus SMU

firing at a similar rate then were the results from the S-type motoneuron and therefore was used in all subsequent simulations.[3]

The first set of studies done on the S_{sh} model motoneuron was an estimate of the reliability of the measurement of response probability at sequential delays following the spike. Human motoneurons show a variation in response trajectory over repeated measures (Fig. 5-1) which may be due to many factors including the effects of synaptic noise or variations in the amount of current received by the motoneuron during voluntary control. To estimate the role of synaptic noise in producing variation in the response trajectories four simulations were run with constant values for the parameters. A depolarizing step current of 2.0 nA was injected into the soma compartment, ± 20 nA of noisy current was injected into d1 and a constant number of 9.0 nA, 1.0 ms current pulses (n=187) were randomly injected into d2 over 4 minutes of simulation time. The mean and standard error bars evaluated over the four trials are shown in Fig. 7-9 (filled squares). A smooth line has been drawn through the data points using the OPSEG method (Chapter 5). Also shown are the means and standard errors for response probability acquired from six human soleus motoneurons with the associated smoothed response trajectory (from Fig. 5-2). The average firing rate of the S_{sh} model motoneuron was 6.7 imp/s which was comparable to the average firing rate of 6.5 imp/s for the six soleus motoneurons. The response trajectory from the model has a similar shape to the data from the human motoneurons with some noticeable differences. At post-spike delays less than 50 ms the model has a lower response probability than the human soleus data and at post-spike delays greater than 50 ms the model has a higher response probability than the soleus data.

In human motoneurons, response trajectories are altered by changes in motoneuron firing rate (Chapter 4; Jones and Bawa, 1995; Olivier et al. 1995). To determine the effect of firing rate on the response trajectories of the S_{sh} model motoneuron, we injected different levels of current

---

[3] The use of the S_{sh} model does not change the qualitative nature of the preceeding results, those results are still considered representative of the modeled motoneurons.

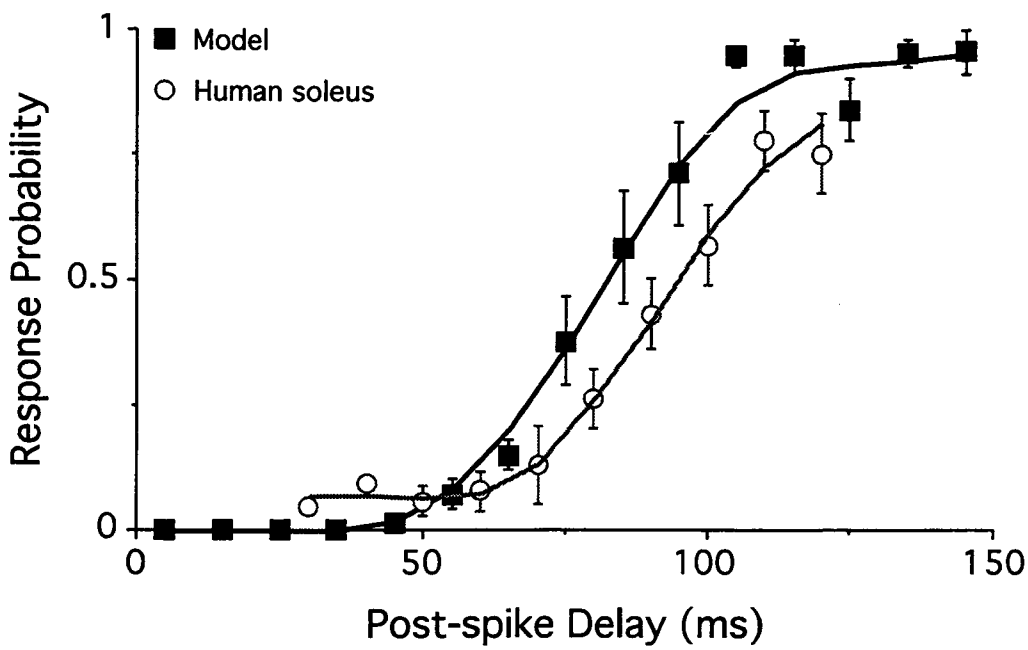

Fig. 7-9 Variability in the S_{sh}-type motoneuron response trajectory and comparison to a human response trajectory.

Four simulations were done on the S_{sh} model keeping the parameters of current pulse input, noisy current and depolarizing current step constant. The mean response probability and standard error were measured over a 10 ms bin width at sequential 10 ms delays following the spike (filled squares). The response trajectory is illustrated by the solid line. There is relatively little variation in response probability at short or long post-spike delays but more during delays from 75-95 ms. The response trajectory from Fig. 6-2 for 6 human soleus motoneurons is illustrated (open circles) for comparison. The mean firing rate of the model was 6.7 imp/s and the mean firing rate of the soleus motoneurons was 6.5 imp/s.

into the soma causing the motoneuron to fire at three different firing rates. A constant amount of noisy current (±20 nA) was injected into d1 and a constant current pulse was randomly injected into d2 (9.0 nA, 1.0 ms). Figure 7-10 illustrates the three response trajectories obtained. The variation in the shapes of the response trajectories with increases in firing rate is similar to the changes seen in human motoneurons (Fig. 4-7). At any given post-spike delay, response probability increased with an increase in the firing rate.

Not only does firing rate affect the shape of human motoneuron response trajectories, they are also dependent on the amplitude of the stimulus input (Fig. 5-4). Figure 7-11 illustrates response trajectories from the S_{sh} model motoneuron that were constructed at the same firing rate for three 1.0 ms current pulse inputs. The sizes of the PPs elicited at rest by the current pulses were 3.4 (open circles, 9.0 nA), 5.8 (open diamonds, 15 nA), and 7.0 mV (open squares, 20 nA). The PPs varied only in size while the other parameters of rise-time and half-width remained constant. As the size of the PP increased the response probability at any given post-spike delay increased. For example response probability at 55 ms is 0.0, 0.56, and 1.0 for the small, medium and large PP respectively. This result is qualitatively similar to the results obtained with human motoneurons.

Discussion

The primary aim of this series of simulations was to contribute to an understanding of the biophysical basis for the results obtained from human motoneurons in previous chapters. This was done by examining the responses of repetitively firing model motoneurons to transient inputs. The models were designed in an effort to identify some of the biophysical factors contributing to two features of the human data: 1) the effect of background firing rate on response probability to an input volley; and 2) the changes in excitability of motoneurons following a spike represented by response trajectories. As an estimate of human motoneuron membrane properties, motoneurons were modeled using the known biophysical properties of adult cat spinal motoneurons. Furthermore, it was intended to investigation to what extent properties of cat

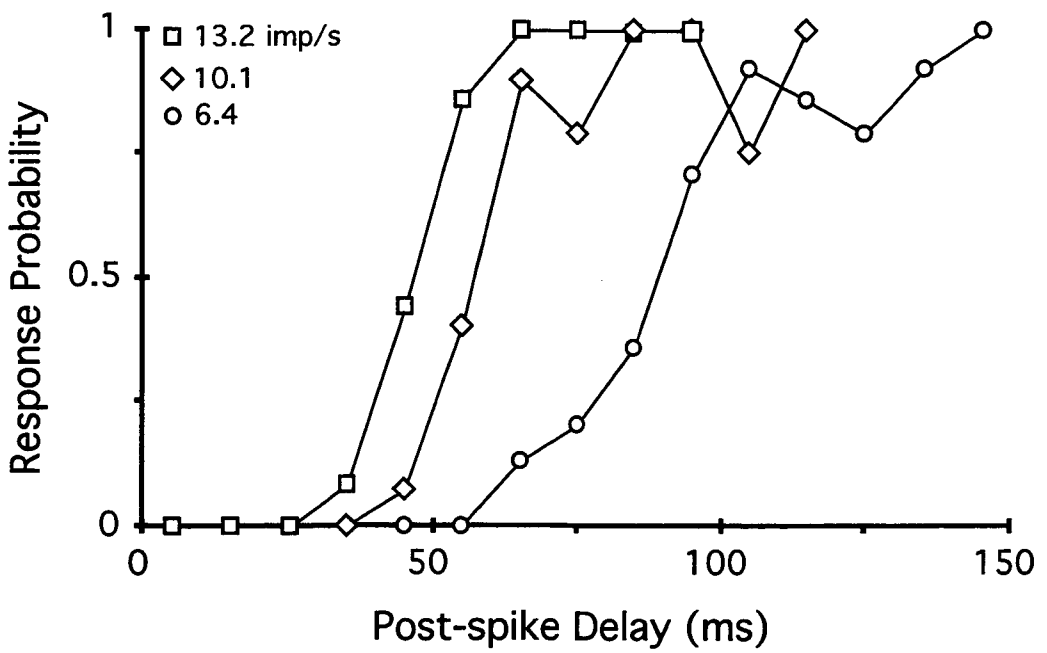

Fig. 7-10 The effect of firing rate on response trajectories.

The S_{sh} model motoneuron was fired at three different rates while being stimulated with a constant current pulse input (9.0 nA, 1.0 ms into d2). The P_r at the three rates was 0.44 (o), 0.39 (◇) and 0.32 (□). The data show that at a given post-spike delay, response probability increases with an increase in firing rate.

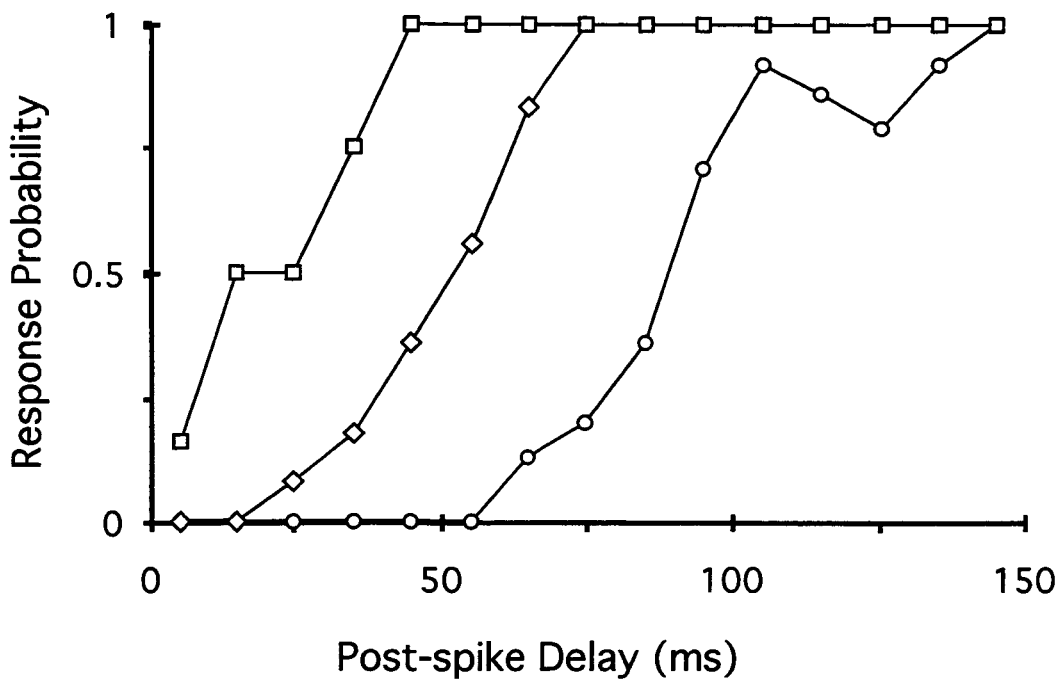

Fig. 7-11 The effect of PP amplitude on response trajectories.

Simulations were done using the S_{sh}-type motoneuron at the same firing rate with different PPs. The smallest PP (○) had an amplitude of 3.4 mV, rise-time of 1.5 ms and half width of 3.2 ms. The intermediate sized PP (◇) had an amplitude of 5.8 mV and the same rise-time and half-width as the small PP. The largest PP (□) had an amplitude of 7.0 mV, that was able to elicit an action potential from rest (see footnote 1), and a similar rise-time and half-width as the small PP. At any given post-spike delay between 25 and 65 ms, an increase in PP was associated with a greater response probability. Outside of this range response trajectories either saturated at 1.0 or fell to 0.0 for input from at least two of the PPs. The P_r values at the different stimulus intensities were 0.44, 0.64, and 0.85.

motoneurons where capable of explaining the behavior of human motoneurons. This information will be valuable as it will determine if the transfer of information from reduced animal experiments to questions of human motoneuron physiology is appropriate. In general, the responses of the model motoneurons were qualitatively similar to those of human motoneurons. That is, an increased firing rate resulted in a decrease in response probability to randomly induced input and motoneuronal excitability at sequential delays following a spike, increased in a monotonic fashion.

Membrane noise

Physiologically, fluctuations in membrane potential are thought to be primarily due to synaptic noise (Calvin and Stevens, 1968) The method of producing noise in the present simulations, however, was achieved through the injection of a white noise current into the model. The noisy current injection was controlled by adjusting the standard deviation of the Gaussian distributed current fluctuation about a mean of zero nA. The resulting membrane potential fluctuations depended upon the site of the current injection. If the noisy current was injected into the soma, the resulting voltage fluctuations had very high frequency components due to the low specific membrane resistance of this compartment. The high frequency nature of these membrane potential fluctuations did not match records of synaptic noise recorded intracellularly from cat motoneurons (Gustafsson and McCrea, 1984). Therefore, the current was injected into the dendrite which resulted in filtering of the fluctuations in membrane voltage measured at the soma. Increasing the standard deviation of the noisy current above a value of 20 nA did not increase the peak to peak value of the membrane voltage noise but instead resulted in higher frequency fluctuations in membrane potential. Therefore, we were unable to adequately test the response trajectories at higher levels of peak to peak membrane voltage noise.

ISI variability at different firing rates

The injection of white noise current into d1 of the S-type motoneuron model resulted in variation of the ISIs to a constant depolarizing step current injected into the soma (Fig. 7-6). The

variation in the ISIs illustrated by the first order histograms is a characteristic of human motoneurons under voluntary control when a subject is asked to maintain a constant firing rate (Chapter 4). The relative variations in the ISIs at different firing rates, measured by the coefficient of variation, is compared for the S-type model and human soleus and FCR motoneurons in Table 7-3. The changes in the coefficient of variation with firing rate was similar for human soleus motoneurons and the S-type model. However, the coefficients of variation at different firing rates were notably different for the S-type model compared to human FCR motoneurons.

TABLE 7-3. Comparison of the coefficients of variation between the model and human data at different firing rates.

Firing Rate (imp/s)	Coefficient of Variation		
	S-type model	Soleus	FCR
5	0.27	0.27	-
7.5 - 8	0.14	0.15	0.30
11	0.09	-	0.16

The difference between the coefficients of variation in the S-type model and human FCR motoneurons is most likely due to differences in the AHP trajectories reflected by their minimal rhythmic firing rates. The minimal rhythmic firing rate of the S-type model was 5.3 imp/s while that for human FCR motoneurons was between 7 - 8 imp/s. At the minimal rhythmic firing rate the coefficients of variation are relatively high and decrease as rates increase. The relatively high coefficient of variation at minimal rhythmic firing rate is most likely due to an asymptotic portion of the membrane potential later in the ISI (Fig. 7-3). This asymptotic region makes the cell relatively sensitive to fluctuations in membrane potential. In the S-type model motoneuron, as firing rates increased the asymptotic region gradually decreased making the cell less sensitive to membrane noise. Relative to the minimal rhythmic firing rate, a firing rate of 7.5 - 8 imp/s is faster for the S-type model than for human FCR motoneurons. Thus the model (and human

soleus motoneurons) will be less sensitive to membrane potential fluctuations at this firing rate compared to human FCR motoneurons, which probably are most sensitive at this minimal rhythmic firing rate.

Effect of background firing rate on response probability

The motoneuron models showed a relationship between background firing rate and response probability to a randomly elicited transient input . The faster the firing rate of the model neuron the lower the response probability to a constant input. This was true for both the S- and FR-type motoneurons for PPs produced by current pulse injection and composite EPSPs produced by synaptic activation. This effect of firing rate on response probability, or "rate effect", was present in the models in the presence and absence of noise.

In the noiseless motoneuron, it is clear that both the membrane voltage and the membrane conductance determine the excitability of the cell. With the same input, the PP increases monotonically during the ISI starting with a relatively small value near the spike. At the same post-spike delay, the PP is smaller at the slower firing rate (Fig. 7-5). The smaller PP added to the lower membrane potential at a specific post-spike delay results in a lower response probability at the slower firing rate. However, during of random stimulation the motoneuron is responsive for a larger percentage of the ISI when it is firing at a slow rate then when it is firing at a faster rate leading to a higher response probability at the slow rate. This higher response probability at slow firing rates may be attributed to the asymptotic nature of the membrane voltage trajectory and low values of conductance in the latter part of the ISI.

With the addition of noise to the simulations and the subsequent stochastic firing of the motoneuron model, a "rate effect" was still observed (Fig. 7-7). The "rate effect" demonstrated by the S-type model motoneuron using a 9.0 nA current pulse input was similar to the "rate effect" described in human soleus motoneurons (Table 7-4, APPENDIX B). This would suggest that the S-type motoneuron model adequately simulates the responses of human soleus motoneurons at different firing rates to Ia input volleys. However, a comparison of the "rate effect" from the S-

type model and human FCR motoneurons suggested that this model was less accurate in describing the behavior of FCR motoneurons (Table 7-4). This may also be a result of differences in AHP trajectories of the model and human FCR motoneurons at different firing rates as discussed above. Although more experiments using the FR model during stochastic firing are needed, it appears from the noiseless data that this model may provide a better description of the behavior of FCR motoneurons (Fig. 7-3). The difference in response probability at relatively slow and fast rates in the FR-type motoneuron is more comparable to that reported for FCR motoneurons.

At rates below 10 imp/s the "rate effect" was clear in the S-type motoneuron with two different amplitudes of input. However, above 10 imp/s the "rate effect" was not present in simulations which incorporated noise. In the absence of noise the "rate effect" persisted at all rates tested to a maximum of 18 imp/s. A possible reason for the lack of "rate effect" in the model during stochastic firing is inadequate levels of membrane noise. This reason is suggested upon examination of Fig. 7-7 at rates near 15 imp/s. At these rates the response probability to a 9 nA current pulse input was similar in the presence or absence of noise. This suggests that the noise added to the simulation has little effect on response probability at this rate. Throughout the simulations the same level of noisy current was added regardless of the mean background firing rate of the model. Perhaps noise levels should be increased at higher firing rates to represent the increased activity and number of synaptic inputs during stronger voluntary contractions. An alternative suggestion is that the "rate effect" does not continue for slow firing neurons for rates above a certain level. This could be tested by examining responses of human soleus motoneurons at rates above 10 imp/s.

An important factor affecting the magnitude of the effect of firing rate on response probability is the depth of the AHP during repetitive firing. This can be seen in the results from the S_{sh} model which, although it exhibited response trajectories whose slopes were more comparable to the human motoneuron data, showed a reduced rate effect (Fig. 7-10). This raises a possible explanation for the previously reported lack of effect of firing rate on response

probability in tibialis anterior motoneurons (Ashby and Zilm, 1982b). Perhaps different populations of human motoneurons exhibit different depths of AHPs during repetitive firing thus giving rise to a lack of significant effect of background firing rate on response probability.

Response trajectories

In the absence of noisy currents and the resulting variation in ISIs, the response trajectories resembled a step function (Fig. 7-8). This finding was expected and predicted earlier in Chapter 4. The reasoning behind this expectation was that if a motoneuron were firing in the absence of noise, its firing could be considered deterministic and the ISI fixed at a constant value.[4] Assuming a fixed voltage threshold and a linear addition of a constant amplitude EPSP to the membrane voltage trajectory, invoking the EPSP at sequential delays following the spike will eventually trigger a spike. At this effectual delay, the amplitude of the EPSP added to the level of the membrane voltage trajectory sum to a level which is sufficient to cross threshold, advancing the forthcoming spike. At any delay greater than this effectual delay, the EPSP added to the membrane potential will always be of sufficient magnitude to trigger a spike. Therefore, the response trajectory will remain zero at all delays shorter than the effectual delay and 1.0 at all delays greater than the effectual delay resulting in a step function. The present results indicate that the PP amplitude cannot be considered constant throughout the ISI (Fig. 7-5), a result which has been reported for other neurons (Reyes and Fetz, 1993a). However, this finding does not alter the prediction of a step function response trajectory because the PP amplitude increases in a monotonic fashion. Likewise changes in the voltage threshold between spikes reported in cat motoneurons (Calvin, 1974; Powers, 1993) and neocortical neurons (Reyes and Fetz, 1993a) would not change the prediction of a step function during repetitive firing in the absence of noise as these changes parallel the membrane voltage trajectory.

---

[4] The assumption of a fixed ISI in the absence of noise is a simplification for it overlooks the possibility of late adaptation that occurs with sustained activation of motoneurons (Spielmann et al., 1993).

The sigmoidal shape of the response trajectory that arose due to the addition of noisy currents to the simulations, was steeper than response trajectories associated with soleus motoneurons at similar firing rates (Chapter 5). Variation in the size of the current pulse input did not change the slope of the response trajectories and, therefore, in an attempt to reconcile this difference, the depth of the AHP was reduced by lowering the maximum conductance of the slow potassium channel in the soma compartment. The resulting S_{sh} model had a smoothed average response trajectory which was comparable to that of the soleus motoneurons firing at the same rate (Fig. 7-9). When the S_{sh} model was examined for variation in its response trajectories due to firing rate and amplitude of input, it showed similar effects as those reported for human FCR motoneurons (Chapters 4 and 5). At increased firing rates of with a greater amplitude of input, the response probability at a given post-spike delay was increased (Fig. 7-10; 7-11).

Membrane voltage trajectories and response trajectories

To what extent do the underlying membrane voltage trajectories determine the shape of the response trajectory? The results of the simulations using the S_{sh} model demonstrate that altering the membrane voltage trajectory will alter the shape of the response trajectory but how does the shape of the response trajectory reflect the underlying membrane voltage trajectory? This is an interesting question as the shape of membrane voltage trajectories in normal human motoneurons is still unknown. Figure 7-12 illustrates the relation between the smoothed response trajectory (dashed line) from the S_{sh} model (Fig. 7-9) and the membrane voltage trajectory (solid line). The response trajectory was acquired during repetitive firing in the presence of noise resulting in an average ISI of 148.5 ± 29.7 ms. The membrane voltage trajectory was acquired during repetitive firing of the model in the absence of noise at a rate equivalent to the mean firing rate in the presence of noise (ISI = 147 ms). In the absence of noise the response trajectory was described by a step function which bore little resemblance to the underlying membrane voltage trajectory.

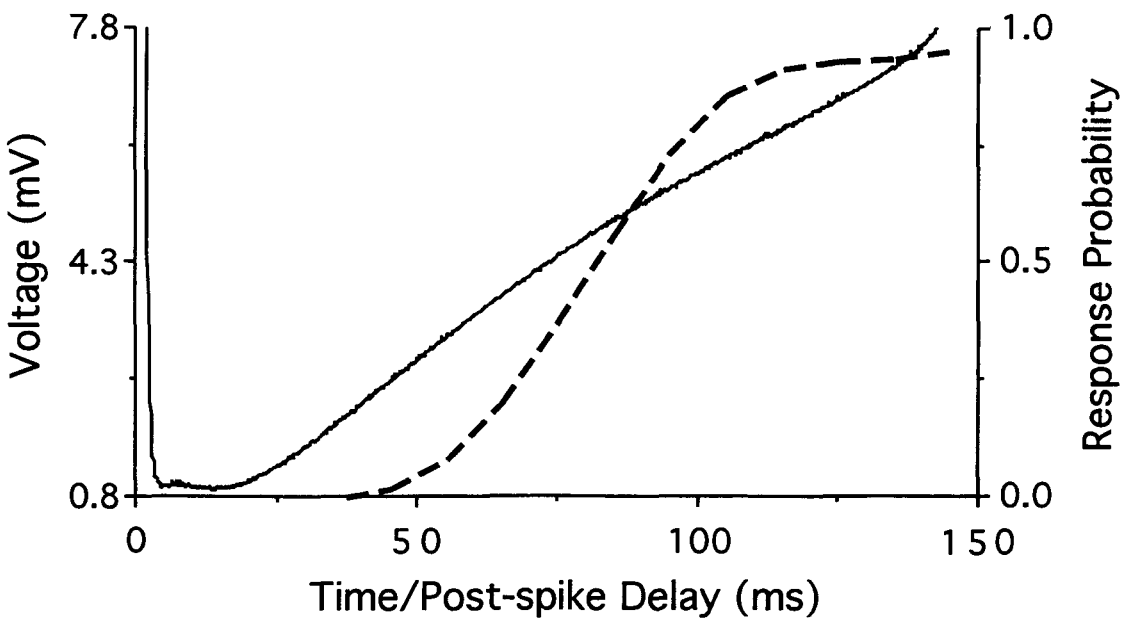

Fig. 7-12 Relationship between the membrane voltage trajectory and a response trajectory of the model motoneuron.

The smoothed response trajectory (dashed line) from Fig. 7-9 from the S_{sh} motoneuron model is shown along with a membrane voltage trajectory (solid line) from the model while firing with a constant ISI of 147 ms which is equivalent to the mean firing rate during the simulations in which the response trajectory was computed. The response trajectory with this level of noise (±20 nA) is not a parallel representation of the membrane voltage trajectory

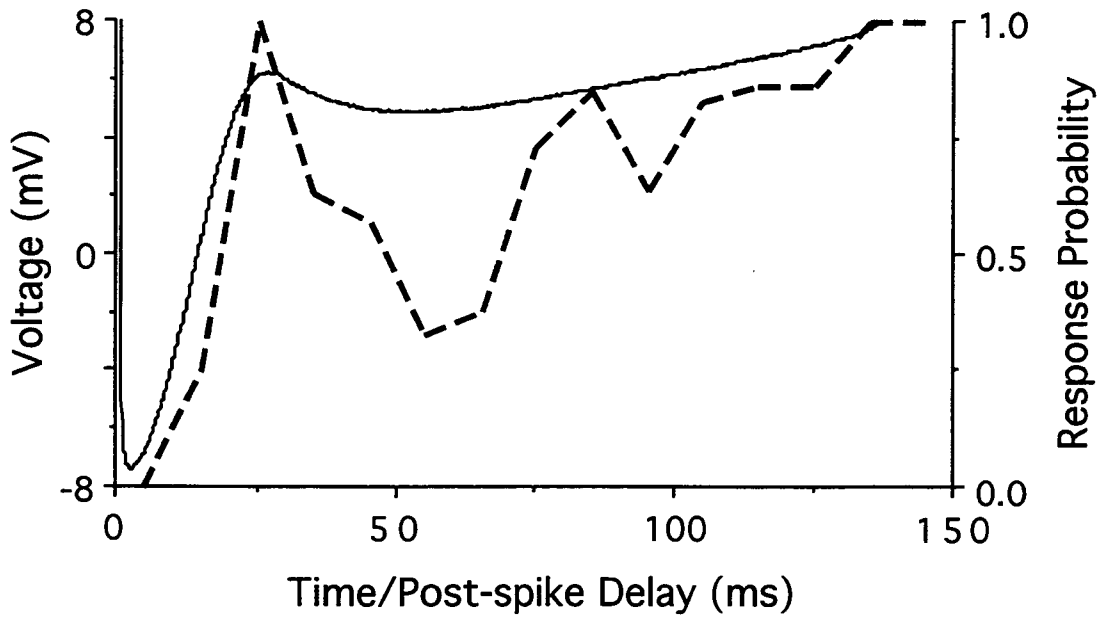

Fig. 7-13 Relationship between the membrane voltage trajectory and a response trajectory in a model with an altered membrane voltage trajectory.

The S-type model was altered to produce repetitive firing with a trajectory that resembled those reported in axotomized motoneurons. The figure indicates that changes in the membrane voltage trajectory (solid line) may be revealed by the response trajectory. The peaks and troughs in the response trajectory (dashed line) coincide with those in the membrane voltage trajectory.

The addition of noise and the subsequent sigmoid shaped response trajectory begin to approximate the shape of the membrane voltage trajectory but the two are still distinct.[5] Perhaps in the presence of additional noise the response trajectory and the membrane voltage trajectory would be more closely approximated.

It is clear that the shape of the membrane voltage trajectory will present itself to some degree in the response trajectory as may be seen in Fig. 7-13. Here the S-type motoneuron has been altered by changing the time constants of the slow potassium channel resulting in a membrane voltage trajectory which is somewhat reminiscent of axotomized motoneurons (Heyer and Llinás, 1977). A depolarizing step current was applied to the soma and noisy current with a standard deviation of 20 nA was injected into d1 resulting in a mean ISI of 142 ± 41 ms. The PSTH resulting from a 9.0 nA current pulse input to d2 looked similar to the data from the normal motoneuron with a $P_r = 0.64$. Construction of the response trajectory, however, revealed a significant deviation from the response trajectories obtained from the normal S-type motoneuron model. It is evident from this figure that the excursions of the membrane potential are reflected in the response trajectory to some extent.

Significance

It is concluded that the present simulations adequately described two features of the human motoneuron data presented in Chapters 4 and 5: 1) an increased firing rate results in a decreased ability of an input volley to alter the firing probability; and 2) excitability following a motoneuron spike increases in a monotonic fashion and this is dependent on noise. This supports the idea that the repetitive firing behavior of human motoneurons may be represented by biophysical processes which are similar to those that underlie repetitive firing in cat motoneurons. Also the results

[5] It must be reaffirmed that the relationship between the response trajectory and the membrane voltage trajectory is dependent on the size of the input. An increase in the size of the input would tend to shift the response trajectory toward lower post-spike delays.

suggest that the use of response trajectories may reveal significant alterations in the underlying membrane voltage trajectories accompanying motoneuron injury or disease.

The next step would be to improve the accuracy of the model, with alterations in membrane noise and conductances underlying the AHP. Then further simulations could be done to estimate the accuracy of the model in predicting a wide range of results from human experiments.

Appendix A

In equation 7-3, the second term represents the sum of the ionic currents in the soma compartment. These currents can be written as:

$$\begin{aligned} I_{ion} &= g_{Na}(V_m - E_{Na}) + (g_{Kf} + g_{Ks})(V_m - E_k) \\ &= \bar{g}_{Na} m^3 h(V_m - E_{Na}) + (\bar{g}_{Kf} n^4 + \bar{g}_{Ks} q^2)(V_m - E_k) \end{aligned}, \qquad \text{A-1}$$

where $\bar{g}_{ion}$ are the maximum conductances for the sodium, fast potassium and slow potassium channels; m, h, n and q are time- and voltage-dependent parameters (represented as η in the following three equations) which determine the magnitude and time course of the activation and inactivation of the respective currents. The time and voltage dependence is given by

$$\frac{d\eta}{dt} = \alpha_\eta(1-\eta) - \beta_\eta \eta = \frac{\eta_\infty - \eta}{\tau_\eta} \qquad \text{A-2}$$

where

$$\tau_\eta = \frac{1}{\alpha_\eta + \beta_\eta} \qquad \text{A-3}$$

$$\eta_\infty = \frac{\alpha_\eta}{\alpha_\eta + \beta_\eta}. \qquad \text{A-4}$$

The time course and magnitudes of the activation/inactivation parameters used in the simulations of Eq. 7-3 are given below.

Initial Segment Currents

Na^+ current

$$I_{Na(IS)} = g_{max} m^3 h (V_m - E_{Na}) \qquad \text{A-5}$$

$g_{max} = 500$ mS/cm^2 $E_{Na} = 115$ mV

m: $$\alpha = \frac{4 + (-0.4 * V_m)}{e^{\left(\frac{V_m - 10}{-5}\right)} - 1} \qquad \text{A-6}$$

$$\beta = \frac{(0.4 * V_m) - 14}{e^{\left(\frac{V_m - 35}{5}\right)} - 1} \quad \text{A-7}$$

h: $$\alpha = \frac{0.16}{e^{\left(\frac{V_m - 37.78}{-18.14}\right)}} \quad \text{A-8}$$

$$\beta = \frac{4}{e^{\left(\frac{V_m - 30}{-10}\right)} + 1} \quad \text{A-9}$$

Fast K^+ current

$$I_{Kf(IS)} = g_{max} n^4 (V_m - E_K) \quad \text{A-10}$$

$g_{max} = 100$ mS/cm^2 $E_K = -10$ mV

n: $$\alpha = \frac{0.2 + (-0.02 * V_m)}{e^{\left(\frac{V_m - 10}{-10}\right)} - 1} \quad \text{A-11}$$

$$\beta = \frac{0.15}{e^{\left(\frac{V_m - 33.79}{71.86}\right)} - 0.01} \quad \text{A-12}$$

Soma Currents

Na^+ current

$$I_{Na(X)} = g_{max} m^3 h (V_m - E_{Na}) \quad \text{A-13}$$

$g_{max} = 140$ mS/cm^2 $E_{Na} = 115$ mV

m: $$\alpha = \frac{7 + (-0.4 * V_m)}{e^{\left(\frac{V_m - 17.5}{-5}\right)} - 1} \quad \text{A-14}$$

$$\beta = \frac{(0.4 * V_m) - 18}{e^{\left(\frac{V_m - 45}{5}\right)} - 1} \quad \text{A-15}$$

h: $$\alpha = \frac{0.15}{e^{\left(\frac{V_m - 34.26}{-18.19}\right)}} \quad \text{A-16}$$

$$\beta = \frac{4}{e^{\left(\frac{V_m - 40}{-10}\right)} + 1} \quad \text{A-17}$$

Fast K^+ current

$$I_{Kf(X)} = g_{max} n^4 (V_m - E_K) \quad \text{A-18}$$

$g_{max} = 35\ mS/cm^2$ $E_K = -10\ mV$

$$n: \alpha = \frac{0.4 + (-0.02 * V_m)}{e^{\left(\frac{V_m - 20}{-10}\right)} - 1} \quad \text{A-19}$$

$$\beta = \frac{0.16}{e^{\left(\frac{V_m - 33.79}{66.56}\right)} - 0.032} \quad \text{A-20}$$

Slow K^+ current: S type motoneuron

$$I_{Ks(X)} = g_{max} q^2 (V_m - E_K) \quad \text{A-21}$$

$g_{max} = 12\ mS/cm^2$ $E_K = -10\ mV$

$$q: \quad \alpha = \frac{3.5}{e^{\left(\frac{V_m - 55}{-4}\right)} + 1} \quad \text{A-22}$$

$$\beta = \frac{0.015}{e^{\left(\frac{V_m + 50}{-0.001}\right)} - 1} \quad \text{A-23}$$

Slow K^+ current: FR type motoneuron

$$I_{Ks(X)} = g_{max} q^2 (V_m - E_K) \quad \text{A-24}$$

$g_{max} = 35\ mS/cm^2$ $E_K = -10\ mV$

$$q: \quad \alpha = \frac{3.5}{e^{\left(\frac{V_m - 55}{-4}\right)} + 1} \quad \text{A-25}$$

$$\beta = \frac{0.035}{e^{\left(\frac{V_m + 50}{-0.001}\right)} - 1} \quad \text{A-26}$$

A larger β_q for the FR motoneuron makes τ_q shorter, resulting in a shorter duration AHP.

Dendritic Synaptic current

$$I_{syn}(t) = g_{syn}(t) * (V_m - E_{syn}) \quad \text{A-27}$$

$$g_{syn}(t) = g_{max} t^{\alpha} e^{-\alpha t/\tau} \quad \text{A-28}$$

$\alpha = 1$ $\tau = 0.2\ ms$ $E_{syn} = 70\ mV$

Appendix B

TABLE 7-4. Comparison of the "Rate Effect" in the model and human data.

Firing Rate (imp/s)	Response Probability to Random Stimuli (mean ± sd)		
	S-type model	Soleus	FCR
Slow (≤ 6)	0.44	0.48± 0.10	-
Fast (> 6)	0.28 ± 0.05	0.27 ± 0.05	-
Slow (≤ 10)	0.34 ± 0.07	-	0.43 ± 0.21
Fast (> 10)	0.24 ± 0.01	-	0.18 ± 0.09

Slow and fast rates are the same as those described in Chapter 4. There are significant differences ($p < 0.02$) between response probability at fast and slow rates in all cases except in the case of the model compared between rates ≤ 10 imp/s and those > 10 imp/s (t-test, $p = 0.075$).

CONCLUSION

The objectives of this thesis were to examine two physiological properties of human motoneurons: 1) recruitment of motoneurons during various tasks; and 2) the biophysics governing repetitive firing behavior in human motoneurons. In meeting these objectives this thesis has made some original contributions to motor control literature.

In addressing the issue of task groups in the flexor carpi ulnaris (FCU) muscle, it was shown that the FCU motor units tested did not show preferential recruitment for the tasks of isometric flexion, non-isometric flexion, isometric ulnar deviation or cocontraction about the wrist joint. This was unlike Denny-Brown's (1949) report in which he stated that the FCU motoneuron pool was fractionated into separate task groups, each task group being activated during a distinct voluntary motor task. The present data an important correction for the literature as neither the flexor carpi radialis (FCR) or extensor carpi radialis (ECR) exhibit fractionation of their motor units into task groups (Riek and Bawa, 1992). Therefore, according to Denny-Brown, FCU appeared to have a significantly different motor organization with little apparent need for such an organization when compared to FCR and ECR. Thus in movements of flexion/extension and ulnar/radial deviation about the wrist, it is suggested that the organizational level of primary importance to ideas of task groups is that of muscle synergies and not subpopulations within a motoneuron pool.

The presence of intramuscular task groups, at first, seems to be predictable based on the anatomy of some muscles. For example, the structurally complex human deltoid muscle has three heads: anterior, middle and posterior. Though all heads may show activity during humeral movements, EMG studies show that each head exhibits maximal activity in a particular direction (Pearl et al., 1992). There are no studies which report intramuscular task groups in the human deltoid muscle, but it seems a likely candidate due to its broad origin which gives rise to different parts of the muscle exerting distinct force vectors on the humerus. Likewise, human jaw muscles, such as masseter, appear to have intramuscular divisions related to task (review Hannam and

McMillan, 1994). Again, intramuscular task groups seem to be predicted by the complex multipinnate nature of the masseter muscle which gives rise to a wide range of force vectors produced by the contraction of the relatively clustered muscle fibers of single motor units in the muscle. The presence of intramuscular task groups in the extensor digitorum communis (EDC; Riek and Bawa, 1992) muscle is compatible with this muscles multiple insertions which serve to extend individual digits. It seems reasonable, therefore, that the presence of intramuscular task groups are more likely in muscles in which different regions of the muscle can direct force through either multiple tendons of different parts of a broad tendon.

In addition to a lack of fractionation of the FCU motoneuron pool into task groups, the study also revealed that the familiar "size principle" recruitment strategy (Henneman et al., 1965) was employed regardless of the task the FCU muscle was engaged in. This raised another question which was addressed in Chapter 3. Most recruitment studies on human motor units have utilized isometric contractions in the classical anatomical planes. If verification for the size principle of human motor unit recruitment were limited to such contractions, extrapolation of the size principle to recruitment during natural movements would be tentative. Indeed a common objection may be paraphrased as, motor unit recruitment studies have only been done during "anatomical" contractions and not during "behavioral" contractions. In an answer to this objection it was shown that motor units of the first dorsal interosseous (1DI) muscle are recruited in the same order during "behavioral" tasks as during isometric abduction of the index finger. This strengthens the idea that the size principle of motor unit recruitment is the normative strategy of recruitment utilized by the central nervous system during all motor behavior.

Following recruitment, if sufficient excitatory drive is available to the motoneuron it will continue to fire repetitively. It is during repetitive firing that motoneuronal excitability has been examined. Motoneuronal excitability throughout this thesis has been defined as the probability that the motoneuron will respond to an input volley. Previously, it has been reported that motoneuron excitability is independent of background firing rate (Ashby and Zilm, 1982b; Miles et al., 1989), however, the present study has shown that for both FCR and soleus motoneurons,

response probability is dependent on background firing rate. The effect of background firing rate depended on whether the stimulus arrived randomly at the motoneuron or at a fixed delay following the motoneuron spike. If it arrived randomly, response probability decreased significantly at the faster firing rate, however, if it arrived at a fixed delay, the response probability increased with an increased firing rate. The results were then explained by drawing upon the known biophysical properties of repetitively firing cat motoneurons and applying that knowledge to the human motoneuron data. This is the first comprehensive documentation of the effect of firing rate on response probability of human motoneurons to Ia afferent input.

The results obtained from the triggered-delay stimulation were used to generate response trajectories under a number of conditions. The response trajectories have been used in this thesis as an analytical tool to investigate: the nature of the refractory period following a motoneuron spike and the factors contributing to it; and, to investigate the similarity between the synaptic distribution from peripheral Ia afferents and corticomotoneurons. Although others have used the idea of response trajectories to investigate human motoneurons (Kudina, 1988; Kudina and Churikova, 1990; Kudina and Alexeeva, 1992) the factors affecting the response trajectory and its relationship to the properties of the motoneuron have not been discussed. The present thesis suggests that the shape of the response trajectory is largely due to the effects of noise, the conductances underlying the AHP, background firing rate and the amplitude and shape of the EPSP resulting from the input volley used to generate the trajectory. With a greater understanding of the factors which give rise to the response trajectories, it is suggested that their potential use as a tool for investigating properties of human motoneurons is encouraging. For example, the results from Chapter 5 illustrating the effects of doublet discharge on response trajectories are interesting as they would suggest a somatic origin for the doublet. Also of interest is the potential for using response trajectories in cases of motoneuron dysfunction to detect changes in the membrane voltage trajectory (Fig. 7-13). If a neuropathy affects the repetitive firing properties of the neuron, use of response trajectories interpreted in light computer simulations may reveal specific biophysical properties affected by the disease.

The final chapter on computer simulations gave a better indication of the biophysical factors that may be contributing to excitability in human motoneurons. The ability to simulate responses from human motoneurons with a model whose basis was cat spinal motoneurons was pleasing as it suggested that the behavior, and perhaps biophysics, of motoneurons from these two species was similar. With some alterations to the model to incorporate an ability to fire doublets and calcium-dependent potassium conductances, more simulations could be done which incorporate other elements the of spinal segmental circuitry. Computer simulations could prove to be a powerful tool in elucidating the details governing the responses seen in human experiments and guiding the development of new ideas of motor control.

REFERENCES

Ashby P, Zilm D (1982a) Relationship between EPSP shape and cross-correlation profile explored by computer simulation for studies on human motoneurons. Exp Brain Res 47: 33-40.

Ashby P, Zilm D (1982b) Characteristics of postsynaptic potentials produced in single human motoneurons by homonymous group I volleys. Exp Brain Res 47: 41-48.

Araki T, Terzuolo CA (1962) Membrane currents in spinal motoneurons associated with the action potential and synaptic activity. J Neurophysiol 25: 772-789.

Baldissera F, Gustafsson B (1971) Regulation of repetitive firing in motoneurones by the afterhyperpolarization conductance. Brain Res 30: 431-434.

Baldissera F, Gustafsson B (1974) Firing behaviour of a neuron model based on the afterhyperpolarization conductance time course and algebraic summation. Adaptation and steady state firing. Acta Physiol Scand 92: 27-47.

Barrett EF, Barrett JN (1976) Separation of two voltage-sensitive potassium currents and demonstration of a tetrodotoxin-resistant calcium current in frog motoneurones. J Physiol (Lond) 255: 737-774.

Barrett JN, Crill WE (1974) Specific membrane properties of cat motoneurones. J Physiol (Lond) 239: 301-324.

Barrett EF, Barrett JN, Crill WE (1980) Voltage-sensitive outward currents in cat motoneurones. J Physiol (Lond) 304: 251-276.

Barrett JN, Crill WE (1980) Voltage clamp of cat motoneurone soma: properties of the fast inward current. J Physiol (Lond) 304: 231-249.

Bawa P (1981) Interaction of excitatory and inhibitory inputs to spinal motoneurones in man. In: Motor Unit Types, Recruitement and Plasticity in Health and Disease. Prog clin Neurophysiol, vol 9, Karger, Basel (ed. JE Desmedt), pp. 212-219.

Bawa P (1982) Interaction of excitatory and inhibitory inputs to motoneurons in man. Can J Physiol Pharm 60: 1562-1566.

Bawa P, Calancie B (1983) Repetitive doublets in human flexor carpi radialis muscle. J Physiol (Lond) 339: 123-132.

Bawa P, Lemon RN (1993) Recruitment of motor units in response to transcranial magnetic stimulation in man. J Physiol (Lond) 471: 445-464

Bigland B, Lippold OCJ (1954) The relationship between force, velocity and integrated electrical activity in human muscle. J Physiol (Lond) 123: 214-224

Booth V, Rinzel J (1995) Dendritic origin of bistability of motoneuron firing patterns. Abstract at Computational Neuroscience Meeting, July 12-15, Monterey, CA. Proceedings to be publised at a later date.

Brock LG, Coombs JS, Eccles JC (1952) The recording of potentials from motoneurones with an intracellular electrode. J Physiol (Lond) 117: 431-460.

Brouwer B, Ashby P, Midroni G (1989) Excitability of corticospinal neurons during tonic muscle contractions in man. Exp Brain Res 74: 649-652.

Brown AG (1981) Organization in the Spinal Cord. Berlin; Springer-Verlag.

Brown SHC, Cooke JD (1981) Amplitude and instruction dependent modulation of movement related electromyogram activity in humans. J Physiol (Lond) 316: 97-107

Brownstone RM, Jordan LM, Kriellaars DJ, Noga BR, Shefchyk SJ (1992) On the regulation of repetitive firing in lumbar motoneurons during fictive locomotion in the cat. Exp Brain Res 90: 441-455.

Burke RE (1967) Motor unit types of cat triceps surae muscle. J Physiol (Lond) 193: 141-160.

Burke RE (1981) Motor units: Anatomy, physiology, and functional organization. In *Handbook of Physiology. The Nervous System* VB Brooks (ed) vol. 2, sect. 1, American Physiological Society, Bethesda, Maryland, pp. 345-442.

Burke RE (1985) Integration of sensory information and motor commands in the spinal cord. In *Motor Control: From Movement Trajectories to Neural Mechanisms*. Society for Neuroscience, Washington, D.C., pp. 44-66.

Burke RE, Jankowska E, Bruggencate G (1970) A comparison of peripheral and rubrospinal synaptic input to slow and fast twitch motor units of triceps surae. J Physiol (Lond) 207: 709-732.

Burke RE, Rudomin P (1977) Spinal neurons and synapses. In *Handbook of Physiology*. vol. 1, *Cellular Biology of Neurons*. ER Kandel (Ed.), American Physiological Soc, Bethesda, Maryland, pp. 877-944.

Burke RE, Walmsley B, Hodgson JA (1979) HRP anatomy of group Ia afferent contacts on alpha motoneurones. Brain Res 160: 347-352.

Buller NP, Garnett R, Stephens JA (1980) The reflex responses of single motor units in human hand muscles following muscle afferent stimulation. J Physiol (Lond) 303: 337-349

Calancie B (1984) Motor unit characteristics of flexor carpi radialis muscle in man. PhD Thesis. Simon Fraser University, Burnaby, BC.

Calancie B, Bawa P (1985a) Firing patterns of human flexor carpi radialis motor units during the stretch reflex. J Neurophysiol 53: 1179-1193

Calancie B, Bawa P (1985b) Voluntary and reflexive recruitment of flexor carpi radialis motor units in humans. J Neurophysiol 53: 1194-1200

Calancie B, Bawa P (1986) Limitations of the spike-triggered averaging technique. Muscle and Nerve 9: 78-83

Calancie B, Bawa P (1990) Motor unit recruitment in humans. In: The segmental motor system, Binder MD, Mendell LM (ed), Oxford Univ Press, New York, pp 75-95

Calvin WH (1974) Three modes of repetitive firing and the role of threshold time course between spikes. Brain Res 69: 341-346.

Calvin WH, Schwindt PC (1972) Steps in production of motoneuron spikes during rhythmic firing. J Neurophysiol 35: 297-310.

Calvin WH, Stevens CF (1968) Synaptic noise and other sources of randomness in motoneuron interspike intervals. J Neurophysiol 31: 574-587.

Clamann HP (1969) Statistical analysis of motor unit firing patterns in a human skeletal muscle. Biophys J 9: 1233-1251.

Clark BD, Dacko SM, Cope TC (1993) Cutaneous stimulation fails to alter motor unit recruitment in the decerebrate cat. J Neurophysiol 70: 1433-1439.

Clements JD, Redman SJ (1989) Cable properties of cat spinal motoneurones measured by combining voltage clamp, current clamp and intracellular staining. J Physiol (Lond) 409: 63-87.

Clough JFM, Kernell D, Phillips CG (1968) The distribution of monosynaptic excitation from the pyramidal tract and from primary spindle afferents to motoneurones of the baboon's hand and forearm. J Physiol (Lond) 198: 145-166.

Coombs JS, Curtis DR, Eccles JC (1957) The generation of impulses in motoneurones. J Physiol (Lond) 139: 232-249.

Cope TC, Clark BD (1991) Motor-unit recruitment in the decerebrate cat: Several unit properties are equally good predictors of order. J Neurophysiol 66: 1127-1138.

Cope TC, Clark BD (1995) Are there important exceptions to the size principle of alpha motoneurone recruitment? In: Alpha and Gamma Motor Sytems. Ed. A. Taylor, M. Gladden and R. Durbaba. Plenum Press, In press.

Cope TC, Fetz EE, Matsumura M (1987) Cross-correlation assessment of synaptic strength of single fiber connections with triceps surae motoneurones in cats. J Physiol (Lond) 390: 161-188.

Cullheim S, Fleshman JW, Glenn LL, Burke RE (1987) Membrane area and dendritic structure in type-identified triceps surae alpha motoneurons. J Comp Neurol 255: 68-81.

Davies L, Wiegner AW, Young RR (1993) Variation in firing order of human soleus motoneurons during voluntary and reflex activation. Brain Res 602: 104-110.

De Schutter E (1989) Computer software for development and simulation of compartmental models of neurons. Compt Biol Med 19: 71-81.

Denny-Brown D (1949) Interpretation of the Electromyogram. Arch Neurol Psych 61: 99-128

Desmedt JE, Godaux E (1977) Fast motor units are not preferentially activated in rapid contractions in man. Nature 267: 717-719

Desmedt JE, Godaux E (1978) Mechanisms of the vibration paradox: excitatory and inhibitory effects of tendon vibration on single soleus muscle motor units in man. J Physiol (Lond) 285: 197-207

Desmedt JE, Godaux E (1979) Recruitment patterns of single motor units in the human masseter muscle during brisk jaw clenching. Arch Oral Biol 24: 171-178.

Desmedt JE, Godaux E (1981) Spinal motoneuron recruitment in man: Deordering with direction, but not with speed of voluntary movement. Science 214: 933-936

Dodge FA, jr, Cooley JW (1973) Action potential of the motorneuron. IBM J Res Dev 17: 219-229.

Edgley SA, Eyre JA, Lemon RN, Miller S (1990) Excitation of the corticospinal tract by electromagnetic and electrical stimulation of the scalp of the macaque monkey. J Physiol (Lond) 425: 301-320.

Fetz EE, Gustafsson B (1983) Relation between shapes of post-synaptic potentials and changes in firing probability of cat motoneurons. J Physiol (Lond) 341: 387-410.

Finegood DT, Thomaseth K, Pacini G, Bergman RN (1988) OPSEG: a general routine for smoothing and interpolating discrete biological data. Comp Meth Prog Biomed 26: 289-300.

Finkel AS, Redman SJ (1983) The synaptic current evoked in cat spinal motoneurones by impulses in single group Ia axons. J Physiol (Lond) 342: 615-632.

Flament D, Goldsmith P, Buckley CJ, Lemon RN (1993) Task dependence of response in first dorsal interosseous muscle to magnetic brain stimulation in man. J Physiol (Lond) 464: 361-378

Fleshman JW, Segev I, Burke RE (1988) Electrotonic architecture of type-identified α-motoneurons in the cat spinal cord. J Neurophysiol 60: 60-85.

Fuglevand AJ, Winter DA, Patla AE (1993) Models of recruitment and rate coding organization in motor-unit pools. J Neurophysiol 70: 2470-2488.

Fujita Y (1989) Dendritic spikes in normal spinal motoneurons of cats. Neurosci Res 6: 299-308.

Fuortes MGF, Frank K, Becker MC (1957) Steps in the production of motoneuron spikes. J Gen Physiol 40: 735-752.

Garnett R, Stephens JA (1980) The reflex responses of single motor units in human first dorsal interosseous muscle following cutaneous afferent stimulation. J Physiol (Lond) 303: 351-364.

Garnett R, Stephens JA (1981) Changes in the recruitment threshold of motor units in human first dorsal interosseous muscle produced by skin stimulation. J Physiol (Lond) 311: 463-473.

Denier van der Gon JJ, Tax T, Gielen S, Erkelens C (1991) Synergism in the control of force and movement of the forearm. Rev Physiol Biochem Pharm 118: 97-124.

Gustafsson B, McCrea D (1984) Influence of stretch-evoked synaptic potentials on firing probability of cat spinal motoneurones. J Physiol (Lond) 347: 431-451.

Gustafsson B, Pinter MJ (1984) An investigation of threshold properties among cat spinal α-motoneurons. J Physiol (Lond) 357: 453-483.

Gustafsson B, Pinter MJ (1984) Influence of post-synaptic properties on the time course of synaptic potentials in different types of cat lumbar alpha-motoneurons. Neurosci Lett 51: 67-72.

Hannam AG, McMillan AS (1994) Internal organization in the human jaw muscles. Crit Rev in Oral Biol & Med 5: 55-89.

Henneman E (1957) Relation between size of neurons and their susceptibility to discharge. Science 126: 1345-1347

Henneman E (1985) The size-principle: A deterministic output emerges from a set of probabilistic connections. J Exp Biol 115: 105-112.

Henneman E, Clamann HP, Gillies JD, Skinner RD (1974) Rank-order of motoneurons within a pool: Law of combination. J Neurophysiol 37: 1338-1349.

Henneman E, Mendell LM (1981) Functional organization of the motoneuron pool and its inputs. In: Handbook of Physiology. The nervous system. Motor control, Brookhart, JM, Mountcastle VB (eds), American Physiological Society, Bethesda, pp. 423-507.

Henneman E, Shahani BT, Young RR (1976) Voluntary control of human motor units. In: Motor systems: Neurophysiology and Muscle Mechanisms, Shahani M (ed), Elsevier, Amsterdam, pp 73-78

Henneman E, Somjen G, Carpenter DO (1965) Functional significance of cell size in spinal motoneurons. J Neurophysiol 28: 560-580

Heyer CB, Llinás R (1977) Control of rhythmic firing in normal and axotomized cat spinal motoneurons. J Neurophysiol 40: 480-487.

Hille B (1992) Ionic Channels of Excitable Membranes, 2nd Edition. Sunderland, Mass.; Sinauer Associates Inc.

Hodgkin AL, Huxley AF (1952) A quantitative description of membrane current and its application to conduction and excitation in nerve. J Physiol (Lond) 117: 500-544.

Hoffer JA, Loeb GE, Sugano N, Marks WB, O'Donovan MJ, Pratt CA (1987) Cat hindlimb motoneurons during locomotion. III. Functional segregation in sartorius. J Neurophysiol 57: 554-562.

Homma S, Nakajima Y (1979) Input-output relationship in spinal motoneurons in the stretch reflex. Prog Brain Res 50: 37-44.

Ito M, Oshima T (1962) Temporal summation of after-hyperpolarization following a motoneuron spike. Nature 195: 910-911.

Jankowska E, Padel Y, Tanaka R (1975) Projections of pyramidal tract cells to α-motoneurones innervating hind-limb muscles in the monkey. J Physiol (Lond) 249: 637-667.

Jones KE, Bawa P (1993) Excitability of motoneurons during different phases of afterhyperpolarization in man. Soc. Neurosci. Abstr. 19:224.9.

Jones KE, Bawa P (1995) Responses of human motoneurons to Ia inputs: effects of background firing rate. Can J Physiol Pharmacol, In press.

Jones KE, Bawa P, McMillan AS (1993) Recruitment of motor units in human flexor carpi ulnaris. Brain Res 602: 354-356

Jones KE, Calancie B, Hall A, Bawa P (1995) A comparison of descending and peripheral inputs on human motoneurons. Can J Physiol Pharm 73: Axii-Axiii.

Jones KE, Calancie B, Hall A, Bawa P (1995) Time course of excitability changes of human α-motoneurones following single spikes and doublets. In: Alpha and Gamma Motor Sytems. Ed. A. Taylor, M. Gladden and R. Durbaba. Plenum Press, In press.

Jones KE, Lyons M, Bawa P, Lemon RN (1994) Recruitment order of motoneurons during functional tasks. Exp Brain Res 100: 503-508.

Kanda K, Burke RE, Walmsley B (1977) Differential control of fast and slow twitch motor units in the decerebrate cat. Exp Brain Res 29: 57-74.

Kanda K, Desmedt JE (1983) Cutaneous facilitation of large motor units and motor control of human fingers in precision grip. In: *Motor Control Mechanisms in Health and Disease.* ed. Desmedt JE, New York, Raven Press, pp.253-261.

Kernell D (1965a) High-frequency repetitive firing of cat lumbosacral motoneurones stimulated by long-lasting injected curents. Acta Physiol Scand 65: 74-86.

Kernell D (1965b) The limits of firing frequency in cat lumbosacral motoneurones possessing different time course of afterhyperpolarization. Acta Physiol Scand 65: 87-100.

Krnjevic K, Puil E, Werman R (1978) EGTA and motoneuronal after potentials. J Physiol (Lond) 275: 199-223.

Kudina LP (1988) Excitability of firing motoneurons tested by Ia afferent volleys in human triceps surae. EEG Clin Neurophysiol 69: 576-580.

Kudina LP, Alexeeva NL (1992) After-potentials and control of repetitive firing in human motoneurons. EEG Clin Neurophysiol 85: 345-353.

Kudina LP, Churikova LI (1990) Testing excitability of human motoneurones capable of firing double discharges. EEG Clin Neurophysiol 75: 334-341.

Lawrence JH, DeLuca J (1983) Myoelectric signal versus force relationship in different human muscles. J Applied Physiol 54: 1653-1659

Lemon RN, Mantel GWH, Rea PA (1990) Recording and identification of single motor units in the free-to-move primate hand. Exp Brain Res 81: 95-106

Lev-Tov A, Miller JP, Burke RE, Rall W (1983) Factors that control amplitude of EPSPs in dendritic neurons. J Neurophysiol 50: 399-412.

Llinás RR (1988) The intrinsic electrophysiological properties of mammalian neurons: Insights into central nervous system function. Science 242: 1654-1664.

Loeb GE (1985) Motoneuron task groups: coping with kinematic heterogeneity. J Exp Biol 115: 137-146

Lüscher H-R, Ruenzel P, Henneman E (1983) Composite EPSPs in motoneurons of different sizes before and during PTP: Implications for transmission failure and its relief in Ia projections. J Neurophysiol 49: 269-289.

Masakado Y, Kamen G, De Luca CJ (1991) Effects of percutaneous stimulation on motor unit firing behavior in man. Exp Brain Res 86: 426-432.

Matthews PBC (1995) A new look at the interval histogram of tonically firing human motor units. J Physiol (Lond) In press.

Mauritz KH, Schlue WR, Richter DW, Nacimiento AC (1974) Membrane conductance course during spike intervals and repetitive firing in cat spinal motoneurones. Brain Res 76: 223-233.

Merton PA, Morton HB (1980) Stimulation of the cerebral cortex in the intact human subject. Nature 285: 227.

Miles TS, Turker KS, Le TH (1989) Ia reflexes and EPSPs in human soleus motor neurons. Exp Brain Res 77: 628-636.

Milner-Brown HS, Stein RB, Yemm R (1973a) The contractile properties of human motor units during voluntary isometric contractions. J Physiol (Lond) 228: 285-306

Milner-Brown HS, Stein RB, Yemm R (1973b) The orderly recruitment of human motor units during linearly changing voluntary contractions. J Physiol (Lond) 230: 359-370

Milner-Brown HS, Stein RB (1975) The relation between the surface electromyogram and muscular force. J Physiol (Lond) 246: 549-569

Monster AW, Chan H (1977) Isometric force production by motor units of extensor digitorum communis muscle in man. J Neurophysiol 40: 1432-1443

Moore JW, Ramon F (1974) On numerical integration of the Hodgkin and Huxley equations for a membrane action potential. J Theor Biol 45: 249-273.

Nardone A, Romano C, Schieppati M (1989) Selective recruitment of high-threshold human motor units during voluntary isotonic lengthening of active muscles. J Physiol (Lond) 409: 451-471.

Nielsen J, Kagamihara Y (1993) Differential projection of the sural nerve to early and late recruited human tibialis anterior motor units: change of recruitment gain. Acta Physiol Scand 147: 385-401.

Nordstrom MA, Fuglevand AJ, Enoka RM (1992) Estimating the strength of common input to human motoneurons from the cross-correlogram. J Physiol (Lond) 453: 547-574.

Olivier E, Bawa P, Lemon RN (1995) Responses to transcranial magnetic stimulation of human motoneurons at different firing rates. J Physiol (Lond) 485.1: 257-269.

Palmer SS, Fetz EE (1985) Discharge properties of primate forearm motor units during isometric muscle activity. J Neurophysiol 54: 1178-1193

Panizza M, Nilsson J, Hallet M (1989) Optimal stimulus duration for the H-reflex. Muscle & Nerve 12: 576-579.

Pearl ML, Perry J, Torburn L, Gordon LH (1992) An electromyographic analysis of the shoulder during cones and planes of arm motion. Clin Ortho & Related Res 284: 116-27.

Person RS, Kudina LP (1972) Discharge frequency and discharge pattern of human motor units during voluntary contraction of muscle. EEG Clin Neurophysiol 32: 471-483.

Phillips CG (1969) Motor apparatus of the baboon's hand. Proc Roy Soc B. 173: 141-174.

Piotrkiewicz M, Churikova L, Person R (1992) Excitability of single firing human motoneurons to single and repetitive stimulation (experiment and model). Biol Cybern 66: 253-259.

Poliakov AV, Miles TS, Nordstrom MA (1994) A new approach to the estimation of post-synaptic potentials in human motoneurones. J Neurosci Meth 53: 143-149.

Porter R, Hore J (1969) Time course of minimal corticomotoneuronal excitatory postsynaptic potentials in lumbar motoneurons of the monkey. J Neurophysiol 32: 443-451.

Powers RK (1993) A variable-threshold motoneuron model that incorporates time- and voltage-dependant potassium and calcium conductances. J Neurophysiol 70: 246-262.

Powers RK, Binder MD (1992) Acceleration of motoneuron discharge rate by hyperpolarizing current pulses. Soc Neurosci Abstr 18: 217.8.

Rall W (1959) Branching dendritic trees and motoneuron membrane resistivity. Exptl Neurol 1: 491-527.

Rall W (1967) Distinguishing theoretical synaptic potentials computed for different soma-dendritic distributions of synaptic input. J Neurophysiol 30: 1138-1168.

Rall W (1977) Core conductor theory and cable properties of neurons. *In*: The Handbook of Physiology, The Nervous System. *Edited by* E.R. Kandel, J.M. Brookhart and V.B. Mountcastle. Bethesda, MD: American Physiological Society, vol I, pp 39-97.

Reyes AD, Fetz EE (1993a) Two modes of interspike interval shortening by brief transient depolarizations in cat neocortical neurons. J Neurophysiol 69: 1661-1672.

Reyes AD, Fetz EE (1993b) Effects of transient depolarizing potentials on the firing rate of cat neocortical neurons. J Neurophysiol 69: 1673-1683.

Riek S, Bawa P (1992) Recruitment of motor units in human forearm extensors. J Neurophysiol 68: 100-108

Schieber MH (1993) Muscular production of individuated finger movements. Soc Neuroscience Abst 19: 228.3

Schoenen J (1982) Dendritic organization of the human spinal cord: the motoneurons. J Comp Neurol 211: 226-247.

Schwindt PC, Calvin WH (1972) Membrane-potential trajectories between spikes underlying motoneuron firing rates. J Neurophysiol 35: 311-325.

Schwindt PC, Calvin WH (1973) Nature of conductances underlying the rhythmic firing in cat spinal motoneurons. J Neurophysiol 36: 955-973.

Schwindt PC, Crill WE (1980a) Properties of a persistent inward current in normal and TEA-injected motoneurons. J Neurophysiol 43: 1700-1724.

Schwindt PC, Crill WE (1980b) Effects of barium on cat spinal motoneurons studied by voltage clamp. J Neurophysiol 44: 827-846.

Schwindt PC, Crill WE (1981) Differential effects of TEA and cations on the outward ionic currents of cat motoneurons. J Neurophysiol 46: 1-15.

Schwindt PC, Crill WE (1982) Factors influencing motoneuron rhythmic firing: results from a voltage-clamp study. J Neurophysiol 48: 875-890.

Schwindt PC, Crill WE (1984) Membrane properties of cat spinal motoneurons. *In*: Handbook of the Spinal Cord. *Edited by* R.A. Davidoff. New York: Dekker, vol II-III, pp 199-242.

Segev I, Fleshman JW, Burke, RE (1990) Computer simulation of group Ia EPSPs using morphologically realistic models of cat α-motoneurons. J Neurophysiol 64: 648-660.

Segev I, Fleshman JW, Miller JP, Bunow B (1985) Modeling the electrical behavior of anatomically complex neurons using a network analysis program: passive membrane. Biol Cybern 53: 27-40.

Segev I, Rinzel J, Shepherd GM (1995) The theoretical foundation of dendritic function: Selected papers of Wilfrid Rall with commentaries. Cambridge, Massachusetts: The MIT Press.

Sherrington CS (1906) The Integrative Activity of the Nervous System. New Haven: Yale University Press, 2nd edition, 1947; reprinted 1961.

Spielmann JM, Laouris Y, Nordstrom MA, Robinson GA, Reinking RM, Stuart DG (1993) Adaptation of cat motoneurons to sustained and intermittent extracellular activation. J Physiol (Lond) 464: 75-120.

Stephens JA, Garnett R, Buller NP (1978) Reversal of recruitment order of single motor units produced by cutaneous stimulation during voluntary muscle contraction in man. Nature 272: 362-364.

Sypert GW, Munson JB (1981) Basis of segmental motor control: motoneuron size of motor unit type? Neurosurgery 8: 608-621.

ter Haar Romeny BM, Denier van der Gon JJ, Gielen CCAM (1982) Changes in recruitment orderof motor units in the human biceps muscle. Exp Neurol 78: 360-368.

ter Haat Romeny BM, Denier van der Gon JJ, Gielen CCAM (1984) Relation between location of a motor unit in thte human biceps brachii and its critical firing levels for different tasks. Exp Neurol 85: 631-650.

Thomas CK, Ross BH, Calancie B (1987) Human motor unit recruitment during isometric contractions and repeated dynamic movements. J Neurophysiol 57: 311--324

Thomas CK, Ross BH, Stein RB (1986) Motor unit recruitment in human first dorsal interosseous muscle for static contractions in three directions. J Neurophysiol 55: 1017-1029

Thomas JS, Schmidt EM, Hambrecht FT (1978) Facility of motor unit control during tasks defined directly in terms of unit behaviors. Exp Neurol 59: 384-395.

Traub RD (1977) Motorneurons of different geometry and the size principle. Biol Cybern 25: 163-176.

Traub RD, Llinás R (1977) The spatial distribution of ionic conductances in normal and axotomized motorneurons. Neuroscience 2: 829-849.

Turker KS, Cheng HB (1994) Motor-unit firing frequency can be used for the estimation of synaptic potentials in human motoneurones. J Neurosci Meth 53: 225-234.

Umemiya M, Berger AJ (1994) Properties and function of low- and high-voltage-activated Ca^{2+} channels in hypoglossal motoneurons. J Neuroscience 14: 5652-5660.

Umemiya M, Berger AJ (1995) Single-channel properties of four calcium channel types in rat motoneurons. J Neuroscience 15: 2218-2224.

Viana F, Bayliss DA, Berger AJ (1993a) Calcium conductances and their role in the firing behavior of neonatal rat hypoglossal motoneurons. J Neurophysiol 69: 2137-2149.

Viana F, Bayliss DA, Berger AJ (1993b) Multiple potassium conductances and their role in action potential repolarization and repetitive firing behavior of neonatal rat hypoglossal motoneurons. J Neurophysiol 69: 2150-2163.

Walmsley B, Stuklis R (1989) Effects of spatial and temporal dispersion of synaptic input on the time course of synaptic potentials. J Neurophysiol 61: 681-687.

Zhang L, Krnjevic K (1987) Apamin depresses selectively the after-hyperpolarization of cat spinal motoneurones. Neurosci Lett 74: 58-62.

Zhang L, Krnjevic K (1988) Intracellular injection of Ca^{2+} chelator does not affect spike repolarization of cat spinal motoneurons. Brain Res 462: 174-180.

Zengel JE, Reid SA, Sypert GW, Munson JB (1985) Membrane electrical properties and prediction of motor-unit type of medial gastrocnemius motoneurons in the cat. J. Neurophysiol. 53:1323-1344.